

**The Mechanical Properties of Bacteria through the Cell Cycle as
Measured by Atomic Force Microscopy**

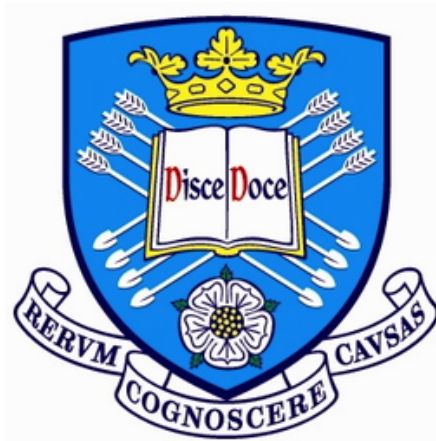
by

Richard Geoffrey Bailey

A thesis presented for the degree of

Doctor of Philosophy

May 2014



Department of Physics & Astronomy

University of Sheffield

Declaration

The work presented and described in this thesis was undertaken at the University of Sheffield between October 2010 and May 2014 under the supervision of Prof Jamie K Hobbs and Prof Simon J Foster. Unless stated otherwise it is the work of the author and has not been submitted, in whole or in part, for any other degree at this or any other institute.

Signed

Richard Geoffrey Bailey

May 2014

Acknowledgements

I would like to thank my two supervisors, Professor Jamie Hobbs and Professor Simon Foster, for their advice and patience through this study. I would also like to thank group members Dr Nic Mullin, Dr Robert Turner, Dr Rebecca Savage, Jacob Albon, Ross Carter, Paul Chapman, Stephen Jackson, Jonathan Burns, Lamiaa Alharbe and Nusrat Sajid, my flatmate Chris Rosslowe and Ana Lorena Morales García, for their continuous help and support throughout the duration of this work.

Thanks also to Dr Chris Hill for his assistance with the Transmission Electron Microscopy experiments, Dr Ken Kennedy for his help in creating the etched silicon wafers used for the project, and Professor Nigel Clarke and Dr Andrew Narracott for helpful discussions.

The calculations concerning continuum plate theory described in Section 6.3 were performed by Professor Nigel Clarke.

Finally I would like to thank EPSRC for providing the funding required for this work, which was also supported by funds from BBSRC.

Abstract

Staphylococcus aureus (SA) is a major cause of infection in humans, including the Methicillin resistant strain, MRSA. However, very little is known about the mechanical properties of these cells. The investigations presented in this thesis use Atomic Force Microscopy (AFM) to examine live SA cells to quantify their mechanical properties. These were explored using force spectroscopy with different trigger forces, allowing the properties to be extracted at different indentation depths. A value obtained with sharp silicon tips of $(0.0134 \pm 0.0068) \text{ Nm}^{-1}$ for the cell wall stiffness has been extracted, along with a second, higher value of $(0.2062 \pm 0.0039) \text{ Nm}^{-1}$ which is found upon indenting at higher forces. This higher value drops by a factor of more than 4 when the cells are exposed to high salt, sugar and detergent concentrations, implying that this measurement contains a contribution from the internal turgor pressure of the cell.

These properties were monitored as the cells progressed through the cell cycle. Force maps were taken over the cells at different stages of the growth process to identify changes in the mechanics throughout the progression of growth and division. These experiments revealed no measurable change in the turgor pressure of the cell, as measured in this way, but it was found that newly formed areas of

cell wall exposed for the first time during the separation of daughter cells gave a higher measured stiffness. This can be related to the structure of the cell wall, which changes as the newly formed cell wall matures during the development of the daughter cells.

The effect of a β -lactam antibiotic, Oxacillin, has also been studied, in an attempt to better understand its mechanism of action. This class of drug is understood to work during division, preventing successful reproduction by inhibiting cell wall production leading to cell lysis. Images were taken throughout the process of β -lactam induced cell death for the first time.

Finally mutant strains of SA and a second species, *Bacillus subtilis* (BS), have been used to link the mechanical properties of the cell walls to structural alterations. Both of these groups of cells contain varied cell wall glycan chain lengths, allowing the study of the effect of chain length on the measured mechanical properties.

Presentations & Publications

Conference Presentations:

UKSPM 2011. Edinburgh, UK. Poster Presentation.

Seeing at the Nanoscale 2012. Bristol, UK. Poster Presentation.

Bruker SPM Conference & User Meeting 2013. Sheffield, UK. Poster Presentation.

UKSPM 2013. Leeds, UK. Poster Presentation.

American Physical Society March Meeting 2014. Denver, USA. Oral Presentation.

Publications:

R G Bailey, R D Turner, N Mullin, N Clarke, S J Foster, J K Hobbs. "The interplay between cell wall mechanical properties and the cell cycle in *Staphylococcus aureus*". Submitted to Biophysical Journal.

R Wheeler, R D Turner, R G Bailey, S A S Mohamad, E J Hayhurst, M J Horsburgh, J K Hobbs, S Mesnage, S J Foster. Working title "Glucosaminidases regulate spherical morphology in *Staphylococcus aureus*". Manuscript in preparation.

List of Figures

2.1	Diagram showing the generalised structure of bacterial cell walls. Top: Gram positive; Bottom: Gram negative.	10
2.2	Diagram showing two models for the structure of peptidoglycan. a) the layered model; b) the scaffold model; c) the coiled coil model. Each shows overall cell model (top) and cross section (bottom).	12
2.3	The structure of oxacillin highlighting the β -lactam ring.	21
3.1	Diagram showing the basic components of the AFM.	25
3.2	Diagram showing the four principal imaging modes of the AFM.	30
3.3	Graph showing the imaging modes of the AFM in terms of the force exerted on the tip by the sample. F = Force on tip, Z = tip height above sample.	31
3.4	Showing the process involved in creating an individual force curve; Top: Cantilever and piezo movement; Bottom: Force curve produced, showing deflection (Volts) against Z - piezo height.	34
3.5	Image showing how the profile of the tip can create artefacts on sharp ridges.	40
4.1	Growth curves for SA (blue diamonds) and BS (red squares).	48
4.2	Plate assay for different SDS concentrations; Top Left 0.01%, Bottom Left 0.1%, Top Centre 1%, Bottom Centre 5%, Top Right 0% (Control).	50
4.3	Contact mode AFM height image of etched silicon wafers for immobilisation of SA cells. Z Scale = 1.0 μm .	56
4.4	Contact mode AFM height image showing SA cells in air, fitting nicely into the etched wells. Z Scale = 1.0 μm .	57
4.5	Contact mode AFM height image in liquid showing cells detached during scanning (tip scanning from bottom to top). Z Scale = 1.0 μm .	58
4.6	Contact mode AFM height image in liquid after polystyrene modification showing cells not detached during scanning. Z Scale = 1.5 μm .	59
4.7	Photograph showing the first sample holder mounted to the JPK NanoWizard 3 stage.	63
4.8	Photograph showing the second sample holder mounted on the Linkam heating stage.	64

4.9	Screenshot of the force curve fitting software, showing the straight line fitted to the curve for an indentation with the 0.01 Nm^{-1} tip.	68
5.1	Graph showing the effect of changing the approach velocity with the 0.1 Nm^{-1} tip.	78
5.2	Graph showing relatively little force relaxation during a constant height dwell time of 10 seconds at 1.0 V deflection setpoint.	80
5.3	Graph showing measurements from three different cantilevers with a full and correct calibration on freshly cleaved mica. The exact location of the contact point is difficult to locate on these curves, and may not be in precisely the true location.	82
5.4	Logarithmic plot of a force curve taken with the 0.07 Nm^{-1} cantilever showing two straight lines in the contact part of the curve, revealing two different power law regions to the original curve.	85
5.5	Histogram showing the two discrete measurement groups for the cell wall (lower) and whole cell compression (higher) indentations. Both data sets contain 36 curves taken on each of 50 cells, a total of 1800 measurements.	88
5.6	Using blunted tips characterised by using a TGT-1 grating (a) to investigate the effect of increased contact area on measured stiffness for 0.01 Nm^{-1} (b) and 0.07 Nm^{-1} (c) cantilevers.	90
5.7	Contact mode vertical deflection image in air showing a field of SA cell walls.	91
5.8	Contact mode vertical deflection image in air showing a single SA cell wall after removal of membrane and contents.	91
5.9	Adding 1.0 M NaCl to SA cells in PBS and monitoring the measured stiffness at high setpoint.	95
5.10	Change in the lowest measured stiffness depending on the concentration of NaCl in the medium.	96
5.11	Graph showing the effect of adding 1.0 M Sorbitol to SA cells in PBS on the measured stiffness at high setpoint.	98
5.12	Monitoring the effect of repeatedly changing the media solute concentration from high to low molarity. Recovery takes much longer the second time around, perhaps because the cell has used up its reserves during the first recovery.	99
5.13	Effect of $1\% \text{ SDS}$ on the stiffness measurements of live cells.	100
5.14	AFM vertical deflection images in air of cells before (left) and after (right) a 1 hour incubation in PBS with $1\% \text{ SDS}$.	102
5.15	Comparing the use of water and PBS as the medium for the addition of NaCl .	103
5.16	Measuring whole cell compression after the addition of both 1 M NaCl and $100 \mu\text{g/ml chloramphenicol}$ to cells in PBS buffer, showing that the cell cannot restore its turgor pressure in this experiment.	104

5.17	Measuring whole cell compression after the addition of both 1 M NaCl and 100 $\mu\text{g}/\text{ml}$ chloramphenicol to cells in water, showing that the cell cannot restore its turgor pressure in this experiment. Here it is also shown that the delay before the measurement dropped, as seen previously in water, does not exist.	105
5.18	TEM images of cells before (1), during (2) and after (3) the drop in whole cell compression stiffness caused by the exposure to 1 M NaCl.	107
5.19	Measured stiffness on live SA cells when under stress due to exposure to NaCl, when indentation setpoint was increased in 0.5 V intervals. Error bars show 1 standard deviation over 5 repeat measurements.	109
6.1	Example slice through the centre of a force map, showing a stiffness vs. position graph for the measurement from each point.	117
6.2	Three examples of cell wall stiffness maps showing little distinguishable variation on each cell, and between different cells.	119
6.3	Three examples of whole cell compression maps on stationary phase cells showing little variation on each cell, and between different cells.	120
6.4	AFM vertical deflection image (left) and force map (right) of an SA cell as the septum shows on the outer wall.	122
6.5	AFM vertical deflection image (left) and force map (right) of an SA cell as the cells start to round up after the septum has finished forming.	123
6.6	AFM vertical deflection image (left) and force map (right) of an SA cell showing new cell wall, indicated by the red circle.	125
6.7	AFM vertical deflection image (left) showing corresponding height profile (right). Arrows indicate the steep region from which data would be unreliable.	126
6.8	AFM vertical deflection images showing typical rings as seen on new septum surfaces.	127
6.9	Three examples of whole cell compression maps taken on exponential phase, dividing cells, showing little variation on each cell, and between different cells.	129
6.10	Measurements of the whole cell compression taken on cells at different stages of the division process. Key: Blue: Stationary phase data; Red: Exponential phase data.	130
6.11	AFM vertical deflection image (left) and corresponding height profile (right) showing the pie crusts of a dividing cell, indicated by the arrows.	132
6.12	AFM vertical deflection image (left) and corresponding 300 nm^2 stiffness force map (right) showing the pie crusts as being stiffer than the central, septal cell wall. Force map Z scale from 0.003 - 0.015 Nm^{-1} .	133

6.13	Histogram showing the measured stiffness of the three regions of the cell wall, from a total of 10 maps.	134
6.14	Sketch showing a cross section of the splitting edge of the septum at initial separation stages, showing a possible conformation of the pie crust and the area being digested by enzymes. This fits with the force data, as the central strip would be softer due to the digestion, and the strip either side of that would be stiffer due to the support of the pie crust under the remaining shallow cell wall at the new corner.	136
7.1	Box and whisker plot showing the measured stiffness for the cell walls of different strains of SA. There appear to be two populations; the first containing <i>SH1000</i> , <i>sagB C</i> and <i>aAH</i> (below the dotted line) and the second containing the other four.	143
7.2	Histograms of raw data taken from different cell mutants, showing <i>SH1000</i> , <i>sagB C</i> and <i>aAH</i> grouped at lower stiffness, and the other mutants grouped at higher stiffness.	144
8.1	Graph showing the temperature measured for the liquid in the Linkam Stage holder compared to the set stage temperature, both with and without the AFM head present.	151
8.2	Graph showing the temperature measured for the liquid in the Linkam Stage holder over a total of 2 hours, to check the stability when set to the desired temperature.	152
8.3	Three AFM vertical deflection images in air showing SA cells after a 1 hour incubation with 5 $\mu\text{g}/\text{ml}$ oxacillin in growth medium (BHI). All the cells appear shrivelled and died during the treatment.	153
8.4	Graph showing the measured diameter of cells that were grown for 1 hour in PBS and oxacillin, BHI and oxacillin, and untreated cells (measurements were taken from cells in both PBS and BHI to check for consistency between the two).	154
8.5	Graph showing the measured whole cell compression stiffness for cells after a 1 hour incubation in 5 $\mu\text{g}/\text{ml}$ oxacillin in growth medium (BHI), much lower than that for healthy cells.	155
8.6	Series of AFM vertical deflection images taken at time intervals of approximately ten minutes of live SA cells showing a cell expanding (a) and then appearing to burst (b) under the effect of oxacillin. The scale bar represents 1 μm .	157
9.1	AFM contact mode height image showing the initial gutter substrates (top) with cross section from marked line (bottom).	162
9.2	3D rendered AFM contact mode height image of etched pillar wafer in air. The height of the pillars is approximately 1.2 μm .	163

9.3	Fluorescence image of BS cells mounted on silicon pillar wafers using the DAPI stain.	164
9.4	Fluorescence images of BS cells mounted on agarose using the live / dead stain. Left: Negative control, dead cells, scale bar is 5 μm ; Right: Positive control, live cells, scale bar is 10 μm .	165
9.5	Fluorescence images of BS cells mounted on silicon pillar wafers using the live / dead stain. Each scale bar represents 10 μm .	166
9.6	Contact mode vertical deflection image of <i>Bacillus subtilis</i> cells imaged in air on freshly cleaved mica.	167
9.7	Contact mode vertical deflection image of <i>Bacillus subtilis</i> cells imaged in liquid on etched silicon wafer. The white arrow indicates one of the larger, healthier looking cells, which detached in the right hand image.	169
9.8	Slope force maps of <i>Bacillus subtilis</i> cells in growth medium. Z scales from 0.002 - 0.016 Nm^{-1} .	170
9.9	Histograms comparing the measured stiffness of the cell wall (top) and the whole cell compression (bottom) for BS and SA cells.	171
9.10	AFM force maps showing a BS cell elongating during growth, the quoted length is the measurement along the blue line. Time between scans is approximately fifteen minutes.	174
9.11	Measuring the length and stiffness for growing BS cells; Top: Cell wall, Bottom: Measured whole cell compression. Time between measurements is approximately fifteen minutes.	175
9.12	300 nm^2 force maps of a small surface area of three different BS cells (1-3) showing (a) height, (b) slope and (c) adhesion. Each scale bar represents 100 nm.	177
9.13	Plot of two retract force curves taken on adhesive (blue) and non adhesive (orange) areas of the same BS cell. The adhesion is quantified by measuring the area below the x axis, within the adhesion 'spike'. Please note, the contact point on these curves has intentionally been chosen marginally incorrectly to visualise the contact part of the two curves without overlap, leading to a larger apparent indentation than in reality.	179
9.14	300 nm^2 adhesion force maps of the surface of BS, taken repeatedly over the same area at 15 minute intervals. Each scale bar represents 100 nm.	180

Contents

Declaration	i
Acknowledgements	ii
Abstract	iii
Presentations and Publications	v
List of Figures	vi
Contents	xi
1 Overview	1
2 Background to Bacteria	4
2.1 Introduction	4
2.2 Species of Interest	5
2.2.1 <i>Staphylococcus aureus</i> (SA)	6
2.2.2 <i>Bacillus subtilis</i> (BS)	7
2.3 Cell Structure	8
2.3.1 Internal Structure	8
2.3.2 The Cell Wall and Membrane(s)	9
2.3.2.1 The (Inner) Cell Membrane	9
2.3.2.2 The Peptidoglycan Cell Wall	11
2.3.2.3 The Periplasmic Space	12
2.3.2.4 Teichoic Acids (only Gram Positive)	13
2.3.2.5 Pili and Flagella	13
2.3.2.6 The Gram Negative Outer Membrane	13
2.4 Growth and Division	14
2.4.1 Cell Wall Hydrolases	15
2.4.2 Division in <i>Staphylococcus aureus</i>	15
2.4.3 Division in <i>Bacillus subtilis</i>	17
2.4.4 Septum Location	17
2.4.5 Cell Shape	18
2.5 Osmotic Stress Response	19
2.6 β -lactam Antibiotics	20
2.7 Industrial Application	21
2.8 Conclusion	22
3 Atomic Force Microscopy	23

3.1	Introduction	23
3.2	Imaging	25
3.2.1	Feedback Controls and Imaging Modes	26
3.2.1.1	Contact Mode	26
3.2.1.2	Dynamic Modes	28
3.2.2	Imaging Modes in Terms of Forces	30
3.2.3	Immobilisation of Samples	30
3.2.4	AFM Imaging of Bacterial Samples	32
3.3	Force Spectroscopy	34
3.3.1	Cantilever Calibration	35
3.3.2	Force Mapping	37
3.3.3	Force Measurements of Bacterial Samples	37
3.4	AFM Artefacts	39
3.5	Why use AFM for Studying Microbes?	41
4	Materials and Methods	43
4.1	Media	43
4.2	Bacterial Strains	44
4.2.1	<i>Staphylococcus aureus</i> (SA)	44
4.2.2	<i>Bacillus subtilis</i> (BS)	45
4.3	Cell Culture Methods	45
4.3.1	Agar Plates	46
4.3.2	Overnight Culture	46
4.3.3	Growth to Exponential Phase	46
4.3.4	Harvesting Cells for AFM	48
4.4	Cell Death	49
4.5	Cell Wall Extraction	51
4.6	AFM Substrate Preparation	52
4.6.1	Unsuccessful Attempts	52
4.6.2	Etched Silicon Wafers	53
4.6.2.1	Design of Wafers	53
4.6.2.2	Etching Protocol	54
4.6.2.3	Preparation of Wafers	55
4.6.2.4	Imaging SA in Liquid	56
4.7	AFM Techniques	61
4.7.1	Sample Holders	61
4.7.2	Imaging	63
4.7.3	Force Measurements	64
4.7.4	Force Mapping	65
4.7.5	Cantilever Calibration	66
4.7.6	Dwell Experiments	66
4.7.7	Live Modification of Buffer Conditions	67
4.7.8	AFM Data Analysis	67

4.7.9	Statistics: Student's T-Test	68
4.8	Fluorescence Microscopy	69
4.8.1	DAPI Stain	69
4.8.2	BacLight™ Stain	70
4.9	Transmission Electron Microscopy (TEM)	71
5	Mechanical Measurements	73
5.1	Introduction	73
5.2	Results	75
5.2.1	Method Development	75
5.2.2	Rate Dependence	77
5.2.3	Possible Calibration Error	78
5.2.4	Dwell	79
5.2.5	Media Dependence	81
5.2.6	Force Curves at 2.5 V with Correct Calibration	81
5.2.7	Common Force Curve Models	83
5.2.7.1	Logging Force Curves	84
5.2.7.2	Rejection of Force Curve Models	86
5.2.8	Quantification of Two Discrete Regions	86
5.2.9	Using Blunt Tips to Understand the Indentations	87
5.2.10	Testing Region 1: The Cell Wall	89
5.2.11	Testing Region 2: Whole Cell Compression with Turgor Component	93
5.2.11.1	NaCl	94
5.2.11.2	Sorbitol	97
5.2.11.3	Reversibility of Change	97
5.2.11.4	SDS	99
5.2.11.5	Using Water as the Medium	102
5.2.11.6	Use of Chloramphenicol to Block Active Processes	103
5.2.11.7	TEM of Cells Exposed to NaCl	106
5.2.11.8	Stress Stiffening Test with Increasing Indentations	108
5.2.11.9	Region 2 Conclusions	110
5.2.12	Targeted Measurements	110
5.3	Conclusions	111
6	Mechanical Mapping	114
6.1	Introduction	114
6.2	Results	116
6.2.1	Measurement Boundary	116
6.2.2	Stationary Phase	118
6.2.2.1	Mapping with Low Force	118
6.2.2.2	Mapping with High Force	119

6.2.3	Exponential Phase	120
6.2.3.1	Mapping with Low Force	121
6.2.3.2	Low Force Measurements During Stage 1 of Division: Septum Visible	121
6.2.3.3	Low Force Measurements During Stage 2 of Division: Cells Rounding Up	122
6.2.3.4	Low Force Measurements During Stage 3 of Division: Exposed Septal Material	124
6.2.3.5	Mapping with High Force	128
6.2.3.6	The ‘Pie Crust’	131
6.3	Continuum Plate Theory	135
6.4	Conclusions	136
6.4.1	The Cell Wall	137
6.4.2	The Whole Cell Compression	138
6.4.3	Separation Questions	139
7	Mutant Strains	140
7.1	Introduction	140
7.2	Strains	141
7.3	Results	142
7.3.1	Discussion for <i>sagB</i> and <i>sagB C</i>	144
7.3.2	Discussion for <i>ABH</i> , <i>aAB</i> and <i>aBH</i>	145
7.3.3	Discussion for <i>aAH</i>	146
7.4	AFM Imaging Observations	146
7.5	Conclusion	147
8	Oxacillin	149
8.1	Introduction	149
8.2	Results	150
8.2.1	Linkam Heating Stage Testing	150
8.2.2	Results from Incubations	152
8.2.3	Live AFM Imaging	155
8.3	Conclusions	158
9	<i>Bacillus subtilis</i>	160
9.1	Introduction	160
9.2	Results	161
9.2.1	Silicon Wafers	161
9.2.2	Fluorescence	163
9.2.2.1	DAPI stain	164
9.2.2.2	BacLight™ Live / Dead Stain	164
9.2.3	Initial AFM Imaging	167
9.2.3.1	Images in Air	167
9.2.3.2	Images in Liquid	168

9.2.4	Initial AFM Force Measurements	169
9.2.5	Consecutive Force Mapping	172
9.2.5.1	Viewing Cell Growth	173
9.2.5.2	Small Scale Force Maps and Adhesion Features	176
9.3	Conclusions	181
10	Conclusions	183
10.1	Overall Conclusions	183
10.2	Future Work	187
	Bibliography	189

1 | Overview

Upon starting this work, the primary objectives were to make mechanical measurements on living bacterial cells. The motivation behind this project was to forward our understanding of the mechanics of the bacterial cell, and particularly the cell wall. Currently there is surprisingly little knowledge in this area, and there is great reason to study it considering the fundamental role the cell wall plays in bacterial mechanical integrity.

Common antibiotics such as penicillin, as discovered by Alexander Fleming in 1928, have been greatly overused in the treatment of bacterial infection. This has led to a dramatic rise in the existence of antibiotic resistant drugs, which pose a significant threat to human health, such as the famous hospital ‘superbug’ MRSA. The requirement for a better understanding of the mechanism of action of antibiotics such as these, and the ways in which bacteria are successfully becoming resistant, is clearly vital.

The cell wall of a bacterial cell is its border to the outside world, and the way in which it interacts with substances in the surrounding environment. It is currently understood that antibiotics in the penicillin family operate by binding to proteins embedded in the cell membrane in order to prevent the manufacture of new cell

wall during division. The cell wall is therefore a vital area of study to forward our understanding of this process and the bacterial cell in general.

The following will now introduce the topics in this thesis, chapter by chapter, beginning with introductions to the subject area, followed by the data acquired during this study.

Chapter 2 introduces a background to bacteria in general, before moving on to discuss the known properties of the two species of interest for this study, SA and BS, in more detail. Following this, Chapter 3 then introduces the Atomic Force Microscope, and discusses specifically the possible uses of AFM in microbiology with examples from the literature where AFM has been used to study bacterial cells.

Chapter 4 discusses the materials and methods that were used throughout the work presented in this thesis, including the microbiology techniques used to culture the bacterial cells and the AFM techniques used to image and measure the live cells.

The first new data obtained in this study is presented in Chapter 5, which includes the separation of the mechanical measurements of the cell wall and the whole cell on SA, with a contribution from the turgor pressure. This chapter also includes experiments performed with the addition of high osmolyte concentration to the surrounding medium, causing changes to the internal turgor pressure of the cell.

Using the properties obtained in the above chapter, Chapter 6 progresses to use mechanical mapping of SA cells, both of the cell wall and the whole cell compression, in order to provide a visual representation of the cells' properties

over the surface. This was performed on cells throughout the division cycle, which allowed a characterisation of changes in these properties as the cells grow and divide.

Using genetically modified mutants of SA, which have longer glycan chains composing the cell wall, made it possible to study the difference that chain length makes to the mechanical properties of the cell wall, as described in Chapter 7.

In the experiments shown in Chapter 8 oxacillin was added to live SA cells in order to attempt to view cell death by exposure to antibiotics, as the method of action of β -lactams is still not fully understood.

Finally, in the experiments analysed in Chapter 9, *Bacillus subtilis* (BS) was studied. This was done mainly for comparison, as it is currently understood that the two species have the same components in their cell walls, but these components are organised differently, with the cell walls of BS containing much longer glycan chains. By using the same techniques as for SA, the mechanical properties of BS were also characterised throughout the cell cycle.

2 | Background to Bacteria

2.1 Introduction

The general term ‘Bacteria’ covers an enormous kingdom of prokaryotic, single celled organisms. These usually have lengthscales on the order of a few microns, and exist in a wide range of shapes, for example the spherical cocci, the rod shaped bacilli, or others including crescents and many irregular shapes.

Bacteria and archaea are believed to have been among the first forms of life on earth, and have been here diversifying since then. Due to their adaptability, they can live almost anywhere, including in temperatures exceeding 100 °C [1] and withstanding enormous pressure 11 km under the ocean surface in and around the Mariana Trench [2]. They also live inside other organisms - it is estimated that there are around ten times more bacterial than human cells inside a person’s body, without which we would not be able to digest certain foods [3], amongst other mutually beneficial requirements.

Despite their abundance, their size and diversity mean that for a long time little was known about these organisms. They were first observed by Antony van

Leeuwenhoek in 1676 [4, 5]. He did this by creating an early form of the optical microscope, involving a convex lens held between two plates designed to magnify a sample that was placed underneath. As Leeuwenhoek observed bacteria in a tiny droplet of water, but at this stage did not know what they were, he initially called them ‘animalcules’ (from the Latin for ‘little animal’). The term ‘bacteria’ was coined much later, in 1828 by Christian Gottfried Ehrenberg, a professor of medicine at Berlin University.

In 1859 Louis Pasteur showed that the fermentation process was caused by the growth of microorganisms. Pasteur and Robert Koch were early supporters of the germ theory of disease, believing that bacteria were responsible for some illnesses, along with viruses and other microorganisms. Koch later proved this with his study into tuberculosis, for which he was awarded the Nobel Prize in Physiology or Medicine in 1905.

As more was being understood about bacteria, and the threat they caused via illness, immunology was becoming an important field. In 1910 the first antibiotic was produced successfully by Nobel Prize winner Paul Ehrlich [6].

This chapter will introduce what is currently known about the bacterial cell, and how that relates to the aims of this study.

2.2 Species of Interest

The two species of interest for this study are *Staphylococcus aureus* and *Bacillus subtilis*. These two species are commonly studied in the laboratory, as they are reasonably robust and easy to grow, with strains relatively harmless to humans

easily available. As they have been studied to an extent already, there are also large numbers of different specific mutants available, allowing the role of particular genes to be determined. Both species have had their genomes fully sequenced [7, 8].

Whilst there has been a considerable amount of research on the structure, genetics and physiology of bacteria, very little is known about their mechanics, and how the physical properties of the cells change during growth and division.

As will be introduced in this chapter, there is a great deal of established knowledge concerning the genetics and biochemistry of bacteria in general and these two well characterised species. Despite this, very little is well understood about the physical properties, the structure and the mechanics of these cells as they grow and progress through the division cycle, and how the physical properties are related to the known genetic and biochemical properties of bacterial cells. Because of this the mechanical properties of bacteria yield a vital area of study. It is during the division process that β -lactam antibiotics, such as penicillin, are believed to work, meaning that antibiotic resistant strains must be dividing successfully whilst simultaneously blocking the antibiotic activity. This study aims to further the understanding of the mechanics of these cells throughout growth, to help towards a greater understanding of bacterial life.

2.2.1 *Staphylococcus aureus* (SA)

SA is a species of micron sized non motile coccoid bacteria, first identified in 1880 by Alexander Ogston [9]. Its name derives from the Greek σταφυλοκοκκος, meaning ‘grape cluster berry’, and the Latin aurum, meaning ‘gold’. It owes

this name to its golden colour, and its ability for dividing cells to not quite fully separate, causing the cells to grow in large connected clusters, like a bunch of grapes.

SA can be completely harmless, and is a common constituent of the normal bacterial flora of the skin and nasal passages, however it can also cause the body serious issues [10]. SA is known to cause a large number of infections including pneumonia [11] and meningitis [12]. Antibiotic resistant strains can cause serious illness and even death, as with the famous ‘super bug’ MRSA (Methicillin Resistant *Staphylococcus aureus*).

2.2.2 *Bacillus subtilis* (BS)

BS is a harmless species of bacteria. It is rod shaped, approximately 2 - 3 microns long and 1 micron wide. BS is usually found in large quantities in the soil, but is also believed to be part of the human gut commensal. Its name comes from the Latin for ‘thin rod shape’. BS is self motile, with flagella at its poles.

Whilst SA is very useful to study to understand better its health threat and antibiotic resistance, BS is studied here as a species commonly found harmlessly in the human gut, which has an affinity for genetic manipulation and sporulation (which have led to its use as a model laboratory organism, although this study does not deal directly with these two features). It is also to be used as a comparator to SA as the cell walls of the two species are believed to have similar composition yet different structures, as discussed later. The genera *Staphylococcus* and *Bacillus* are closely related, and have been grouped in the same order *Bacillales* and class *Bacilli* [13] (all living things are currently classified as follows: Life > Domain >

Kingdom > Phylum > Class > Order > Family > Genus > Species).

2.3 Cell Structure

2.3.1 Internal Structure

Bacteria are prokaryotes, which means that they do not have any membrane bound organelles. Instead all of the cellular contents are collected together in the cytoplasm of the cell rather than being individually contained within their own membranes. This means that the cells can appear more homogeneous than eukaryotes, which have large bound areas of different density where the large organelles are located. The genetic information of the bacterial cell is coiled together in a large nucleoid, with other nucleic acid fragments looped into plasmids also located in the cells' cytoplasm. The cell also contains large quantities of ribosomes, similar to those found in eukaryotic cells, used as the site for protein synthesis and folding. A few species of bacteria also contain specific organelles, such as chromatophores in phototropic bacteria and magnetosomes in magnetotactic species.

From the point of view of this study, the arrangement of the cellular components is not particularly important. The intracellular structure of these cells means that the cell can be viewed as a container of liquid of relatively homogeneous density.

2.3.2 The Cell Wall and Membrane(s)

At the outer edge of a bacterial cell is a cell membrane encased by a cell wall. Bacteria are grouped into two main types by the structure of this wall, which depends on the thickness of the wall and whether or not there is a second, outer membrane present.

The two types are classified as either Gram positive or Gram negative, which depends on their ability to take up the Gram stain [14]. The general overall structures of the two types of wall are shown in Figure 2.1. The general structure in both cases consists of a phospholipid bilayer membrane on the inside edge, covered with a cell wall made up of peptidoglycan. In Gram positive cells this layer is much thicker than in Gram negative, where there is a thinner peptidoglycan layer topped with a second lipid membrane [15]. The structures and functions of the various components are summarised below.

2.3.2.1 The (Inner) Cell Membrane

Bacterial cell membranes have similar structure to eukaryotic membranes, consisting of a phospholipid bilayer. The inner cell membrane of bacteria primarily functions as a permeability barrier for passage of materials into and out of the cell. Small molecules and ions can diffuse across the membrane at no energy cost to the cell. The membrane is also studded with proteins which can actively transport larger molecules across the membrane, such as sugars and amino acids crucial for growth.

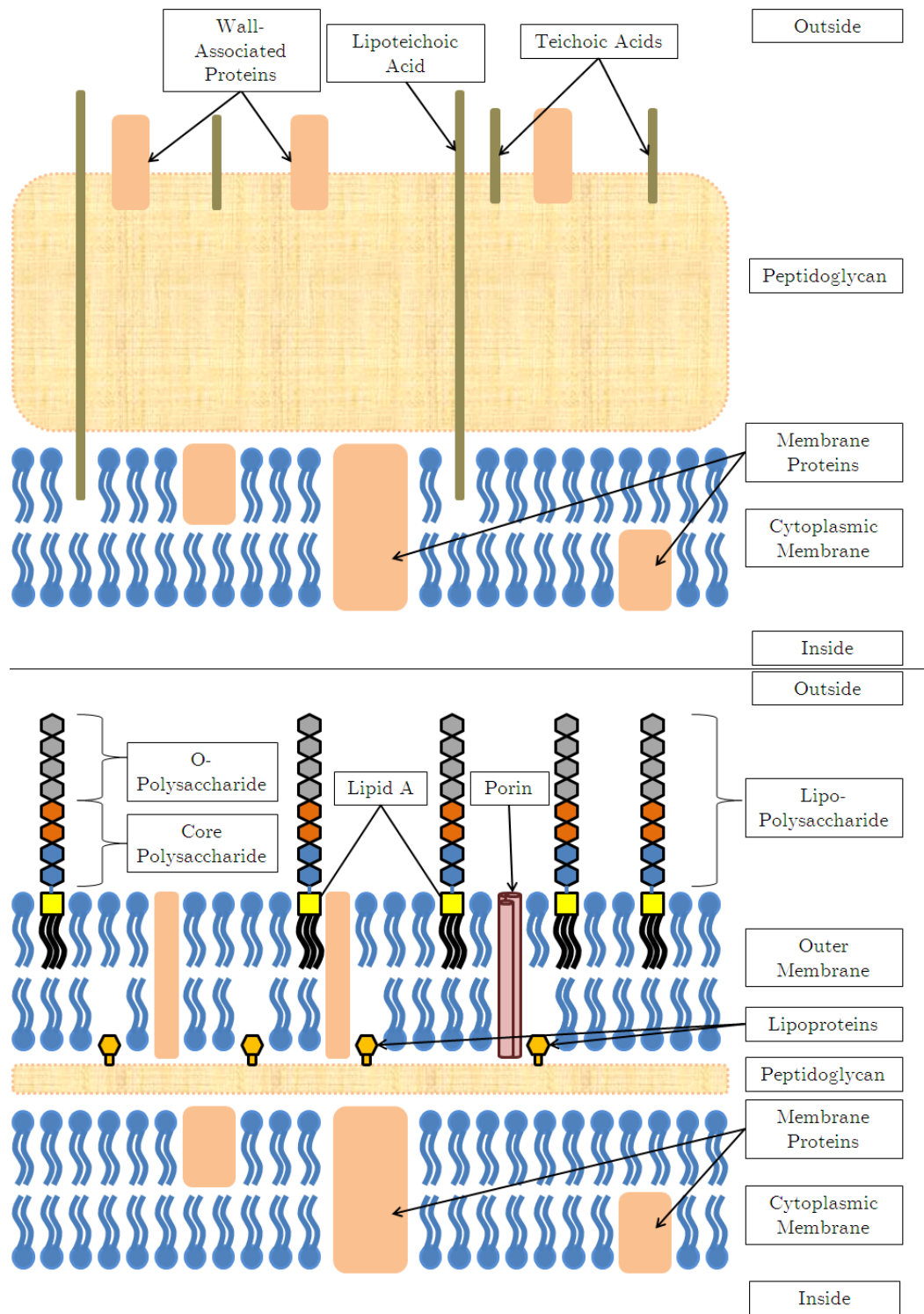


Figure 2.1: Diagram showing the generalised structure of bacterial cell walls. Top: Gram positive; Bottom: Gram negative.

2.3.2.2 The Peptidoglycan Cell Wall

The structure and function of the peptidoglycan is still the subject of debate. It is generally accepted that the function is to both contain the large turgor pressures that exist in bacteria (up to 5 atm in Gram positive species) and also to provide a barrier against the environment.

The structure of the peptidoglycan layer is still unresolved. It is understood that the primary structure of the peptidoglycan consists of chains of alternating N- acetylglucosamine (GLcNAc) and N- acetylmuramic acid (MurNAc) residues, which are connected by β 1 - 4 glycosidic bonds [16]. The way in which these are arranged together is still unclear, and there are a number of models currently available to attempt to describe possible arrangements [17, 18, 19].

The first of these models, known as the Layered Model, has both the glycan strands and the peptide crosslinks lying in the plane of the cell wall, as shown in Figure 2.2a [20, 21]. This forms a network of peptidoglycan over the surface of the cell which can be stacked to form a thicker wall. When the wall is put under stress it is likely that it forms the 'chicken wire' conformation shown rather than being perfectly linearly arranged. This is currently believed to be the conformation of Gram negative peptidoglycan [22], and some believe that it could also be the case for Gram positive [23].

The second common model is shown in Figure 2.2b, known as the Scaffold Model. In this case the glycan chains are much shorter than in the Layered Model, sitting perpendicular to the cell surface, still linked by the same cross links [24, 25, 26].

There is also a third model, that was proposed more recently in 2008. This model suggests a ‘coiled coil’ arrangement of the peptidoglycan of *Bacillus subtilis*, more complex than either of the two previous models thought [27]. A similar structure to this has also been proposed for *Lactococcus lactis* with periodic bands of peptidoglycan wrapped around the cell [28]. See Figure 2.2c.

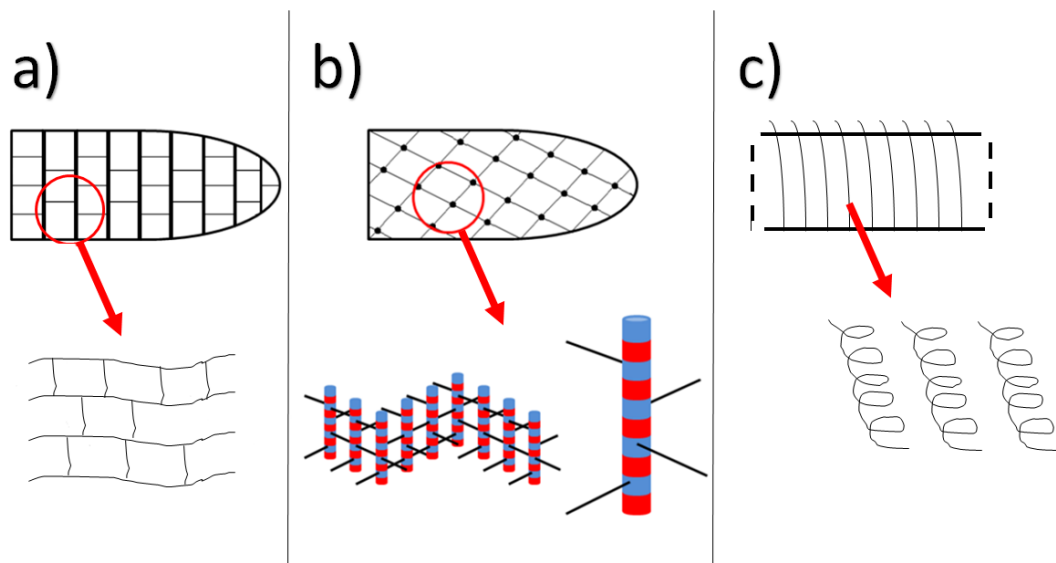


Figure 2.2: Diagram showing two models for the structure of peptidoglycan. a) the layered model; b) the scaffold model; c) the coiled coil model. Each shows overall cell model (top) and cross section (bottom).

2.3.2.3 The Periplasmic Space

Electron microscopy of thin slices through cells has shown that there is a low density gap between the inner phospholipid membrane and the peptidoglycan layer of the cell wall, known as the periplasmic space [29, 30, 31, 32]. In Gram negative bacteria this space is located between the inner and outer phospholipid membranes, encompassing the thin peptidoglycan layer. It is unclear exactly what this space is, but it would appear that it is largely formed of lipoteichoic acid in Gram positive bacteria.

2.3.2.4 Teichoic Acids (only Gram Positive)

There are two chief types of teichoic acids, those that are anchored to the lipid cytoplasmic membrane, which are called lipoteichoic acids, and those that are covalently bound to the peptidoglycan, called wall teichoic acids. These have a number of functions, including stabilising the membranes by attracting cations, assisting in cell morphogenesis [33] and growth regulation by limiting the binding of autolysins that cleave the glycosidic bonds in the cell wall [34].

2.3.2.5 Pili and Flagella

Many bacteria show external ‘hairs’, or pili (from the Latin pilus). These are protein structures that are believed to be used either for cell - cell interactions (conjugative pili) or for providing motile forces for the cell (type IV pili) [35]. Pili are generally located relatively homogeneously over the surface of the cell. Flagella (from the Latin meaning ‘whip’) are helical protein structures used primarily for propulsion by rotating like a corkscrew, either clockwise or anticlockwise [5]. These are often only located at the poles of rod shaped cells, but can also be found over the whole surface in other species.

2.3.2.6 The Gram Negative Outer Membrane

The outer membrane is a lipid bilayer but also contains lipopolysaccharide and membrane proteins, which allow diffusion of molecules through the outer membrane, and act as specific channels for different molecules. The lipopolysaccharide (LPS) has a purpose roughly equivalent to the teichoic acids of the Gram positive wall,

anchored by Lipid A. All cells that have these features have the core polysaccharide layer, known as a rough LPS layer, which are more hydrophobic than those which also have the O-polysaccharide section, known as a smooth LPS layer.

2.4 Growth and Division

Bacteria primarily divide through a process called binary fission, a form of asexual reproduction. This involves the DNA of the bacterium being duplicated, before it is pulled to opposing ends of the cell. A septum is then formed to separate the two halves of the parent cell to produce two separate, but identical, daughter cells. The exact method through which this occurs is slightly different for different species of bacteria.

The general process involves the fabrication of new peptidoglycan by the high molecular weight penicillin binding proteins [36], which is then assembled by an array of further cellular machinery [37]. Part of this process involves the breaking of bonds in the peptidoglycan chains by the cell wall hydrolases [38].

When bacteria are growing in a culture, with finite resources, the culture goes through a number of distinct growth phases. Initially there is a lag phase, as the cells adapt to their new environment, as they usually do not start to grow immediately. This is followed by the exponential phase, where each cell divides into two causing the number of cells in the culture to double every set amount of time (the time for this varies between different species). Thirdly there is a stationary phase, where there are no longer enough resources to maintain the exponential growth, creating an upper limit on the number of cells that the culture

can sustain. As the bacteria start to use up the remaining resources the culture can enter the death phase, where some of the cells die due to nutrient starvation and the numbers begin to decrease.

2.4.1 Cell Wall Hydrolases

The length of the peptidoglycan chains and the degree of crosslinking in the cell wall are controlled by a group of enzymes called the cell wall hydrolases which are used by the cell during growth and development [39]. Although these enzymes are often linked to the destruction of the cell wall, they are utilised by the cell in a tightly regulated form in order to manufacture new areas of cell wall during growth and division, and without them the cell would not survive. They are also believed to be used during the separation of the two daughter cells during division where the old cell wall attaching the two new cells is eaten away, allowing the two cells to separate.

2.4.2 Division in *Staphylococcus aureus*

Division in SA begins with the formation of the septum, before any changes to cell size or shape. The septum forms by growing inwards from the outer edges of the cell, like the closing of a camera aperture [40].

Once this septum is complete, the outer edges start to split, revealing the location of the septum on the outer edge of the cell. It is currently not well understood how the cell goes from being in this state to being two separated daughter cells, although it is believed that the cell does not make any new wall material once the

septum is complete. This means that the daughter cells have to go from being two connected hemispheres to being two separate spheres, effectively doubling in size, without the creation of any new material. This leads to the current theory that the septum should be formed of more dense material than the rest of the wall, as it has to expand to cover a much larger area.

In the study by Kailas *et al* [41] AFM was used to study live SA cells, and contact mode imaging was used to view cell growth and division. During this process it was possible to view the splitting of the outer cell wall along the division plane of the new septum, and view the separation of the two halves as the daughter cells were beginning to pull away from each other. During this separation, the splitting along the edge of the septum is seen to begin with small holes appearing along the division line, which goes on to involve quite a sudden burst as the daughter cells appear to be forced apart, leading to an idea that it could be related to a rise in pressure of the daughter cells, forcing the hemispheres apart and providing the force to expand them into full spheres.

The area at which the septum meets the edge of the cell wall forms a thick band of material called the ‘pie crust’. This is thought to be a marker for the start of formation of the septum [42], and leaves a visible mark on the cell even after the daughter has fully grown and is ready to start the next round of division, called a ‘rib’. These ribs are markers of the plane of division, and can be used to demonstrate the architecture of consecutive division planes in SA. When an SA cell divides, the new plane of division is always perpendicular to the previous one [41, 42, 43]. This feature, combined with the fact that the daughter cells often do not completely separate, but stay slightly attached together even when fully grown, lead to the characteristic grape cluster formation after which they are

named [44].

2.4.3 Division in *Bacillus subtilis*

In contrast to the above, division in BS occurs in a different order. In this case the cell elongates first, and it is thought that it does this by inserting patches of new cell wall into the existing wall along the cell's length, rather than adding it to the growing ends [45] (this patchy insertion also occurs in *E. coli* [46, 47]), a process called cell wall turnover. Once the cell has reached a suitable length the septum starts to grow inwards, but there is no constriction of the outer wall until the septum has fully formed. At this point the two daughter cells are sealed off from one another, although again they do not fully separate, leading to the potential for BS to form long chains of many cells after several rounds of division [48].

2.4.4 Septum Location

As the septum starts to grow inwards from a point around the edge of the inside of the cell wall, the cell must have some way of deciding where to start this growth. It is thought that the protein FtsZ (filamentous temperature sensitive protein Z) is responsible for this. This is a protein that, along with a group of others, forms a ring (the Z ring) around the circumference of the division site [49, 50], anchored to the inside of the membrane by the FtsA protein (without this binding protein, the Z rings do not form). Whilst many of the other proteins that gather here do not seem to be directly required for Z ring formation, a combined loss of certain ones can lead to 'synthetic lethality'. This is when two non lethal mutations combine to become lethal. The Z ring is composed of repeating subunits of FtsZ filaments,

arranged head to tail several times around the circumference of the division site of the cell. It is understood that this does not play any part in shaping the cell [51]. It has also been proposed that the Z ring contributes to the constrictive forces required to help the cell divide [52, 53], although it is not believed to be able to provide enough force on its own [54].

The exact structure of the Z ring, and the mechanism by which the ring is able to locate at the exact midpoint of the dividing cell, are also currently unknown. There are a small number of different models available [55, 56], demonstrating a range of FtsZ formations including short chains bundled together, and long chains wrapped several times around the cell circumference.

2.4.5 Cell Shape

Whilst the shape of SA is easily understandable, as a sphere is a stable shape when modelled as a homogeneous membrane full of fluid at high pressure, the shape of BS (and other non - spherical bacteria) is a little more complicated. When rod shaped cells are boiled and the sacculi extracted they maintain their rod shape, but there must be some kind of internal scaffold that directs the initial growth of the cell in this direction, defining the shape.

A number of protein structures have been proposed to explain this. In BS and other cylindrical rod shaped cells the protein MreB has been shown to play a part in maintaining the rod shape, as in mutants that do not produce it the cells lose their shape [37, 57]. It is currently believed that MreB forms a cytoskeletal structure inside the cell wall that helps the cell keep its shape [51, 58]. A number of publications [59, 51, 57, 60, 61] describe three different models for the formation of

this MreB cytoskeleton, with hoops, a spiral and an internal scaffold proposed.

2.5 Osmotic Stress Response

SA is part of a group of bacteria called salt tolerant non - halophiles. This means that it is able to grow at abnormally high salt concentrations (or very low water activity, a_w) [62]. When a cell is exposed to a high exterior salt concentration, the difference in concentration between the outside and the inside of the cell creates an osmotic pressure across the membrane, as water diffuses out of the cell due to the concentration gradient. Under normal circumstances this would dehydrate the cell, reducing its turgor pressure to a point that the cell could no longer function. However SA, along with other halotolerant bacteria, have mechanisms that can be used to restore turgor pressure in these situations, allowing them to survive.

An early study on the subject found that the cells had higher quantities of solutes when grown in low water activity [63]. Further studies on the subject have identified the key components, called compatible solutes [64]; Choline, Glycine Betaine, Proline and Taurine [65]. These act as osmoprotectants, protecting the cell against the high salt concentration. Supplementation of these in a high salt medium was found to vastly increase the growth rate of SA [10]. It is believed that cells are able to take these solutes up from the surrounding medium, should they be available, by two different transport systems [66]. SA cells grown in the presence of high salt concentrations have also been shown to be larger than those grown in normal conditions, despite growing at a much slower rate, and were found to have shortened interpeptide bridges in the cell wall. Addition of compatible solutes into the high salt growth medium restored the growth of these cells to more regular

sizes [67].

Although these solutes protect the cells against the high salt concentration, when cells are suddenly exposed to this it is still understood that they suffer from the initial water loss due to the osmotic pressure across the membrane, but that the solutes are then accumulated, from the surrounding medium or formed within the cell, which allows the cell to restore its turgor pressure and survive [68]. This has been studied recently using fluorescently tagged *E. coli* cells, which demonstrated an initial shrinkage cell volume, indicating the time where the water leaves the cell, followed by a slower and more complex recovery procedure [69].

2.6 β -lactam Antibiotics

β -lactam antibiotics are a group of drugs that kill bacteria by interacting with penicillin binding proteins (PBPs) on the cell surface. These proteins are understood to play a significant part in the manufacture and regulation of cell walls and division [70]. Therefore the drug is believed to inhibit the successful division of cells by blocking the completion of the manufacture of new cell wall and septa (PBPs are found in large quantities at the division site [71]), leading to cell lysis. Figure 2.3 below shows the structure of oxacillin, the β -lactam used in this study, with the β -lactam ring structure highlighted.

The exact mode of action of these drugs is still a little unclear, however it is believed that they bind to the PBPs of a dividing cell, by containing a structure (the β -lactam ring) that is very similar to the terminal amino acid residues of the peptide subunits of the peptidoglycan layer. The β -lactam ring binds irreversibly

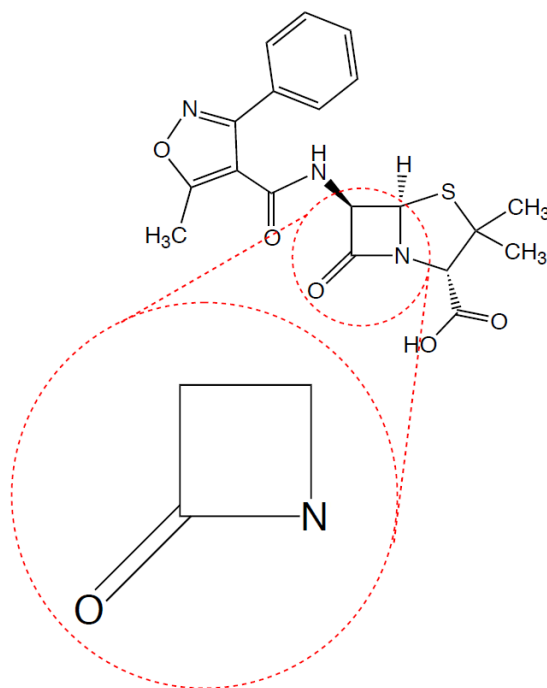


Figure 2.3: The structure of oxacillin highlighting the β -lactam ring.

to the PBP active site, preventing the required crosslinking of the peptidoglycan layer. Without a properly formed cell wall, the bacteria cannot form an intact septum during division, or add to their currently existing wall during growth, causing the cell to eventually lyse.

2.7 Industrial Application

A better understanding of the structure, growth and division of bacteria has a large industrial interest. Bacteria are used in a wide range of industrial applications. These include those where bacteria are vital to the process, including brewing, waste processing and food manufacture; and those where bacteria are unwanted and need to be removed, such as medical processes. Their ability to uptake, replicate and use DNA can also be exploited, for example to produce insulin.

2.8 Conclusion

Whilst there has been a great deal of successful research into certain aspects of the bacterial cell, such as the genetics and the biochemistry, there is still a wide range of unsolved issues relating to the mechanical properties and the structure of the cells, and particularly the cell wall.

To probe the mechanical properties of live cells, the atomic force microscope is ideal. It can be used in a liquid environment, allowing cells to be maintained in their growth medium or a suitable buffer, and the probe can be used to indent the cell surface in order to measure the mechanical response of the cell. The following chapter will introduce the AFM in more detail.

3 | Atomic Force Microscopy

3.1 Introduction

The Atomic Force Microscope (AFM) was invented by Binnig *et al* in 1986 [72]. A modern day AFM is composed of four main components: a cantilever with a sharp tip, an optical deflection system consisting of a laser and photodetector, a piezoelectric scanner, and an electrical feedback system.

The cantilevers are usually made of either silicon or silicon nitride, fixed at the base to the chip which is held in place by a holder, the design of which varies between different microscopes. As the base of the cantilever is therefore fixed in place, it can be used to measure attractive or repulsive forces between the tip and a sample by measuring the deflection of the tip end of the cantilever towards or away from the surface. AFM cantilevers can be thought of as springs, and therefore can be described by Hooke's Law at small deflections: $F = -kx$; where $x = -aV$. Here a is the deflection sensitivity of the cantilever and V is the cantilever deflection, measured in Volts.

In most modern AFMs cantilever deflection is measured by the optical deflection

system. A laser spot is focused onto the back of the cantilever in such a way that it reflects onto a position sensitive 4-quadrant photodetector. As the force between the tip and the sample changes, the cantilever deflection changes and so the position of the laser spot on the photodetector moves. This set up is sensitive enough that it can detect deflections as small as 10^{-4} Å. The system uses a detector with 4 quadrants to allow the deflection of the cantilever to be measured in two different directions, both the vertical deflection and the lateral twisting of the cantilever.

The piezoelectric scanner is mounted either in the AFM head or within the sample stage, depending on the microscope's design. This allows precise movement of the tip relative to the sample in three dimensions. This is of particular use with the feedback loop, which allows the AFM to not only measure tip - sample forces, but also to regulate them. This process allows very soft samples to be imaged by keeping the force applied to the surface as low as possible.

The feedback loop works to keep the deflection of the cantilever constant, at a pre-set value. During a measurement the cantilever deflection is constantly measured, and any changes to this trigger a response that changes the voltage on the piezo, changing the height of the tip (or the sample) to keep the deflection constant.

With this basic set up, the AFM can be used in a number of different ways for many different applications, as will be discussed in the following sections. Figure 3.1 shows the basic components of the AFM.

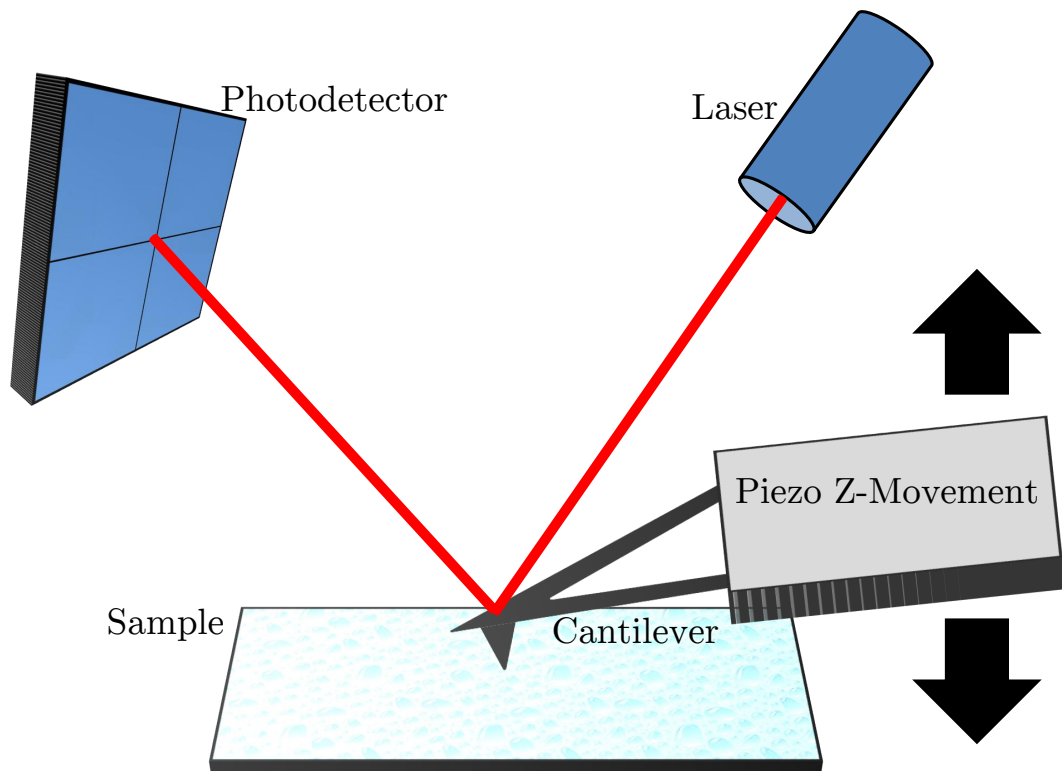


Figure 3.1: Diagram showing the basic components of the AFM.

3.2 Imaging

In this section the technique through which the AFM tip is scanned over the surface will be discussed for each of the main imaging modes. Details on how the feedback loop is utilised in order to keep tip - sample forces constant will also be covered, along with the reasons that samples are required to be strongly immobilised for study by AFM.

3.2.1 Feedback Controls and Imaging Modes

3.2.1.1 Contact Mode

The most basic imaging mode is contact mode. In this case the tip is scanned over the surface, and the cantilever deflection measured. This can be done with no feedback, just scanning laterally and measuring the deflection signal, which is known as ‘constant height’ imaging. The problem with this is that the higher parts of the sample will experience a much larger force than the lower parts, as the force applied by the cantilever is proportional to the deflection.

The feedback loop constantly adjusts the height of the tip relative to the sample as the tip moves over higher and lower parts of the sample, causing all parts of the sample to experience approximately the same force.

There are two controls that adjust how the feedback loop responds, known as the integral and proportional gains. These controls adjust how quickly the feedback loop responds to adjust the measured cantilever deflection to the pre-set value (the ‘setpoint’), which need to be adjusted and optimised for individual imaging conditions, depending chiefly on sample topography and scan speed. As the setpoint is a measured deflection of the cantilever, a lower setpoint provides a lower force to the sample.

The proportional gain works by calculating the difference between the measured deflection of the cantilever and the desired value, selected by the setpoint. This is multiplied by a constant (the user inputted value) to produce the output signal. This, therefore, only reacts to the surface directly under the tip, so can only be used for relatively flat surfaces imaged at low scan speeds.

The integral gain calculates the integral of the difference between measured and desired deflection over time, and again multiplies this with a user inputted constant. This reacts much slower than the proportional gain, allowing correction on rougher surfaces and higher scan speeds. For both gain controls, a higher constant value leads to a faster response from the feedback loop.

As the feedback loop adjusts the height of the tip, the time it takes to respond to deflections of the cantilever means that at surface features that cause large deflections the feedback cannot react fast enough to prevent measurable deflections. It is these slight errors in the feedback that are used to create the vertical deflection image, so the image is created from the deflection of the cantilever away from the target setpoint, before the feedback loop has had time to correct the deflection back to the desired value. Altering the gains to increase or decrease the response time of the feedback loop will decrease or increase the amount of information on this image, respectively. A perfect feedback loop would react instantly, creating a perfectly flat deflection image, but in reality this is not possible.

With this feedback system in place, all parts of the sample should experience the same applied force, so this is now known as ‘constant force’ imaging, rather than constant height. In these cases where the deflection of the cantilever is used to set the feedback, is known as contact mode imaging.

The biggest concern when using contact mode, particularly with soft biological samples, is the large lateral force that the tip applies to the sample. This can be a problem in some situations, damaging very soft samples and dislodging cells (for example) that are not well immobilised. In other situations though, this can be exploited, such as when the friction between the tip and the sample is of interest, which could reveal information about different chemical properties within a sample

that would otherwise not be visible.

Although the lateral forces can be high in this mode, the vertical force can be controlled through the setpoint, so compression of the sample can be limited.

3.2.1.2 Dynamic Modes

It is also possible to scan the AFM in dynamic modes, where the cantilever is oscillated close to its resonant frequency, and this oscillation is measured. In air the cantilever is usually driven directly, however in liquid this is not possible due to the damping effect of the liquid, so in these cases the cantilever is commonly driven acoustically through the liquid.

In dynamic modes, the setpoint is set as a certain amplitude, frequency or force, rather than the deflection used in contact mode. The feedback loop then acts to adjust the tip height to match this preset value.

When a sample is imaged in dynamic mode, the scan produces height and error signal images, the same as for contact mode imaging. However in this mode it also produces a phase image, which is the difference between the drive signal phase and the response phase of the cantilever. This phase image can reveal information about the mechanics of the sample, such as stiffness and adhesion, which would not be seen in the other images [73].

There are three main different types of dynamic modes, the difference between them being how much the tip interacts with the sample surface, and what is used as the feedback source. The most common of these is often referred to as intermittent contact mode, where the tip is oscillated just above the surface so

that it only interacts at the very bottom of its oscillation. The amplitude of the resonating tip is used as the feedback for this mode, so it is also known as amplitude modulation mode. This provides much lower lateral forces than contact mode, since the tip only touches the sample very briefly and doesn't move laterally whilst in contact. Because the setpoint is proportional to the amplitude, a higher setpoint means less damping by the sample and so gives lower imaging forces.

The two other modes are not used as often. The first of these is known as frequency modulation, where the tip is oscillated close to the sample surface without actually touching it, using the frequency of the oscillating tip for the feedback (frequency modulation mode). This is particularly difficult to do since there is a possibility of the tip jumping into contact with the surface, meaning that very stiff cantilevers often have to be used. In ambient conditions the capillary forces between the tip and the sample make this technique very tough to control. The benefit though is that as the tip never touches the sample, it should not cause any damage.

The final mode is known as force modulation mode, where the tip is oscillated at the sample surface but never breaks contact during its oscillation, so lies somewhere between contact mode and dynamic mode, using the force on the tip for the feedback. This is also not used very often due to the difficulties of operation and the likeliness of damage to soft samples.

Figure 3.2 shows a cartoon of the four main imaging modes of the AFM, showing the tip movement in relation to the sample surface.

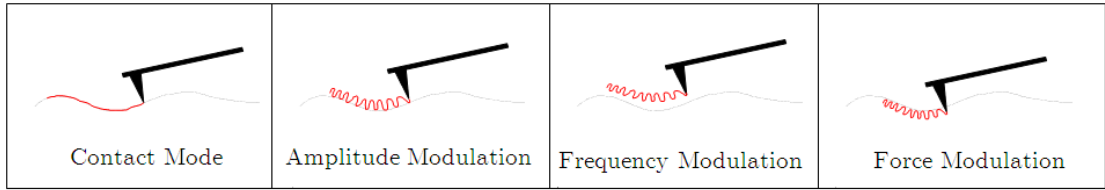


Figure 3.2: Diagram showing the four principal imaging modes of the AFM.

3.2.2 Imaging Modes in Terms of Forces

These imaging modes can also be viewed in terms of the forces that the tip applies to the sample. Interactions between two objects change as they get closer to one another. At long ranges van der Waals and capillary forces provide an attraction, but at short range contact between the two objects provides a strong repulsive force as the objects' electron orbitals start to overlap. This is a very simplified view and the situation becomes much more complex in reality.

In general, the forces between two objects can be visualised as in Figure 3.3, showing the force between the tip and the sample against the distance between the two. The imaging modes can then be seen in terms of the forces and distances between the tip and the sample. This shows attraction as negative force, and repulsion as positive force, as this is what the tip will experience.

3.2.3 Immobilisation of Samples

As the tip exerts a lateral force on the sample, the sample must be prepared suitably to deal with this. Where the sample is biological, particularly when individual cells are to be studied such as the ones in the work presented here,

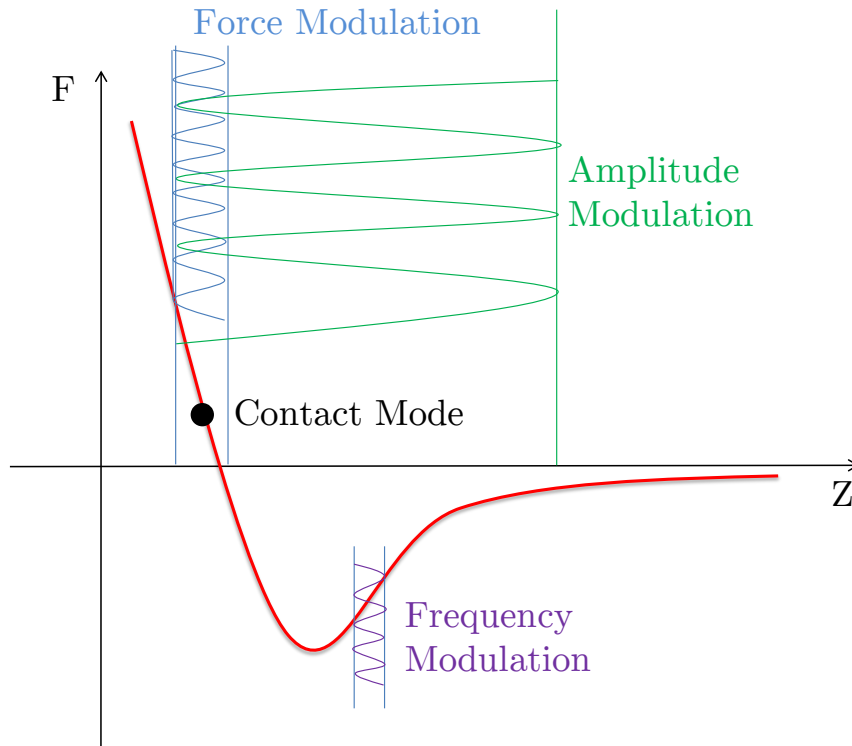


Figure 3.3: Graph showing the imaging modes of the AFM in terms of the force exerted on the tip by the sample. F = Force on tip, Z = tip height above sample.

the cells must be immobilised on the surface to prevent them being kicked off the surface by the scanning tip. There are a range of ways to do this, with relevant pros and cons for each.

The commonly used immobilisation techniques for bacterial cells can be grouped into two main types, chemical fixation and mechanical entrapment. Chemical fixation involves binding the cells to the surface by covalent bonds via a surface coating of EDC-NHS or glutaraldehyde, or the use of an adhesive protein [74]. This anchors the cells strongly to the surface, but it is possible that the process could affect the cells or the properties of their cell walls due to the binding activity.

Mechanical entrapment is a good alternative to the chemical techniques. Although

it can be more difficult to immobilise cells in this way, there is no alteration to the cell or the cell wall as there is no interaction or binding, the cells are simply held in place by edges of wells or similar. This can be done using a gelatin layer [75], wells carved into a PDMS surface [76, 77], trapping the cells in the pores of a suitably sized filter [42, 78, 79], a porous polymer membrane [80] or trapping the cells in wells etched into silicon wafers [41]. The effect of patterning the surface on the ease of bacterial cell detachment during scanning has itself been investigated, as shown by Whitehead *et al* [81]. In this study a tip was scanned over a cell covered surface repeatedly with higher and higher imaging forces, observing the detachment of cells with each successive scan.

3.2.4 AFM Imaging of Bacterial Samples

The AFM is an excellent tool for the study of bacteria, due to its high resolution and its ability to be used in liquid, allowing the study of cells in their natural environment. This section will give a brief summary of some examples of this from the literature, further to the immobilisation papers referenced above.

This combination of high resolution and liquid environments allows the study of membranes, and the proteins embedded in them, without causing damage to their natural form by having to dry them out [82]. It is also possible to achieve high resolution images of the cell wall of bacteria, whilst they are alive, leading to clues about the formation and structure of the cell wall [83]. Details of the structure and components of the photosynthetic membrane of *Rhodobacter sphaeroides* have also been studied by high resolution AFM [84], similarly details of the cell surface of *Streptomyces coelicolor* [85], along with magnetosomes extracted

from the magnetotactic bacteria *Magnetospirillum magneticum* [86].

As rod shaped, self motile bacteria are difficult to immobilise for AFM measurements in liquid, some studies on them are currently performed in air [87, 88] although this can cause shrinkage of the cells as they dry out [89]. Scanning in air allows the imaging of extracellular structures such as pili and flagella [88, 90], which tend to move about and avoid the tip in liquid [75].

As the cells can be kept in their growth media, the AFM can also study live processes in real time, as shown by the cell division ‘filmed’ by Kailas *et al* [41] and also observed by Touhami *et al* [40], and the effects of added extras to the media, such as adhesion modifying chemicals [91], Lysozyme (an enzyme that damages bacterial cell walls by catalysing hydrolysis of glycosidic bonds) [92], Lysostaphin (an enzyme that cleaves peptidoglycan in SA) [93], Cefodizime (an antibiotic) [70] and glutaraldehyde [94].

Although this is becoming more common, many biological processes happen much too fast for the AFM to be able to detect. Recent advances in AFM technology have allowed much faster scanning, so that now processes such as those in photo-activated bacteriorhodopsin [95] and the kinetics of antimicrobial peptide activity [96] can not be followed, but there is still some way to go in this field.

AFM is often combined with fluorescence microscopy, allowing the AFM to target cells that have been fluorescently tagged for certain properties [33, 97, 98].

3.3 Force Spectroscopy

Force spectroscopy is used when the mechanical properties of the surface are of interest [99]. In this mode, the piezo moves the tip down towards the surface until the cantilever has made contact and deflected by a certain amount (the setpoint), at which point the piezo moves the tip away from the surface again. The deflection of the cantilever is monitored throughout this process, building up a force curve, as shown in Figure 3.3. In these force curves, the height position is usually shown on the x axis and the cantilever deflection on the y.

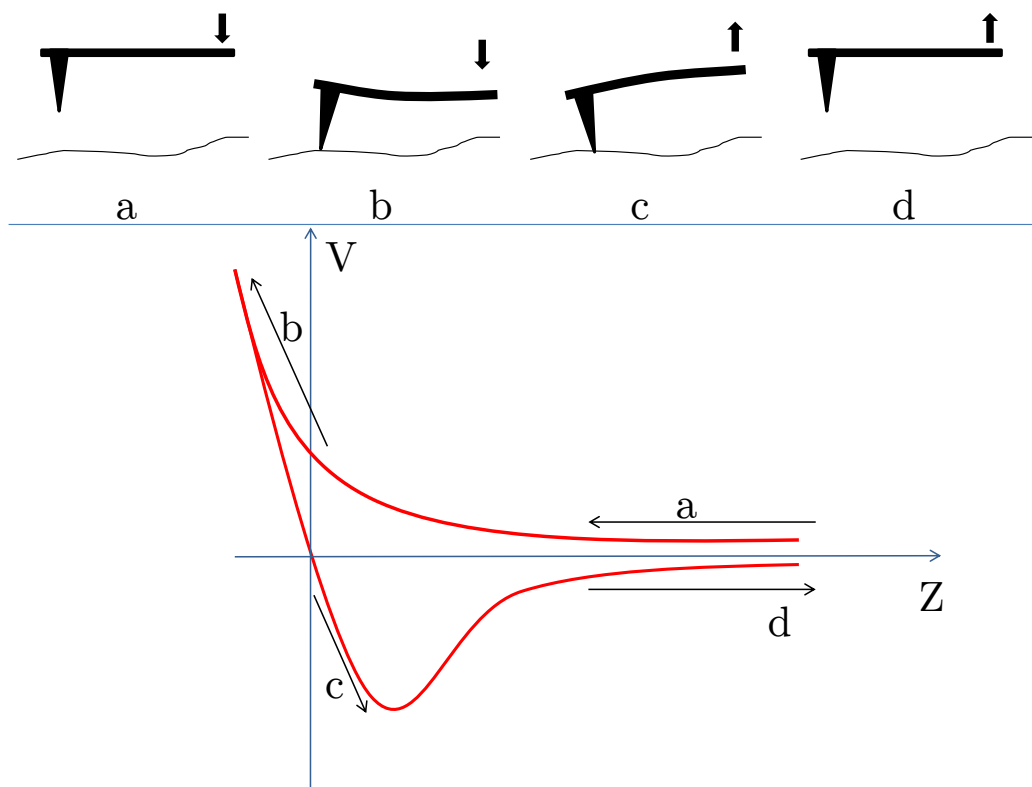


Figure 3.4: Showing the process involved in creating an individual force curve; Top: Cantilever and piezo movement; Bottom: Force curve produced, showing deflection (Volts) against Z - piezo height.

The general shape of the force curve will be similar for all samples, and can be explained as follows. Initially the cantilever is moved towards the surface by the piezo, as shown during stage 'a'. The tip then gets close to the surface and starts to be repelled (for a hard surface in air this may be preceded by a jump - to - contact attraction, due to van der Waals and capillary forces). The piezo continues to lower the cantilever until the deflection due to the repulsion from the surface reaches the setpoint, as shown in stage 'b'. The gradient of this part of the force curve is directly related to the stiffness of the surface, from which values can be extracted, as explained below. At this point the piezo reverses direction and pulls the cantilever away from the surface. There is often a hysteresis between the approach and retract parts of the force curve due to the surface under examination not being perfectly elastic. The force curve also often extends into negative forces as shown at point 'c', as the tip remains stuck to the surface, bending downwards until the force is great enough to overcome the adhesion force between the tip and the sample. The piezo then moves the cantilever away to a pre set distance, shown by stage 'd'.

The raw data taken from a force curve will plot the measurements as a cantilever deflection measured in Volts by the photodetector against the piezo movement, as a distance. To get this into a more useful form, the cantilever properties must be calibrated for each individual experiment.

3.3.1 Cantilever Calibration

There are two parts to the calibration required to analyse force curves, firstly the deflection of the cantilever and secondly the height need to be calibrated. The

cantilever deflection is used to convert the measured photodetector signal into a quantitative force measurement. This is done in two stages, initially calibrating the distance that the cantilever deflects for a given photodetector measurement (known as the optical lever sensitivity) and secondly the spring constant of the cantilever.

The sensitivity is measured by indenting a hard surface in air. This gives an experiment where the contact part of the curve is perfectly linear, and the hard surface is not indented into, allowing a conversion from Volts into nanometers. This is most commonly performed at the end of an experiment as the hard surface is reasonably likely to damage the tip.

The most common way to measure the spring constant of a cantilever is by the thermal noise method [100, 101]. In this case the cantilever is held fixed at the base, and the spectrum of the noise from thermal vibrations is plotted. The first resonant peak is fitted using a simple harmonic oscillator fit which gives a value for the spring constant (other resonances can be used provided a suitable correction factor is used within the fitting). The only correction applied here was for the ten degree tilt of the cantilever, applied automatically by the JPK software, as described by Hutton [102]. Further corrections, including that for the v-shape of the cantilever as described by Stark *et al* [103], were not applied. This was largely due to the software that was used (JPK Data Processing software) not having the option to perform these corrections, and the time required to examine the cantilevers with electron microscopy to check dimensions of each particular tip, as they are often not identical. The thermal noise method is the most common technique due to its use in air or liquid, during, before or after an experiment, with a fast and automated software analysis.

The force curves from this experiment can now be plotted in terms of force (N) against the tip - sample separation (m), allowing a direct measurement of the properties of the surface. This is done by fitting the gradient of the contact part of the curve, usually on the approach, to yield a value of stiffness in terms of Nm^{-1} .

3.3.2 Force Mapping

Force mapping is a technique where an image is created by taking a force curve at each pixel. The image can then be constructed by showing whichever property of the force curve the user desires, most commonly sample surface height, measured stiffness and adhesion. Each pixel is set to part of a colour scale depending on its value, and the image is formed. This is a very useful technique for visualising the difference in properties across a sample, for example areas on a cell surface that may be shown to have different mechanical properties.

The force curves in a force map are taken in the same way as for individual force curves described above, and can therefore be individually analysed, so the force maps can be used to both visualise the mechanics of the surface, and also to extract measurements from required areas.

3.3.3 Force Measurements of Bacterial Samples

Using the AFM to measure forces on biological samples has attracted a large amount of attention in the last 10 to 15 years. Two main topic areas are included in this, firstly measuring the mechanical stiffness of the samples, and secondly

measuring the adhesion forces on the retraction part of the force curve.

Examples of stiffness measurements include data taken on different mutants of *E. coli* expressing different surface proteins [104], fibrillated and non fibrillated *Streptococcus salivarius* [105], a range of bacteria in direct comparison [106], the external surface of spores of *Clostridium tyrobutyricum* [107], Manin-Darby canine kidney (MDCK) cells [108], and Leukaemia cells [109]. Vadillo-Rodriguez *et al* used colloidal probes and an indentation force of 6 nN combined with a dwell to measure the viscoelasticity of rod shaped bacteria [110]. This paper presents a model for the viscoelastic behaviour of the cells studied in which a spring is connected in series with a combination of a spring and dashpot in parallel, in order to accurately model both the instantaneous and delayed components of the cells' elastic response. This study also showed a significant difference in the amount of creep deformation measured on Gram positive and negative cells, with only a very small change observed on the thicker walled Gram positive species. Force mapping has also been used to display properties of cells over their surface [111, 112].

As with the imaging described earlier, force measurements taken over time can reveal information about time dependant factors, a recent example of which used the addition of antibiotics to induce a change in the bacteria's mechanical properties [113], in which the authors saw a reduction in the measured stiffness of their cells when under the influence of ampicillin.

Further to these stiffness measurements, the AFM is a useful tool to measure adhesion forces as the tip is retracted from the surface. This is usually done with a modified tip, to target specific interactions, and displayed on a force map to show the areas with different adhesive properties. Examples of this include using hydrophobic tips to measure the hydrophobicity of different areas of the cell

surface [114, 115], chemically modified tips with COOH - terminations to study the surface charge distributions [116], tips coated with polysaccharide targeting molecules (lectins) to examine the surface polysaccharide distribution [117], tips coated with antibodies and adhesins targeted at specific surface proteins [118, 119], and by attaching a single, live cell to the cantilever to study cell - cell interaction forces [120].

3.4 AFM Artefacts

Due to the nature of AFM, as the image is constructed by the movement of a sharp tip across the sample surface, it is not uncommon for artefacts to appear on the image. An artefact is anything that appears on the image that should not be there.

One common artefact is due to tip shape. These are most commonly formed by features on the surface that are sharper than the dimensions of the tip, such as steep ridges and very narrow features. In these cases it is usually because the edge of the tip makes contact with the feature before the end of the tip, as shown in Figure 3.5.

The best way to avoid getting artefacts such as these on an image is to use a very sharp tip with a very high aspect ratio, like the lower image in Figure 3.5. The problem with very sharp tips such as these is durability, due to their shape these tips are extremely fragile and are very easily snapped off at some point along their length.

The choice of tip to be used is usually therefore a trade off between sharpness and

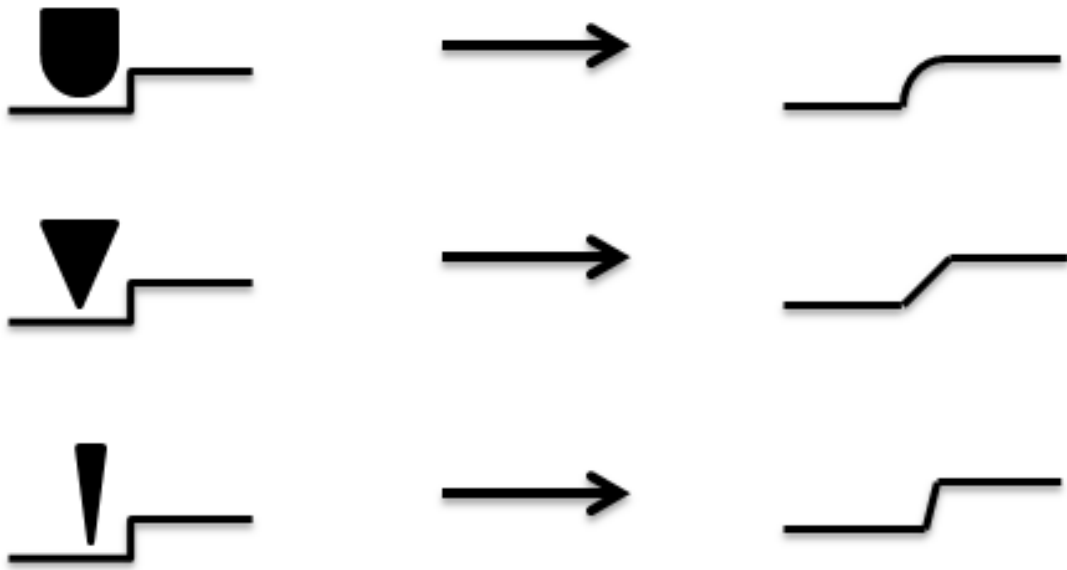


Figure 3.5: Image showing how the profile of the tip can create artefacts on sharp ridges.

durability, although it also depends on the sample being scanned. Using a super sharp tip on a very soft sample such as a biological membrane is not advisable as the tip will be likely to cut into the surface.

Other ways to reduce the presence of these artefacts include reducing the scan speed and altering the gain settings, allowing the feedback loop more time to adjust to changes in height of the sample.

Other artefacts can be created by having either damaged or contaminated tips; these both result in tips that do not have a regular shape, or perhaps do not have a sharp point on the end. These are commonly seen as repeated identical features appearing across the surface where the irregular part of the tip has interacted with the surface. Loosely bound contamination on the tip can also lead to streaks and lines appearing across the image as the contamination is moved around by the scanning movement of the tip.

Examples of artefacts and issues due to the force of the tip on the cell seen during imaging can be found in the literature. Examples of this include the grooves that Boonaert *et al* observed along the scanning direction on the surface of *Lactococcus lactis* cells, caused by the force exerted on the cells by the scanning tip [121]. Artefacts caused by the edges of the tip interacting with the sample rather than just the end of the tip as desired are discussed by Velegol *et al* [122] and Alsteens *et al* [123]. Other artefacts, caused by the tip radius being larger than the features being imaged, are shown by Bustamante and Keller [124].

3.5 Why use AFM for Studying Microbes?

AFM has many advantages over other commonly used microscopes. Traditional optical microscopy has its limitations when used in the microbiology field, due to the resolution limit provided by the wavelength of light, and the requirement for samples to be relatively thin and non opaque to allow for the transmission of light through the sample. These issues are all overcome by the AFM, which can be used to gain a much greater resolution and does not require the transit of light through the sample.

The electron microscope overcomes some of the limitations provided by optical microscopy, due to the wavelength of electrons being much lower than visible light, giving much better resolution. There are two types of electron microscope commonly in use for the study of bacteria, the transmission electron microscope (TEM) and the scanning electron microscope (SEM). Whilst both of these techniques can provide suitable resolution for studying on the nanoscale, they both have issues which would render them unsuitable for use in this study.

The TEM requires that samples are extremely thin, much thinner than an individual bacterial cell. To prepare samples for TEM thin slices of the cells have to be taken, meaning that whole cells cannot be imaged.

The SEM does not need the samples to be as thin, but it does require that the samples are electrically conductive, which usually requires coating the sample in a thin layer of gold, or similar. This therefore also cannot image live cells.

The AFM has many advantages over these other types of microscopy, the greatest of which is its ability to image live cells, in a liquid environment. This keeps the cells alive, and indeed allows active cellular processes to be imaged in real time [41]. Aside from the imaging, the AFM can also be used to provide mechanical information on the sample, as described above, which the other types of microscopy cannot provide.

In terms of measuring the mechanical properties of cells, there are other techniques available. These include rheology, tracking an oscillatory magnetic sphere attached to a cell, and optically studying a cell during deformation (for example by flow or micropipette aspiration). However, since AFM allows the user to simultaneously image and measure the cell surface at high resolution, this was the method of choice for this study.

4 | Materials and Methods

4.1 Media

All media was prepared in deionised water and autoclaved at 121 °C for 20 minutes.

The growth media for SA is Brain Heart Infusion Broth (Sigma - Aldrich), dissolved into deionised water at a concentration of 37 g/l. For solid medium 23 g/l nutrient agar (Sigma - Aldrich) was added. For BHI containing higher salt concentrations NaCl was also added at a concentration of 50.4 g/l, calculated from the mass needed for 1M NaCl (55.4 g/l) minus the mass of NaCl already in BHI (5 g/l). Other NaCl concentrations were also used, by dissolving the corresponding quantity of NaCl into the medium required, by the same technique. D-Sorbitol (Sigma - Aldrich, C₆H₁₄O₆) was also used in place of the NaCl, dissolved into BHI to the required concentration. Oxacillin (Sigma - Aldrich) was used as an antibiotic agent in growth medium, added at a concentration of 5 mg/l to both BHI and PBS (see below).

The growth medium for BS is Nutrient Broth No. 3 (Sigma - Aldrich); dissolved

into deionised water at a concentration of 13 g/l. As for BHI, for solid medium 23 g/l nutrient agar (Sigma - Aldrich) was added.

Phosphate Buffered Saline (PBS) was used as an imaging buffer when active processes were not required. This is composed of NaCl, 8g/l; KCl, 0.2 g/l; Na₂HPO₄, 1.4 g/l; NaH₂PO₄, 0.2 g/l. Supplied as a dispersible tablet by Sigma - Aldrich. A Potassium Phosphate Buffer was created from KCl, 0.2 g/l; Na₂HPO₄, 1.4 g/l; NaH₂PO₄, 0.2 g/l. This was made from constituent parts as an NaCl-free version of PBS. HEPES buffer (4-(2-Hydroxyethyl)piperazine-1-ethanesulfonic acid; C₈H₁₈N₂O₄S) was also used as a buffer for some AFM experiments, as supplied by Sigma-Aldrich.

Cell death was performed with a detergent called Sodium Dodecyl Sulphate (SDS, CH₃(CH₂)₁₁OSO₃Na, Sigma - Aldrich); dissolved into PBS at 0.01%, 0.1%, 1% and 5% by volume. Active cell processes were blocked, whilst keeping the cells alive, with the addition of 100 µg/ml of a bacteriostatic antimicrobial substance known as chloramphenicol (2,2-dichloro-N-[1,3-dihydroxy-1-(4-nitrophenyl)propan-2-yl]acetamide; C₁₁H₁₂Cl₂N₂O₅, Sigma - Aldrich).

4.2 Bacterial Strains

4.2.1 *Staphylococcus aureus* (SA)

Seven strains of SA were used in total. For the most part, and unless otherwise stated, the common laboratory strain *SH1000* was used. The other strains used were the mutants *sagB*, the complemented version of the same strain (labelled

as *sagB* C), and four "triples", so called as they each have 3 cell wall hydrolase enzymes removed. *sagB* and the triples have more heavily crosslinked cell wall polymers, due to the removal of up to 3 of the 4 enzymes that control the hydrolysis of peptidoglycan chains in the cell wall. Like many other mutant strains, these also have engineered antibiotic resistance. This allows growth in media with added antibiotic, killing off any contamination from regular strains, ensuring that the resulting culture is made only of the particular cells of interest. All strains use BHI as the growth medium, with the addition of the relevant antibiotics for regular and complemented *sagB*. The triple strains were not grown in the presence of antibiotic since so many are required that the growth of the cells is retarded beyond a workable level. The antibiotics used were neomycin and kanamycin for *sagB* and the same two plus tetracycline for the complemented strain.

4.2.2 *Bacillus subtilis* (BS)

Only one strain of BS has been used, again a common laboratory strain, named *BS168*. This was grown in Nutrient Broth (NB) growth medium.

4.3 Cell Culture Methods

Unless otherwise stated, the culture method was the same for each different strain used. Stocks of each strain were kept long term at -80 °C. All cultures were grown in duplicate, so that if one culture failed there was always a backup.

4.3.1 Agar Plates

Agar plates were prepared by melting the relevant growth medium with agar and dispensing into Petri dishes, to a depth of approximately 5 mm, and allowing to cool and solidify. A sterile wire loop was used to transfer cells from the -80 °C stock to the agar plate, spreading the cells in a streaked pattern. This spreads the cells out to suitable extent that individual colonies do not overlap once grown. As each colony on a grown plate originates from a single parent cell, this is the best way to maximise the possibility of ending with a genetically identical sample set. Plates were incubated overnight at 37 °C, and the resulting cultures were kept at 4 °C for up to 1 month.

4.3.2 Overnight Culture

Overnight liquid cultures were made by using a sterile metal loop to transfer a single colony from an agar plate culture into a sterile universal tube filled with 10 ml of the relevant growth medium (plus antibiotic if growing mutant strain) and incubated overnight, on a rotary shaker set to 250 rpm, at 37 °C. The rotary shaker kept cells suspended in the medium and prevented them settling together at the base of the tube, which would limit access to nutrients, damaging both growth and survival rates.

4.3.3 Growth to Exponential Phase

After the overnight incubation, the culture was always at stationary phase. This meant that a point had been reached where the culture was supporting the maxi-

imum quantity of viable cells, so that no more growth was possible. Cells were either harvested at this point, or grown to exponential phase.

The advantages of using cells in exponential phase is that the cells are still in a rapid growth phase, so features related to cell growth and division will be visible on a large proportion of the sample.

The correct stage of growth was calculated by plotting growth curves for both species of bacteria that were to be used. In order to acquire the desired initial starting point, the optical density of the overnight culture was determined by measuring the optical density of 1 ml of the sample at a wavelength of 600 nm (OD_{600}) using a spectrophotometer. The new culture was to be grown in 50 ml conical flasks, so the required initial OD_{600} (0.05) was multiplied by 50 (as the OD_{600} measurements were taken on 1 ml), and divided by the reading gained from the overnight culture. This calculation gave a volume to be added to 50 ml of growth media in the conical flasks, which were then incubated as for the overnight.

At time points of 30 minutes, three samples of 1 ml of each of the cultures was extracted and the OD_{600} measured on each, so that the OD_{600} could be plotted as a function of time. Three samples were taken so that multiple curves could be plotted to check for consistency. These curves are usually plotted with the logarithm of the optical density against time, so that the exponential growth phase is displayed as a straight line. This allows a point towards the centre of this phase to be easily chosen as the time to harvest the cells. These growth curves are shown in Figure 4.1.

From these curves, harvest times of 2.5 and 3.5 hours for SA and BS respectively

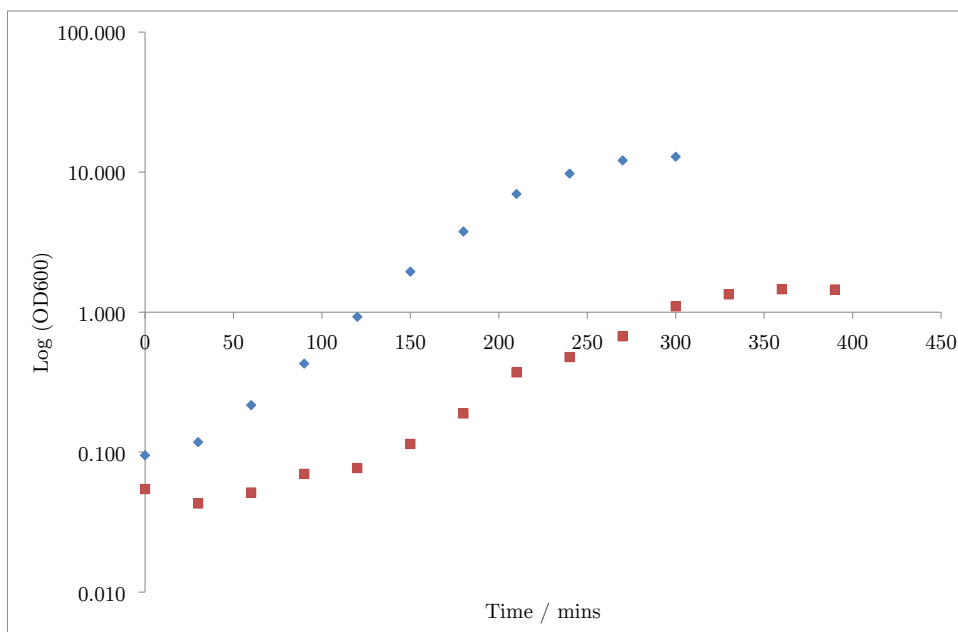


Figure 4.1: Growth curves for SA (blue diamonds) and BS (red squares).

were selected. From an overnight culture cells were now able to be grown to mid exponential phase, by incubation for this amount of time. The preparation for this culture is as for the conical flasks in the growth curve experiment, except that 10 ml universal tubes were used instead of the larger 50 ml flasks. After this incubation the cultures gave an OD_{600} of approximately 0.8, as required for mid exponential phase.

4.3.4 Harvesting Cells for AFM

Once the culture had reached the required optical density the cells were ready to be harvested. This was performed by centrifuging 1 ml eppendorfs of the culture for 3 minutes at 13,200 rpm. This process caused the cells to drop out of suspension

and form into a pellet at the base of the tube. The supernatant was then pipetted off and discarded, and the tube filled with 1 ml PBS, resuspending the cells. This process was repeated 3 more times to remove all growth media from the sample. At this stage the cells were ready to be deposited onto the imaging substrate.

4.4 Cell Death

Some of the experiments performed during this study required the use of dead cells; the detergent SDS was used, which dissolves away the cell membrane, allowing the majority of the cell contents to evacuate, but leaving the cell wall intact.

To determine the concentration of SDS required, a plate assay was performed. In this case, a culture was grown to the required OD_{600} , as normal. Cells were then incubated for a further 1 hour in a solution of PBS containing SDS in the following concentrations: 0% (pure PBS, control), 0.01%, 0.1%, 1% and 5%.

After the second incubation, the cultures were diluted into pure PBS in consecutive 10% dilutions, giving sample concentrations of 10%, 1%, 0.1%, 0.01% and 0.001%. Everything was then plated up onto growth medium with agar, with a separate plate for each concentration of SDS, each split into 5 segments, one for each dilution of the sample. Three 10 μ l droplets were placed into each corresponding segment. The plates were then incubated overnight, allowing any cells that had not been killed by the SDS incubation stage to establish colonies on the plates.

The finished plates are shown in Figure 4.2, where the number in the centre of the plate refers to the SDS concentration, and the numbers around the outer edge refer to the sample dilution concentration in that particular segment. The two

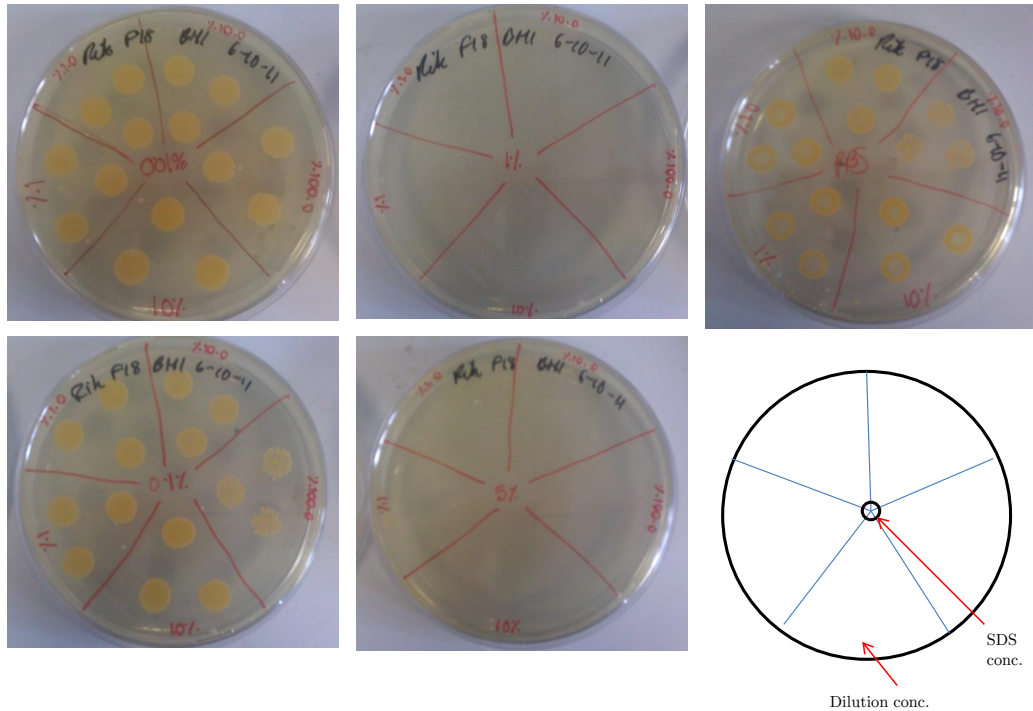


Figure 4.2: Plate assay for different SDS concentrations; Top Left 0.01%, Bottom Left 0.1%, Top Centre 1%, Bottom Centre 5%, Top Right 0% (Control).

plates on the left show a high level of cell growth, so these two concentrations (0.01% and 0.1%) do not contain enough SDS to kill the whole cell population. However the two plates in the centre (1% and 5%) show no cell growth at all. The plate at the top right contained 0% SDS and was only used as a control. From these results it was concluded that 1% SDS was a sufficient quantity to use in the cell death experiments.

In order to kill the cells in a culture but leave the cell walls intact, the culture was first boiled in a water bath for 10 minutes. The cells were then resuspended in PBS containing 1% SDS and boiled for a further 25 minutes, harvested, resuspended in 1% SDS, and boiled for 15 minutes. Finally the cells were washed 6 times in

distilled water to remove the SDS, using the standard protocol for harvesting cells. By this stage the culture only contained the intact cell walls, and minimal cellular contents.

4.5 Cell Wall Extraction

The cell death technique described above is successful in killing all the cells in the population, however as the cell walls remain intact, some of the cellular material from inside the cell is unable to escape through the wall. Where it was required for all of the contents to be removed and only cell wall to be left behind, an extra step was taken in this method.

Once the culture had been boiled for 10 minutes, but before the cells were re-suspended in SDS, the cells were chilled on ice until cooled. The cells were then harvested and resuspended in distilled water to a 'custard' consistency. This solution was then put into FastPrep tubes. These are small 1 ml tubes containing tiny, sharp glass beads, which get mixed in with the sample. The FastPrep machine was used to shake these tubes at high speed (6 times at speed 6 for 30 seconds each time). This process shook the beads and the cells very quickly together, so that the beads ruptured the walls of the cells. After the FastPrep, the solution was spun down for 20 - 30 seconds at 1000 rpm to remove the beads, after which the protocol is identical to the standard cell death technique, from the first SDS boiling stage onwards.

4.6 AFM Substrate Preparation

A few different techniques for immobilising bacteria for AFM imaging were tried before one was found to be repeatable and consistently successful.

4.6.1 Unsuccessful Attempts

All of the initial attempts that used methods of binding cells to a flat surface proved to be unsuccessful. Both APTES and Polylysine use a charge interaction to create an attraction between the cell and the substrate. When dried and imaged in air, large clusters of cells were seen on the surface. However, as soon as the samples were immersed in liquid, there were no cells seen whilst scanning. One possible explanation for this is the amount of NaCl in the medium, as these samples were all imaged in PBS. The presence of Na^+ and Cl^- ions in the liquid would have screened the charge interaction binding the cells, reducing the strength of the immobilisation. It could also be possible that as SA is spherical and the contact area is extremely small, the interaction may not have been strong enough to bind the cells in the liquid.

Cell-TakTM a strongly adhesive polyphenolic protein extracted from the marine mussel *Mytilus edulis*, used as an alternative surface binding agent. Meyer *et al* [74] describe the use of this method for immobilising multiple rod-shaped bacterial species for AFM. However, when used in this study to immobilise SA the results were the same as for APTES and Polylysine described above. One possible explanation for the unsuccessful use with SA is the vastly reduced contact area when immobilising spherical cells as compared to the rod shaped cells used by

Meyer *et al*, causing the binding between the cell and the surface to be insufficient with SA.

4.6.2 Etched Silicon Wafers

The first technique to work, and work well, was the use of physical confinement, similar to that described by Kailas *et al* [41]. In this case silicon wafers were etched to create customisable patterns on the surface to hold deposited cells in place during AFM scanning. Two different designs were used, one for SA and one for BS.

4.6.2.1 Design of Wafers

Since SA is a spherical, micron diameter cell, the design for a substrate to confine these cells was to create a set of wells in the wafer. These were required to be slightly larger than 1 μm in diameter and approximately 750 nm in depth. This allowed for the cells to settle down into the holes well enough to be immobilised for AFM scanning whilst also being visible enough to be examined.

The design for a substrate to immobilise BS was more complex, due to the rod shaped nature of these cells. As BS divides by initially extending lengthways, the cells in a culture are often a range of different lengths, so the design of the wafer could not restrict the length of the cells. The designed wafer formed almost an exact negative of the set of wells for SA, with a bed of nails type pattern. This would allow BS cells to lie along the base of the substrate, immobilised along their length by supporting pillars, whilst also being unrestricted enough to allow long

chains to lie unbroken.

4.6.2.2 Etching Protocol

The method for creating the two different substrates was almost identical, apart from the type of photoresist used. For the wells, MaN 1410 negative resist was used, and for the pillars SPR 350 positive resist.

Once the wafer had been cleaned (using N-butyl acetate, acetone and propanol), and spin coated with the relevant photoresist, the grid pattern was marked into the resist layer. This was performed using a Suss MJB 3 mask aligner with a UV 300 optical set-up. This exposed the resist to UV light through a grid mask, to mark out a regular series of micron sized squares, the pattern required for etching.

The resist was developed in MF26A developer, until the pattern in the resist became visible on the surface of the wafer. At this point the different photoresists were key. As the UV light reached the same parts through the mask, it was the behaviour of the resist that determines whether the sample ended up with wells or pillars. With a negative resist, the UV light changed the chemical properties of the resist so that it became more soluble in the developer. The exposed areas from the mask were therefore exposed in the etch, forming wells. When the positive resist was exposed to UV light, it changed to become more insoluble in the developer, so that these regions remained coated and the rest of the wafer was etched, forming pillars.

The wafers were etched in an OPT 100 ICP etcher. This used a plasma of SF₆, O₂ and Ar. The depth of the etch was controlled by varying the time of exposure. An oxygen plasma barrel etcher was used to remove any excess photoresist, before

cleaning the wafer in acetone and propanol.

Whereas Kailas *et al* used a custom built mask to form diamond shaped wells with a depth of approximately 450 nm, these wells were formed with a standard commercial mask forming rounded square holes, of roughly the same diameter but a longer exposure created a depth of 750 nm. Other than these two modifications, the techniques used were very similar.

4.6.2.3 Preparation of Wafers

Initial AFM imaging of the wafers enabled a check that they had been created successfully, and also to check that the very topographic surface was able to be imaged without damage to the tip or the substrate during scanning. Figure 4.3 shows a height image of the etched wafer. From this image it appeared that the wafers had turned out exactly as planned, with wells slightly larger than 1 μm in x and y, and a depth of 750 nm (not visible in this image).

The dimensions of the wells were checked by depositing a droplet of harvested cells onto the wafer, allowing the liquid to dry, then imaging the sample in air. Figure 4.4 shows a contact mode image of the cells dried onto the surface, fitting comfortably into the etched wells. Whilst some of the cells are inevitably sat on top of either other cells or the ridges of the silicon, the majority of the wells on the surface have been filled by cells.

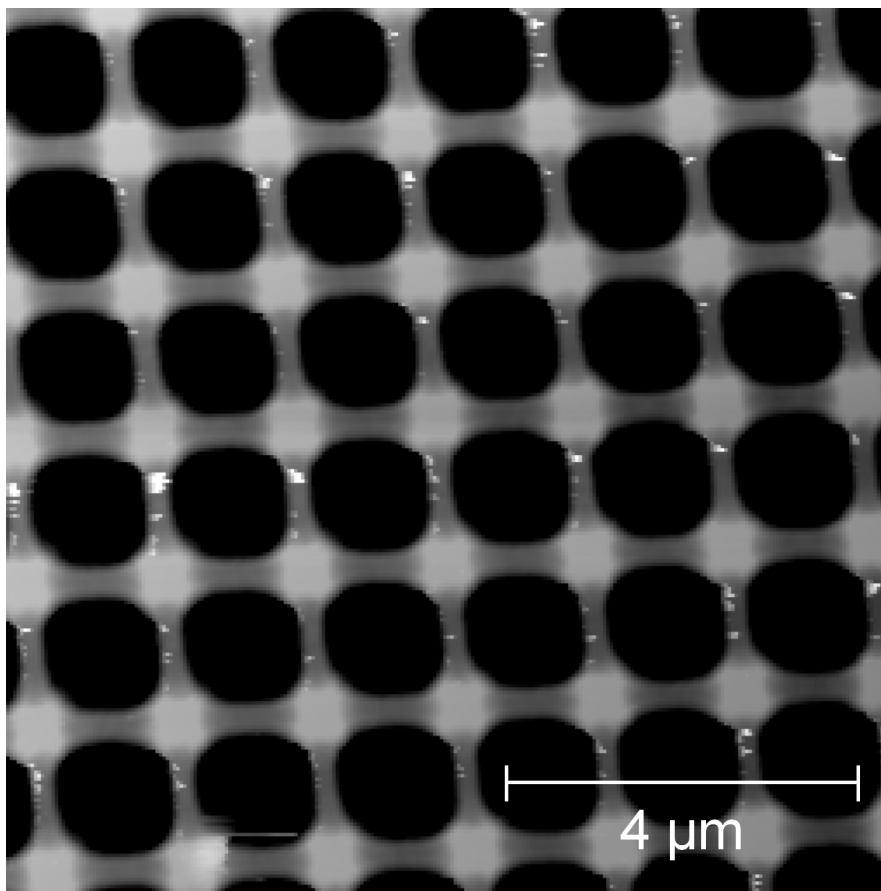


Figure 4.3: Contact mode AFM height image of etched silicon wafers for immobilisation of SA cells. Z Scale = 1.0 μm .

4.6.2.4 Imaging SA in Liquid

Whilst the wafers were performing exactly as desired in air, there were still issues when the samples were imaged in liquid. When tapping mode was used, there was nothing at all seen on the surface, all of the wells that were full of cells in air had become empty with the addition of liquid. Contact mode imaging gave slightly better results, as the scan was able to start imaging immobilised cells, but as soon as the tip got more than approximately 20 - 50% of its way across the cell it would remove the cell from the well, losing it into the liquid. This meant that whilst the cells were in the wells to begin with, they were not sufficiently immobilised

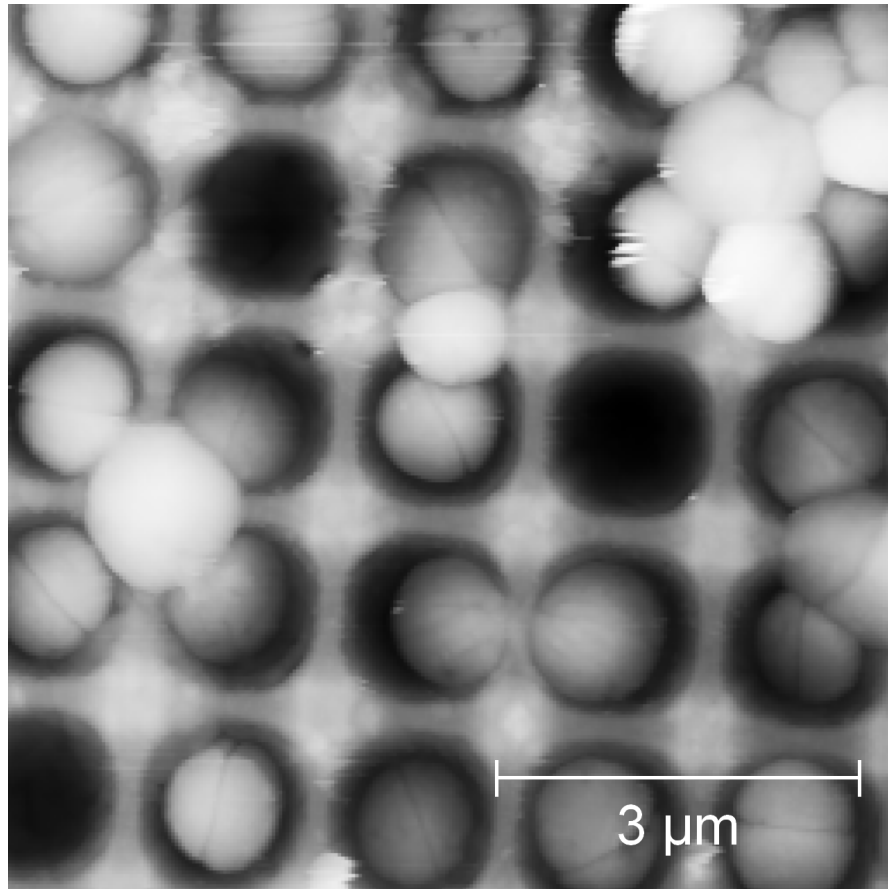


Figure 4.4: Contact mode AFM height image showing SA cells in air, fitting nicely into the etched wells. Z Scale = 1.0 μm .

there to remain stuck during the scan. Figure 4.5 shows three cells that have been removed by the tip whilst scanning.

One theory for this detachment was that the silicon wafer will have been coated in a very thin native layer of silicon dioxide (SiO_2), even just from exposure to the air. Because this layer on the surface is hydrophilic, it is inevitable that when the liquid medium was added to the sample, the water would have been attracted to the substrate surface. This could have created a water layer between the edges and base of the well, effectively lifting the cells out of the wells, causing them to be lost more easily during scanning.

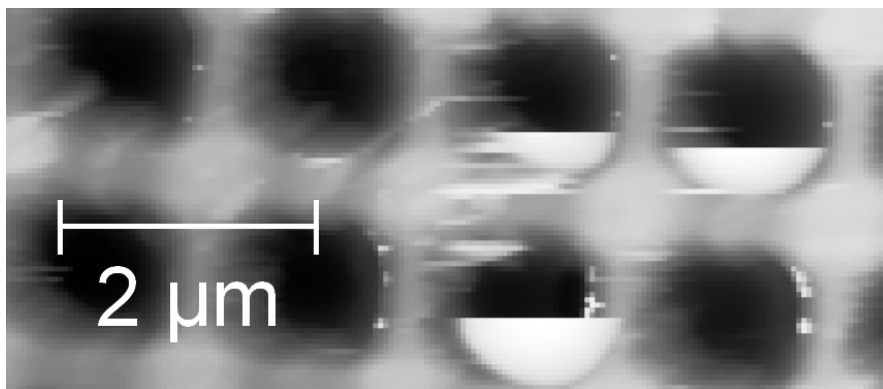


Figure 4.5: Contact mode AFM height image in liquid showing cells detached during scanning (tip scanning from bottom to top). Z Scale = 1.0 μm .

In order to test this idea, the surface had to be made hydrophobic. This was done by adding a polystyrene layer to the surface, by dropping 10 μl of 1 mg/ml 35,000 M_w polystyrene in toluene solution and allowing the toluene to evaporate in a fume hood. This created a very thin layer over the surface, such that when the wafers were imaged without cells, they did not appear any different to before the polystyrene was added when imaged at low resolution in air. However when cells were added, and the sample was imaged in liquid, it was now possible to scan over whole cells several times in contact mode without them becoming detached. Figure 4.6 below shows a contact mode height image in liquid over a small group of cells, showing no detachments. These samples have been imaged continuously for as long as 8 hours, which demonstrates the stability of the technique.

The wafers were cleaned between experiments by an overnight sonication in toluene, which removed all of the cells from the sample and stripped off the polystyrene layer. The following morning the wafers were dried in a nitrogen flow, the polystyrene layer was added and they were stored in a sterile Petri dish ready for their next use. Experiments were run attempting to use the same polystyrene layer, just washing to remove the cells, but this did not provide successful immobilisation on

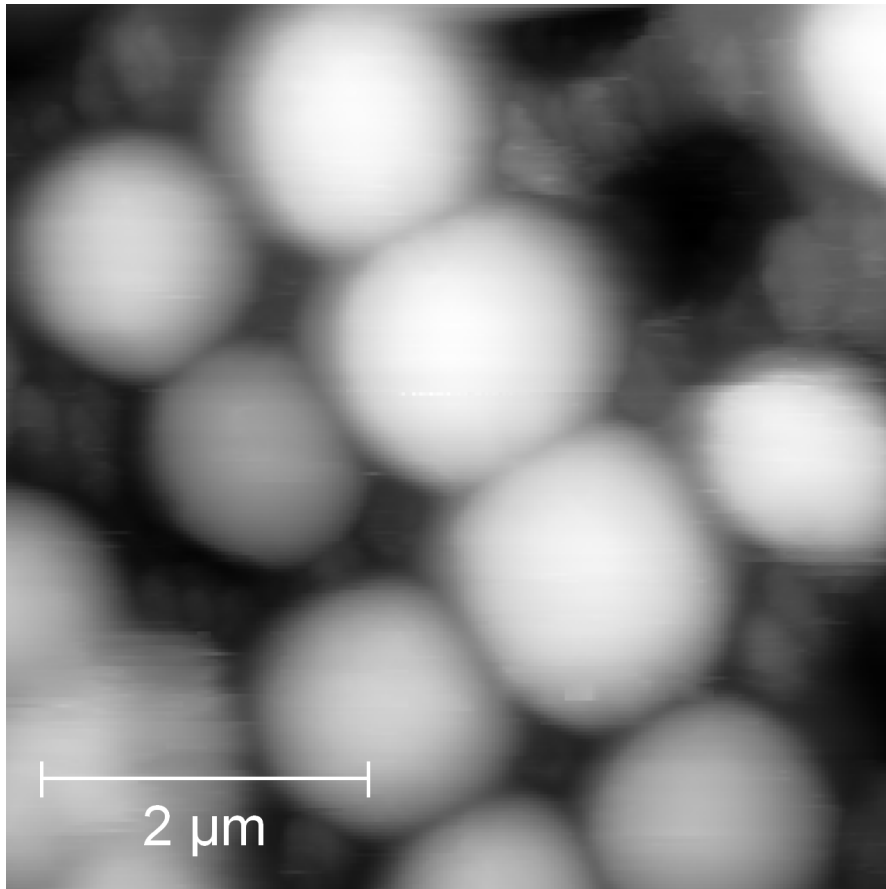


Figure 4.6: Contact mode AFM height image in liquid after polystyrene modification showing cells not detached during scanning. Z Scale = 1.5 μm .

the following experiment. This could be due to damage to the polystyrene layer as cells attach and are then removed, or even just during the immersion in buffer and the scanning of the tip. Cleaning everything off and depositing a new polystyrene layer from solution, however, did lead to repeatable immobilisation, and the same wafers have been used for all experiments with SA.

Whilst it was now possible to image cells repeatably in liquid in contact mode, switching to intermittent contact mode still caused the cells to become detached from the surface, even when they had been imaged immediately before in contact mode. Initially this appeared unusual, as the higher lateral forces exerted on the

sample by the tip in contact mode were expected to detach cells from the surface much more than in intermittent contact mode.

It is likely that contact mode is working well with these samples because the cells are set relatively deep into the etched wells. As the tip scans over the cell, the lateral forces just push the cell up against the walls of the well, with the vertical force due to the tip pressing down slightly on the top of the cell keeping the cells secured within the wells. The net force exerted on the cell by the tip is down and across, and there is no force to lift the cells up and out of the wells.

As for intermittent contact mode, it is still unclear exactly why it was never possible to image the cells in liquid by this technique. It is possible that the motion of the oscillating cantilever, when close to the sample surface, creates corresponding disturbances in the liquid environment around the tip. When this gets close to the cells, the cells themselves could pick up the vibrations, shaking themselves free of the wells.

In liquid the damping of the surroundings on the cantilever mean that the cantilever cannot be oscillated as directly as in air, but instead it is driven acoustically by transmission of an acoustic wave through the liquid. This could cause the whole system to act as an effective ultrasonic cleaner. A more direct drive, such as oscillating the cantilever with a magnetic drive or similar could have solved this problem, but contact mode was found to be suitable for the experiments performed.

It is also possible that as the tip taps on the surface, as there is sometimes a slight adhesive force between the tip and the sample, the tip could pull the cell slowly upwards, and ultimately out of the well. However this is less likely than

the first reason, due to the fact that most of the time no cells were seen at all in intermittent contact mode. For this to be happening, the start of a cell would have been regularly seen whilst scanning before it detached, similar to when imaging in contact mode before the polystyrene layer was added (Figure 4.5).

4.7 AFM Techniques

Two AFMs were used in this study. Some of the preliminary method development was performed using a Veeco Dimension 3100, although all of the data presented here was obtained using a JPK NanoWizard® 3.

Harvested cells were put onto the substrates by pipetting a small (approximately 100 μ l) droplet of the cell / PBS suspension onto the surface and allowing to dry for 20 - 30 minutes. This process encouraged the cells to drop out of suspension and settle onto the surface, falling into the wells (or around the pillars) ready for imaging.

All experiments presented here used Bruker MLCT silicon nitride cantilevers with pyramidal tips.

4.7.1 Sample Holders

Two different sample holders were designed specifically for this study, one for each of the microscopes used. The standard imaging technique for AFM imaging in liquid is to add a small droplet of the imaging buffer to the sample, and scan using this droplet as the liquid environment for the sample. However this

is unsuitable for this study as many of the experiments require several hours of imaging in liquid. On these timescales the droplet suffers from significant evaporation, either reducing in volume or drying the sample out completely. This will cause a large increase in the concentration of the salts and other molecules in the droplet, causing problematic conditions and even toxicity for the cells in the sample. Sample holders were therefore designed to allow imaging of the samples in a holder containing a much larger volume of liquid, reducing the effects of the small amount of evaporation, and also allowing the liquid to be added to more easily in particularly lengthy experiments.

The first of these was required for normal imaging in liquid on the JPK NanoWizard 3, as the microscope stage is only suitable for anchoring standard glass microscope slides. The silicon wafer substrates were superglued onto small, 1 cm metal discs, allowing them to be temporarily attached to holders by magnetic attraction. The holder itself was then created by supergluing a shallow Petri dish to the top and a magnet to the bottom of a glass slide, as shown in Figure 4.7. The dish allowed a sufficient volume of imaging buffer to be used whilst being small enough to be used under the AFM with the magnet providing a non-invasive way of holding the sample in place during scanning. The Petri dishes used were BD FalconTM 100 mm x 15 mm Bacteriological Petri Dishes (BD Biosciences). The magnets were 14 mm diameter ceramic ferrite magnetic discs (RS Components).

The second holder was designed for use with a Linkam heating stage. The growth of the cells that were being studied is relatively temperature sensitive, if there was much deviation from the ideal 37 °C conditions then the growth of the cells was severely compromised. Therefore, when experiments that required active cell processes were run, the temperature of the laboratory, which ranged between

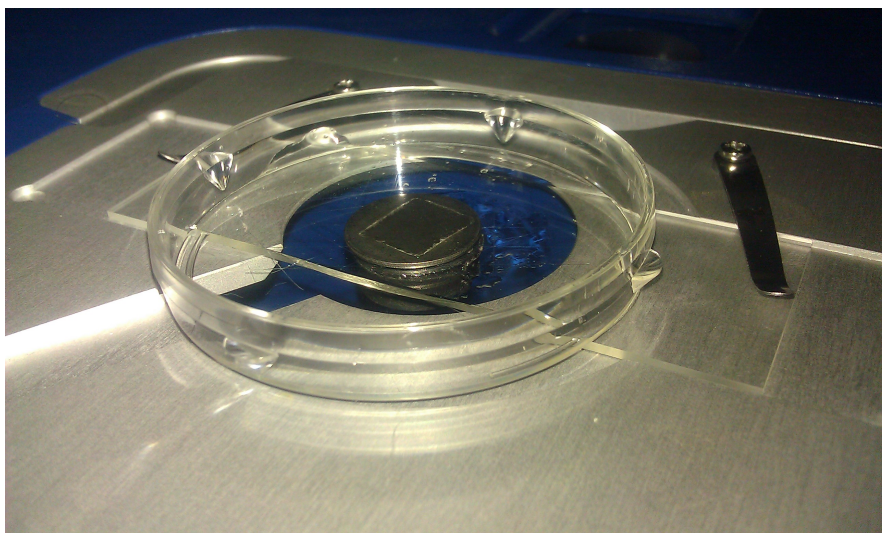


Figure 4.7: Photograph showing the first sample holder mounted to the JPK NanoWizard 3 stage.

approximately 15 and 25 °C, was insufficient. For these experiments the Linkam Heating Stage was used to provide a temperature as close as possible to the ideal 37 °C, so a sample holder had to be designed to attach onto the heating stage. A metal dish was designed to attach tightly onto the stage, providing a reservoir for the sample and imaging buffer to be scanned by the AFM head whilst being warmed from below, as shown in Figure 4.8.

4.7.2 Imaging

As the majority of biological samples are very soft, it is common to image them by intermittent contact mode, rather than contact mode, as the reduced lateral forces greatly reduce the chance of damaging the sample. At the start of this study, all of the samples were imaged in intermittent contact mode for this reason, however there was no success with this, on any of the substrates. When the imaging mode was switched to contact mode, it was common to see large areas on the etched



Figure 4.8: Photograph showing the second sample holder mounted on the Linkam heating stage.

silicon wafers with cells immobilised, so the imaging technique of choice quickly became the combination of the etched silicon wafers, imaged with contact mode. In order to minimise the forces experienced by the cell during imaging, the samples were imaged with the lowest setpoint possible that gave a high quality image. This was true for both of the AFMs that were used.

Samples were initially imaged in contact mode in air before the liquid experiments were started. This allowed the cells to be scanned before any were detached by the liquid, ensuring that there were cells suitably located within the wells of the silicon wafer samples. It also allowed a quick check that the cells looked healthy and alive, and were not damaged by the preparation procedure.

4.7.3 Force Measurements

All of the force measurements performed during this study were done on the JPK NanoWizard 3. As the cells are so small, there was no possible way of

viewing them on the optical camera of the AFM, as these optics are far from being powerful enough for this. It was therefore necessary to locate cells by first imaging in contact mode, as described above. Cells from this image could then be selected for examination either by individual force curves, where the locations of curves were manually selected at the required points, or by force mapping, creating a visual image of the measured properties. Depending on the specific requirements of the experiment in question, these were taken at a range of setpoints over a range of timescales. Unless otherwise stated, all force curve measurements were taken at an approach velocity of $1.0 \mu\text{ms}^{-1}$. Any faster than this and the curves, particularly for the softer cantilevers, started to experience large hysteresis due to the hydrodynamic drag experienced by moving quickly through liquid. Indentations were taken up to a deflection of 1 Volt on the photodiode, corresponding to applied forces of 130 pN and 1.3 nN for the 0.01 Nm^{-1} and 0.07 Nm^{-1} tips respectively.

4.7.4 Force Mapping

Force maps were taken once a relevant area had been found by imaging. During a force map, a force curve is automatically taken at each pixel, then properties such as height and stiffness can be displayed by processing the force curves and expressing their values as a colour scale image. The curves were set to have an approach velocity of $1.0 \mu\text{ms}^{-1}$, as for individual force measurements.

4.7.5 Cantilever Calibration

In order to quantify any of the measurements taken during AFM force measurements, the properties of the cantilever must be known. Calibrations of the cantilevers used were always performed immediately after measurements were taken, by switching the sample for freshly cleaved mica and calibrating by the thermal tuning method described in Chapter 3.

The calibration was always done after taking measurements on cells, rather than before, as part of the calibration procedure involves pressing the tip onto a hard surface (mica), and this has the potential to damage and blunt the tip.

4.7.6 Dwell Experiments

It was also possible to add a dwell to the force curves. This was done to test for a viscoelastic relaxation of the cell during prolonged indentation by the AFM tip. The tip was approached as normal, but instead of retracting immediately once it was reached its maximum indentation, the tip was held at a constant height between the end of the approach and the start of the retract. By plotting this part of the curve as a force versus time graph, any relaxation in the sample would be seen as an exponential decay in the force on the cantilever during the time of the dwell.

4.7.7 Live Modification of Buffer Conditions

As the samples were contained in dishes with an accessible liquid reservoir, it was reasonably easy to add to this liquid, changing the conditions of the buffer and observing the effects on the cells as it happened. This was done by inserting a syringe with a long needle into the liquid at the edge of the dish, and using this to inject the required new medium into the reservoir. By using measured volumes of known media, it was possible to modify imaging buffers to contain accurate required concentrations of the substances involved. The four substances used for this were solutions of NaCl, D-Sorbitol, SDS and oxacillin.

4.7.8 AFM Data Analysis

Force curves were analysed using the JPK 'Data Processing' software. Raw curves were first calibrated with the cantilever stiffness and sensitivity values from the calibration that was run at the end of each experiment. The stiffness value was extracted from each curve by fitting a straight line tangent to the curve at a point dependant on the tip being used. For the 0.01 Nm^{-1} tip this was at an indentation depth of approximately 10 nm, and for the 0.07 Nm^{-1} tip at approximately 50 nm, in order to quantify the measured stiffness. These points were chosen as they were at the maximum indentation for the parameters used, and fitted well to the majority of the upper parts of the curve. A screenshot of the fitting software is shown in Figure 4.9 for reference. These fits had to be done manually for each and every data point as it was found that the software's option for automatic fitting did not fit the curves well. The value for each force curve was entered into Microsoft Excel for processing into the averaged values, histograms and other presentations

of the data shown in this thesis. Where data is presented averaged over a number of samples, the resulting value is quoted along with an error, calculated as the standard deviation of the sample.

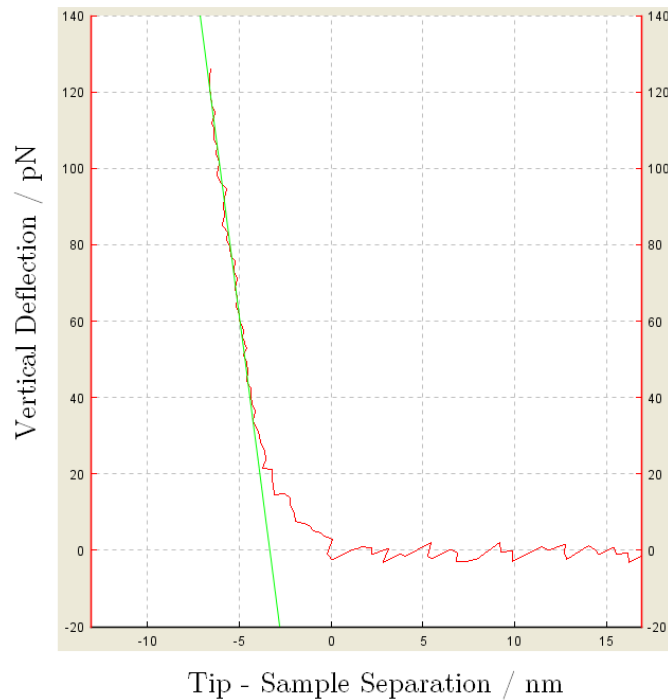


Figure 4.9: Screenshot of the force curve fitting software, showing the straight line fitted to the curve for an indentation with the 0.01 Nm^{-1} tip.

4.7.9 Statistics: Student's T-Test

Where two different groups of measurements were to be compared to see if they were the similar or different, a Student's t-test was performed on the data. This test compares the two data groups and produces a result called a p value. This number is the probability that the two data sets are from different populations, expressed as a decimal. Where p is less than 0.05 it can be assumed that the two data sets are not the same, since there is only a 0.05% chance that they are of the same population. Where $p > 0.05$ it is generally accepted that the data is

comparable.

4.8 Fluorescence Microscopy

Fluorescence images were taken of BS on a silicon pillar wafer, prepared as for AFM, using a Deltavision optical microscope. Two different stains were used.

Fluorescence imaging was used to test the viability of the BS cells once they were immobilised on the silicon wafers, as BS has never been immobilised successfully in this way. Fluorescence was not done with SA since the immobilisation technique used was very similar to that of Kailas *et al* [41], so it is established that SA can survive this preparation procedure.

Since fluorescence microscopy usually uses samples mounted on transparent glass slides and this experiment required the cells to be immobilised on silicon wafers, and initial DAPI stain was used to check that it was possible to image the cells in this way, before a more detailed experiment was run with BacLightTM staining.

4.8.1 DAPI Stain

DAPI nucleic acid stain (Invitrogen). Cells were harvested at exponential phase, washed in PBS and pipetted onto the silicon substrate, as for AFM. The DAPI stain was prepared by creating a 300 nM solution in PBS, and adding this to the surface of the wafer until coated. After a 15 minute incubation the sample was imaged.

DAPI stains cells by passing through the cell wall and membrane and binding to double stranded DNA. As DAPI is only fluorescent when it has successfully bound to DNA, it is very useful for locating cells on a surface, although it does not provide any information on cell viability.

DAPI has an absorption maximum at 358 nm (ultraviolet) and an emission maximum at 461 nm (blue).

4.8.2 BacLight™ Stain

Live/Dead BacLight™ stain, kit number L13152 (Invitrogen), supplied as pairs of applicator sets with the components desiccated in individual sealed pipettes ready for use. Exponential phase cells were harvested and washed in PBS, as usual.

This stain utilises two different components, SYTO 9 and propidium iodide. SYTO 9 is a green fluorescent nucleic acid stain, which is able to penetrate intact cell membranes, causing all of the cells in the sample to stain green. Propidium iodide, a red fluorescent nucleic acid stain, cannot pass through the membrane. It cannot therefore stain cells with intact membranes, only those which have been compromised. When this stain is present in a cell, it reduces the SYTO 9 fluorescence. Therefore, when both dyes are used in the correct balance, bacteria with intact cell membranes (viable cells) stain fluorescent green, whereas cells with compromised membranes (mostly dead cells) stain fluorescent red.

Both stains can be excited at the same time, as SYTO 9 is excited at 480 nm and propidium iodide at 490 nm. The emission maxima are at 500 nm and 635 nm

respectively.

In order to combine the stain and the cells, a stock solution of the reagent mixture was prepared by dissolving the contents of one of each of the pipettes into a universal tube containing 5 ml distilled water, before being dropped onto the silicon wafer which was prepared with the cells as per AFM. After 15 minutes of settling time the sample was ready for imaging. The final concentrations of the constituents of the stain were 6 μM SYTO 9 and 30 μM propidium iodide.

As well as the cells prepared on the silicon, two control samples were also imaged. In the first, the cells were harvested, washed, stained and then imaged on agarose. This was a positive control, as the majority of the cells in the sample should still have been alive. A negative control was prepared by adding in a step before the washing where the cells were incubated in ethanol for 10 minutes, killing all of the cells in the sample.

4.9 Transmission Electron Microscopy (TEM)

TEM was performed on the samples that were exposed to high NaCl concentrations in an attempt to view any visible changes to the internal parts of the cell. At the relevant stage during the NaCl exposure, a 3% solution of glutaraldehyde was added to the cells to fix them. This was performed at three timepoints, firstly before the addition of any NaCl, secondly seven minutes after the addition (during the phase where the measurements of the whole cell compression were lowered) and 30 minutes after the addition, significantly after the cells had been seen by the AFM measurements to recover their turgor pressure. The solution was then

briefly vortexed and placed on a rotary shaker for 15 minutes to avoid the cells becoming clumped together during the fixing process.

The preparation of the cells for TEM was performed by Chris Hill, Electron Microscopy Unit, Department of Biomedical Science. The samples were then viewed at up to 16,500x magnification using a FEI Tecnai TEM with a Gatan digital camera and analysed.

5 | Mechanical Measurements

5.1 Introduction

Once a repeatable, reliable immobilisation technique had been established, it became possible to move on to start taking mechanical measurements on cells.

As SA is a Gram positive bacterium, it has a relatively homogeneous, strong cell wall, so it was initially unclear exactly how much information could be gathered simply by doing AFM force spectroscopy on living cells. However as experiments were done, and information started to be collected and analysed, it became clear that there was a large amount of information available.

This chapter discusses this process, from initial measurements, to quantification of different parameters, and the difference between these measurements at different stages of the cell cycle. The experiments in this chapter were all performed on the standard laboratory strain *SH1000*.

The Force Spectroscopy mode of the JPK NanoWizard 3 was used for the work presented in this chapter. Once an image had been taken in contact mode, individual locations were selected on the image to be the locations of force curve

measurements.

The main motivation for studying the mechanical properties of these cells is to try to better understand the cell division process. The basic process of division is understood, it is known that the cell duplicates its contents, then creates a septum from new cell wall, then the two halves separate. Finally the two hemispheres expand to form fully spherical daughter cells, ready for the next round of division. This process is described in detail in Chapter 2.

However, little is known about what happens to the mechanical properties of the cell as it progresses through this cycle, both from the perspective of the cell wall, new or old, and also the pressure inside the cell. For example, what causes the two hemispheres to pull apart from each other once the septum has finished forming?

These division properties become even more important to study when one considers the action of antibiotics. β -lactam antibiotics such as penicillin are thought to act by stopping the cell creating any new cell wall, so that a dividing cell cannot create a septum, meaning it cannot successfully divide. However the exact mechanism of action of these drugs is not particularly well understood, so studying this area can potentially lead to better healthcare in the future.

5.2 Results

5.2.1 Method Development

Measurements were taken on live cells, in stationary phase, in PBS. In this growth stage, the majority of cells in a sample will not be expressing any growth features, such as septa within the cell or newly made cell wall exposed on the outside. This helped to give a broad overview of the general properties of the population, and any changes that occurred during the division cycle could then be studied at a later time by examining cells in exponential phase. SA can survive in PBS for several hours, but will not be able to grow due to the lack of nutrients, allowing multiple stationary phase measurements to be taken in an experimental session.

When the cells were being imaged, the choice of cantilever was not of huge importance, as the only difference between imaging with one stiffness cantilever to another on the same chip is a slight change in force applied whilst scanning, which can be altered using a different setpoint. As long as the cells remain immobilised during the scan, then any cantilever can be used, and cells have been imaged in this study using cantilevers of nominal stiffness between 0.01 and 0.1 Nm^{-1} . However when force measurements were to be made, the choice of cantilever was vital due to stiffer cantilevers applying a higher indentation force to the sample than softer ones. For example, a very stiff cantilever indenting a very soft sample will not deflect by much, vastly decreasing the accuracy of the measurement. For this reason, it is common to use a cantilever with a nominal stiffness similar to the stiffness of the sample being measured. Indentation and deflection can both be accurately measured - or at least the error in the two is similar.

As it was difficult to know what cantilever would be best to use for indenting SA cells, initial experiments were run using a range of cantilevers to indent at low setpoint (1.0 V deflection). These cantilevers were all part of the Bruker MLCT chips, with nominal stiffness values of 0.01, 0.03, 0.07 and 0.1 Nm^{-1} .

Raw force curves were processed from voltage versus distance curves into force versus tip - sample separation curves via tuning the cantilever and subtracting the deflection sensitivity, as explained in Chapter 3. The stiffness was quantified by fitting a straight line tangent to the top of the force curve at its maximum point of indentation. Each cantilever was used to indent 10 cells, and the surface stiffness measurements averaged across all 10. The results from this are as follows. For the 0.01, 0.03 and 0.07 Nm^{-1} cantilevers, values of (0.0131 ± 0.0004) , (0.0127 ± 0.0008) and (0.0110 ± 0.0014) Nm^{-1} , respectively, were obtained for the sample stiffness. As these values are in relatively good agreement, it was believed that these measurements were of the same property. However the 0.1 Nm^{-1} tip gave a measurement of (0.104 ± 0.016) Nm^{-1} for the sample stiffness, which is significantly different.

As these measurements were all taken with a setpoint of 1.0 V, the cantilever indented the sample until the laser spot had moved a set distance on the photodiode. Therefore the cantilevers were indenting to a certain deflection, rather than a certain force or indentation depth. As these cantilevers were all of different stiffness, the amount of force applied to the sample must have been different in each case. This could explain why the stiffest cantilever gave such a different value for the measured sample stiffness. Further experiments were run with a setpoint of 2.5 V rather than the 1.0 V used here, so that all of the cantilevers were applying a higher force to the sample, to see if that made any difference to

the measurements. There was also a possibility of the calibration of the cantilever being slightly wrong, due to the use of peripheral areas of the wafer rather than clean mica or glass for this purpose.

It was also considered that as all of these experiments were performed with a tip approach velocity of $1.0 \mu\text{ms}^{-1}$, then the rate of application of force from the tip to the sample was higher for the stiffer cantilevers, which could bring about a viscoelastic response from the cell. In order to test this, dwell and rate dependence experiments were also run.

5.2.2 Rate Dependence

In order to test whether the rate of application of force on the sample was having any effect on the measurements, each tip was used in turn to approach at a range of approach velocities. Any change in the fitted gradients of these curves would show that there was a rate dependence in the measured stiffness of the sample.

The curves were processed by fitting the contact part of the curve to get a value for the measured stiffness, and the indentation depth at a measured applied force of 0.7 nN was also measured to see if a higher rate of application of force was giving a greater or smaller indentation at a specified force. This data was collected from a total of ten cells for each data point.

However, it appeared that there was no change to either of these measured properties during this experiment. Figure 5.1 shows the result for one of the tips, the 0.1 Nm^{-1} , as an example. Even though the approach velocity was varied over a large range, from 0.01 to $2.0 \mu\text{ms}^{-1}$, there was very little noticeable change in the

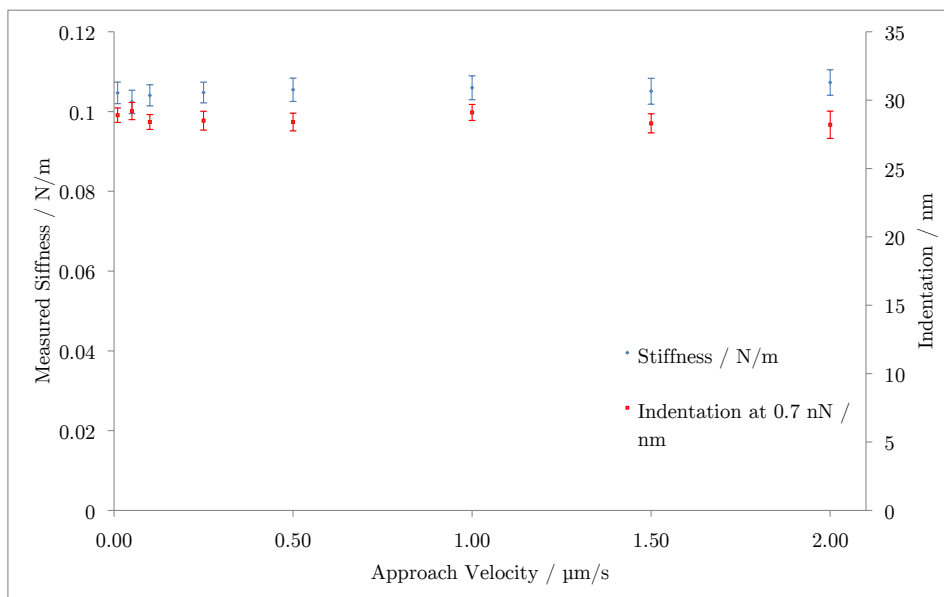


Figure 5.1: Graph showing the effect of changing the approach velocity with the 0.1 Nm^{-1} tip.

measurements.

This shows that the cells reacted to an applied force the same, no matter how quickly that force was applied. It also showed that any difference obtained in earlier force curves was not due to an effect of rate dependence.

5.2.3 Possible Calibration Error

When these initial measurements were taken, the tip calibration was performed on the silicon wafer, at a point around the cell where the silicon appeared to be bare. However, even though the wafer appeared to be bare, it is likely that it was coated in a thin covering of waste cellular material, bits of contaminants from the

media during the settling out time, or something similar, meaning that the hard surface was not actually as hard as it should have been, and was therefore likely to have been unsuitable for calibration.

All of the experiments from this point forward were calibrated on freshly cleaved mica rather than a part of the wafer. This ensured a better calibration of the sensitivity, meaning that the results would be more reliable.

All of the data presented in the following sections of this study use the correct calibration on mica apart from the studies involving the use of salt and sorbitol, which were incorrectly calibrated using the wafer as the hard surface. However, because these sections do not specifically require the actual numbers in the data to be accurate, they only require that the patterns in the data over time are correct, this data can be examined qualitatively rather than quantitatively. The error in the calibration is a systematic error not a random one for each particular data set, but the timescales and other conditions are all comparable, so the patterns and changes within each data set are still correct.

5.2.4 Dwell

In order to test for viscoelastic relaxation, the cells were indented with a dwell between the end of the approach and the start of the retract. The cantilever was held at a constant height, so the tip was free to experience any changes in force applied to it.

During a regular force curve, when plotted as deflection versus time, the deflection will increase during the approach and then decrease back to its starting value

during the retract. When there is a dwell involved, the viscoelastic behaviour of the sample is observed by the state of this deflection versus time plot during the dwell time. If there were to be any relaxation of the sample, the deflection would decay exponentially during the dwell time. However, it quickly became clear that there was only a small decay in the deflection of the cantilever during the dwell for this experiment. Cells were tested with a range of dwell times from 1 to 60 seconds inclusive, all of which showed relatively little measurable decay, meaning that there was negligible relaxation of the sample during the dwell. Figure 5.2 shows an example of this, for the contact region of an experiment with a 10 second dwell. The non-contact parts of this curve have been removed for clarity.

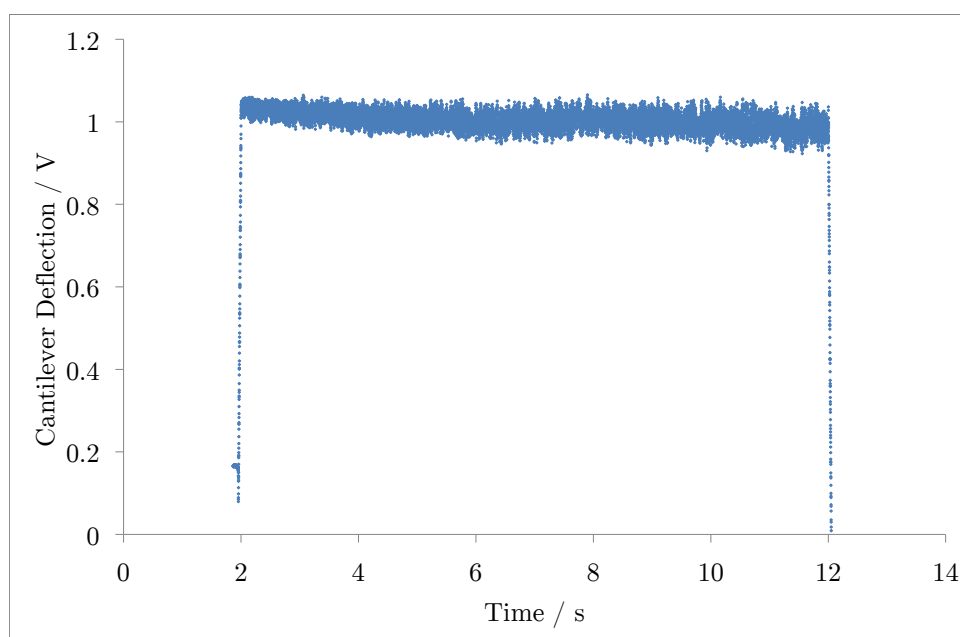


Figure 5.2: Graph showing relatively little force relaxation during a constant height dwell time of 10 seconds at 1.0 V deflection setpoint.

5.2.5 Media Dependence

Measurements were taken on cells in PBS, HEPES buffer and BHI growth medium. All of the measurements taken were in good agreement with one another, indicating that there was no direct dependence of the properties of the cells on the media they were in. This is perhaps not entirely surprising, since these media have been designed as buffers for use with bacteria, so will be suited to their needs and shouldn't cause a major response from the cells.

5.2.6 Force Curves at 2.5 V with Correct Calibration

When the 0.01, 0.07 and 0.1 Nm^{-1} cantilevers were tested with a full and correct calibration on freshly cleaved mica, the results were much more interesting. They all lay on top of each other very well, indicating that the measurements were consistent across the three levers. The contact point was still difficult to determine, as with many force curves taken in liquid, but the curves did appear to match with each other very well. Figure 5.3 shows measurements recorded with each of these three cantilevers, plotted on the same axes. The changes in end point (maximum force) are due to the different stiffness cantilevers all being indented to the same deflection setpoint. Whilst the contact point is probably in reality slightly further to the left on these curves (around the current 10 nm mark), this is not crucial at the moment.

The most important check required by these curves was to determine whether or not the two discrete measurements that were initially obtained were due to measuring two different features, or whether they were just taken at different

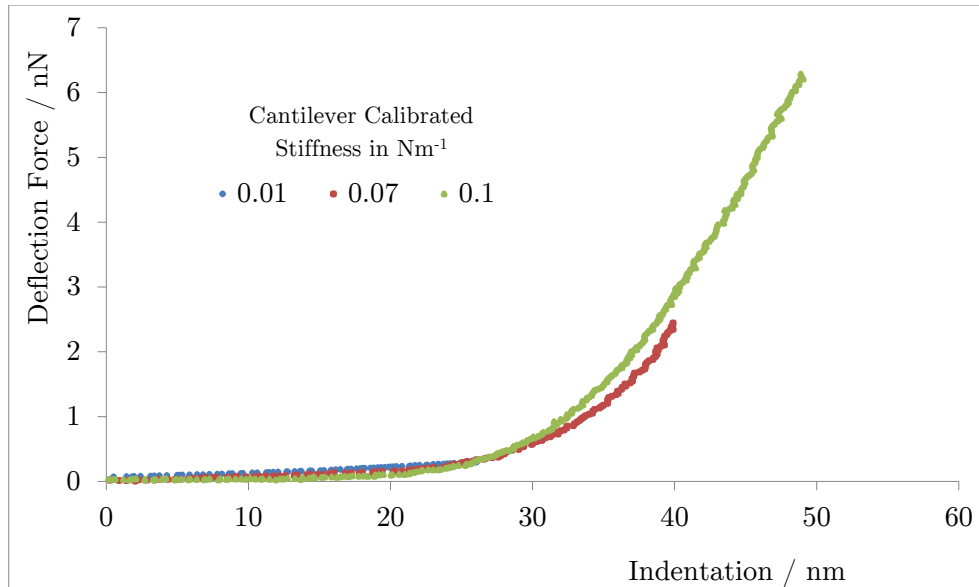


Figure 5.3: Graph showing measurements from three different cantilevers with a full and correct calibration on freshly cleaved mica. The exact location of the contact point is difficult to locate on these curves, and may not be in precisely the true location.

points of a continuum. The data acquired with the softer cantilevers matched well with the early parts of the curves taken with stiffer cantilevers when the two were overlaid, so it would be possible that the soft cantilevers and the early parts of the stiff cantilever curves were both measuring one property at small indentations, and the higher parts of the stiff cantilever curves were measuring a different property at larger indentation depths. It was therefore investigated whether or not the stiffer cantilever force curves contained different properties, or were just a continuation of one single property which increased slowly but steadily with increasing indentation depth.

5.2.7 Common Force Curve Models

All of the stiffness measurements quoted to this point have been given in terms of Nm^{-1} . Models of contact mechanics can potentially be used to extract the mechanical properties information from force curve data such as that presented here, by fitting a modelled curve to the measured one. There are a small number of such models that have been applied to AFM data in the literature similar to that presented here, but each of these models has associated assumptions that are not true with this data. As the tip indents further into a sample, the contact area between the tip and the sample surface will increase continuously, creating a non-linear force curve. The exact form of this curve will depend on the nature of the contact mechanics. The usual contact models, for example Hertz, Sneddon, JKR, DMT etc [125], each have a different power law dependence of the force on the cantilever as the indentation depth increases. For a particular homogeneous sample it would be expected that one of these models would fit, as the force curve data would follow a constant power law. By plotting the force curve data on a log-log plot therefore, normally the data would fit along one straight line, the gradient of which describes the power of the power law which the original data followed. Therefore, if there were really two different regions being measured in the data presented here, there should be two straight lines on a log-log plot, with an intercept between the two at the indentation depth at which the homogeneity of the surface stiffness changes.

5.2.7.1 Logging Force Curves

Normally a force curve will follow a given power law, as the indentation increases the contact area between the indenter and the sample will increase causing a much higher force on the indenter. Due to this, plotting a force curve with \log_{10} axes should give a straight line, the gradient of which describes the power law of the original curve. In order to check that there were indeed two discrete sections to these curves, and that they were not just one long continuous curve that appeared as 2 regions, the data was plotted with both axes as the \log_{10} of their original value. This would highlight the difference between two discrete regions, with a different straight line gradient on the log plot for each different power law in the curve, and the point where the two regions changed appearing as a change in gradient.

Figure 5.4 shows an example of the resulting plot acquired using the \log_{10} data, for the 0.07 Nm^{-1} cantilever used in Figure 5.3. It shows that there are three regions to which straight lines can be fitted well. The first of these, on the left hand side of the graph, has a gradient of zero. This is the non-contact part of the force curve, where the contact point for the original curve had not quite been selected in the correct place. It does however give a nice visual aid to the log-log plot here where the flat line of the non-contact part of the curve would not otherwise be seen. At the real contact point, where the log-log plot's gradient changes, there is an initial section with a gradient of 2.03 ± 0.05 before another clean change to a second straight line with a gradient of 3.94 ± 0.05 . This appears to confirm that the original curve was composed of two discrete regions, as the data taken from both soft and stiff cantilevers suggested might be possible. This data was collected from a total of 30 curves for each cantilever, where the 0.01 Nm^{-1} lever

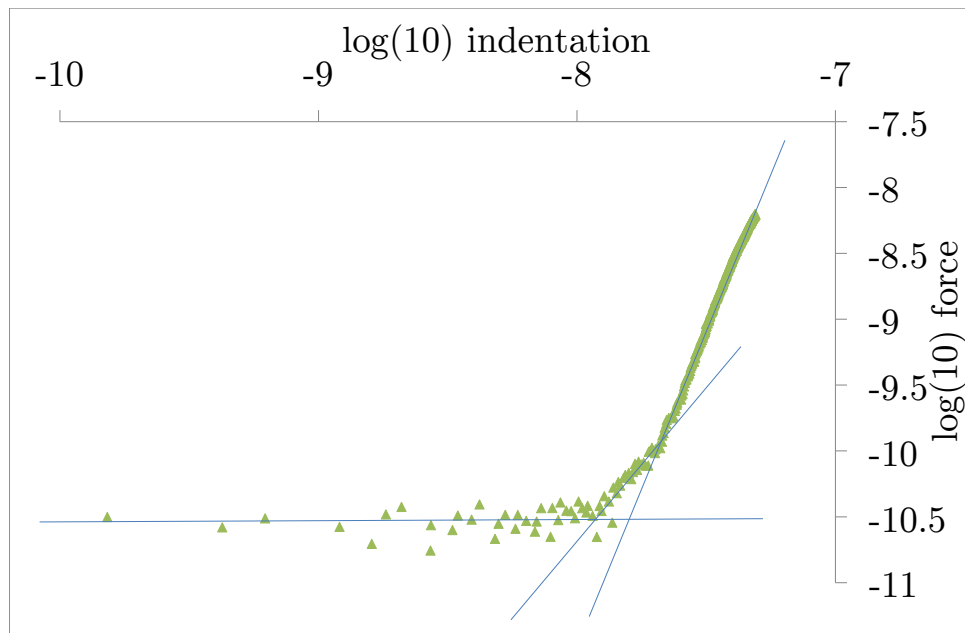


Figure 5.4: Logarithmic plot of a force curve taken with the 0.07 Nm^{-1} cantilever showing two straight lines in the contact part of the curve, revealing two different power law regions to the original curve.

only measured the initial property as it was triggered before the change, and the 0.07 and 0.1 Nm^{-1} levers both measured both regions.

It was possible to calculate the point at which the gradient changes on the log - log graph, to find the depth of indentation at which the stiffness measurement changed, by finding the distance between the contact point and the change in the contact part gradients. This was due to the point of intersection of best fit lines of the two straight sections of the log - log plot giving a specific point. From these plots, that point was found to be $(21 \pm 2) \text{ nm}$.

5.2.7.2 Rejection of Force Curve Models

As this data clearly contains two different force curve power law dependences, the contact models (which require a single power law dependence) cannot be applied. In addition, common models are only strictly valid for samples that are an infinite elastic half space, which is not true of a sample containing an outer layer that is 20 - 35 nm thick, and when the sample as a whole is deformable. When indenting to such depths as in this study, this assumption is not valid. Because none of these common models can be realistically applied to the data, the simple linear stiffness in terms of Nm^{-1} is presented for all measured data.

5.2.8 Quantification of Two Discrete Regions

It was proposed at this point that the data shows measurements of two different features. Initially there is a softer outer region, before an indentation at which the measured force becomes much higher. The critical feature of this change in stiffness is its depth within the sample. From Figure 5.4 it appears that the change happens at an indentation of approximately 21 nm. This may not be exactly correct due to the difficulty of selecting the contact point when measuring soft samples in liquid, but it should be close to the true value. This is a very important depth when considering the indentation of SA. Previously published data by Matias and Beveridge [31] and by Cui *et al* [126] suggest that the thickness of the SA cell wall is between 20 and 35 nm, which corresponds well with this force curve data.

It was therefore proposed that the first region of the data shown in Figure 5.3 is as the cell wall is indented. At the point where the force on the cantilever

became much higher, as this matches well with the reported depth of the cell wall, it is possible that the increased force was due to a change in indentation regime, moving from an indentation of the cell wall to a compression of the whole cell, containing contributions of the turgor pressure within.

Once values had been obtained from the data for both of these regions, experiments were designed to test this proposal. Force curves were collected over a large range of cells, indenting in the centre of each one. The resulting values obtained from this were as follows. For the first region, proposed as the measurement of the cell wall, the gathered data gave a value of $(0.0134 \pm 0.0068) \text{ Nm}^{-1}$. This is in good agreement with the previously published value, during a study of Lysostaphin digestion of SA cell walls by Francius *et al* [93]. The second region, thought to have some contribution from the turgor pressure below the wall, was measured at $(0.2062 \pm 0.0039) \text{ Nm}^{-1}$. The two discrete data sets are shown on the histogram in Figure 5.5.

5.2.9 Using Blunt Tips to Understand the Indentations

0.01 and 0.07 Nm^{-1} tips were blunted in order to see the effect of a larger contact area on the measured stiffness values obtained with these cantilevers. The blunting was performed by scanning the tips over a large ($30 \mu\text{m}^2$) area of empty etched silicon wells at high tip velocity, and indenting onto freshly cleaved mica repeatedly with high deflection setpoints. The bluntness of the tip was then quantified by using a TGT-1 test grating from NT-MDT. This grating consists of a set of high aspect ratio pins, with diameters much smaller than that of the tip. This means that when scanned, the image produced is that of the tip rather than the surface

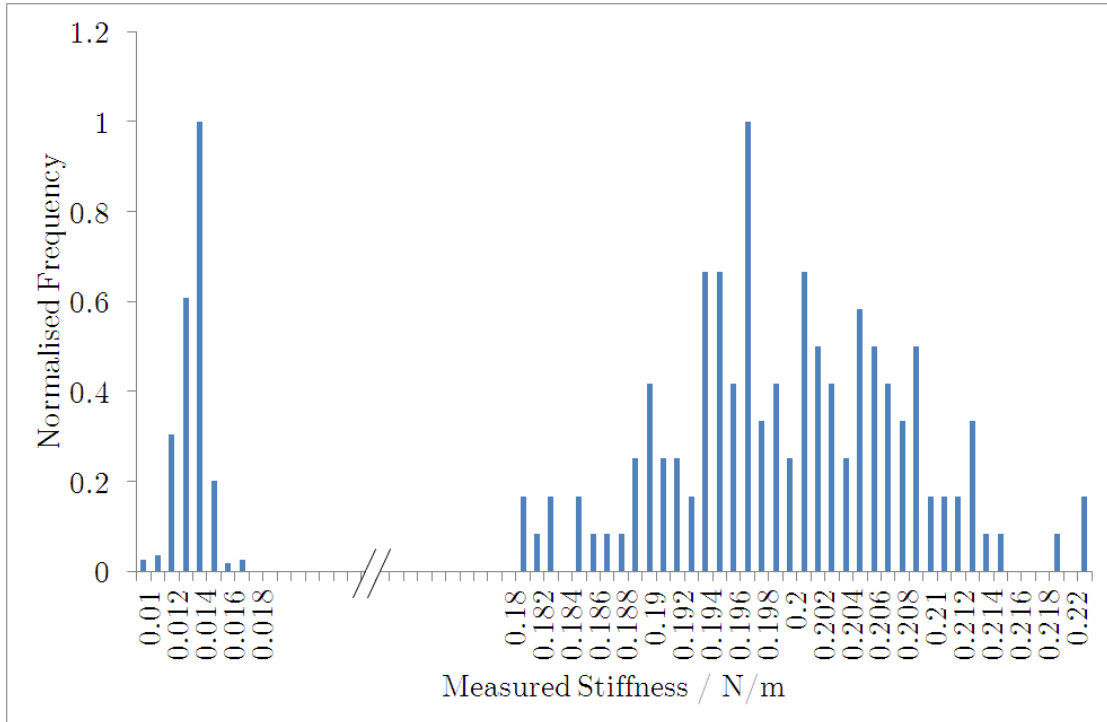


Figure 5.5: Histogram showing the two discrete measurement groups for the cell wall (lower) and whole cell compression (higher) indentations. Both data sets contain 36 curves taken on each of 50 cells, a total of 1800 measurements.

feature itself, as shown in the sketch in Figure 5.6a. Taking a cross section through this image allows the diameter of the tip to be measured.

For each stiffness, three tips were used in total, one which had not been blunted and two which had, to different levels. The tip diameters measured on these are as follows: For the 0.01 Nm^{-1} tip 55.88, 73.04 and 104.9 nm, and for the 0.07 Nm^{-1} tip 52.90, 61.31 and 93.73 nm. The resulting measured stiffness, from an average of 30 measurements per tip, are shown in Figure 5.6b & c. This data shows that as the tip is blunted, so as the contact area with the cell surface increases, the measured stiffness with the 0.01 Nm^{-1} tip increases slightly while the 0.07 Nm^{-1} tip shows very little change.

This data helps towards a confirmation of the indentation idea proposed above.

If the shallow indentations are due to a small indentation of the cell wall, then a blunter tip will be expected to experience a higher stiffness, as seen in the data, due to a larger area of the surface needing to be indented. The larger indentations, proposed as a compression of the whole cell, would not be expected to show a change in stiffness as the compression would be broadly similar regardless of the exact size of the tip, as also seen in the data.

5.2.10 Testing Region 1:

The Cell Wall

The first part of testing this proposal was to take measurements on cell walls that had no turgor pressure inside. This was done by breaking open the cell wall, dissolving the membrane and removing the contents of the cell, as described in Chapter 4.

These cell walls were deposited onto mica and imaged in air; it has not yet been possible to immobilise them sufficiently well for liquid measurements. Figure 5.7 shows an area of mica coated in cell wall fragments, showing that many large fragments have survived the preparation procedure. Some of the cell walls had kept almost all of their structure intact, with just a small broken area through which the material was removed, such as the example shown in Figure 5.8. These larger sections were chosen for measurements since they were much closer to the original wall conformation than any smaller fragments.

As these large fragments almost always appeared to be two layers thick, it was possible to take measurements of the thickness of the cell wall, both to aid the

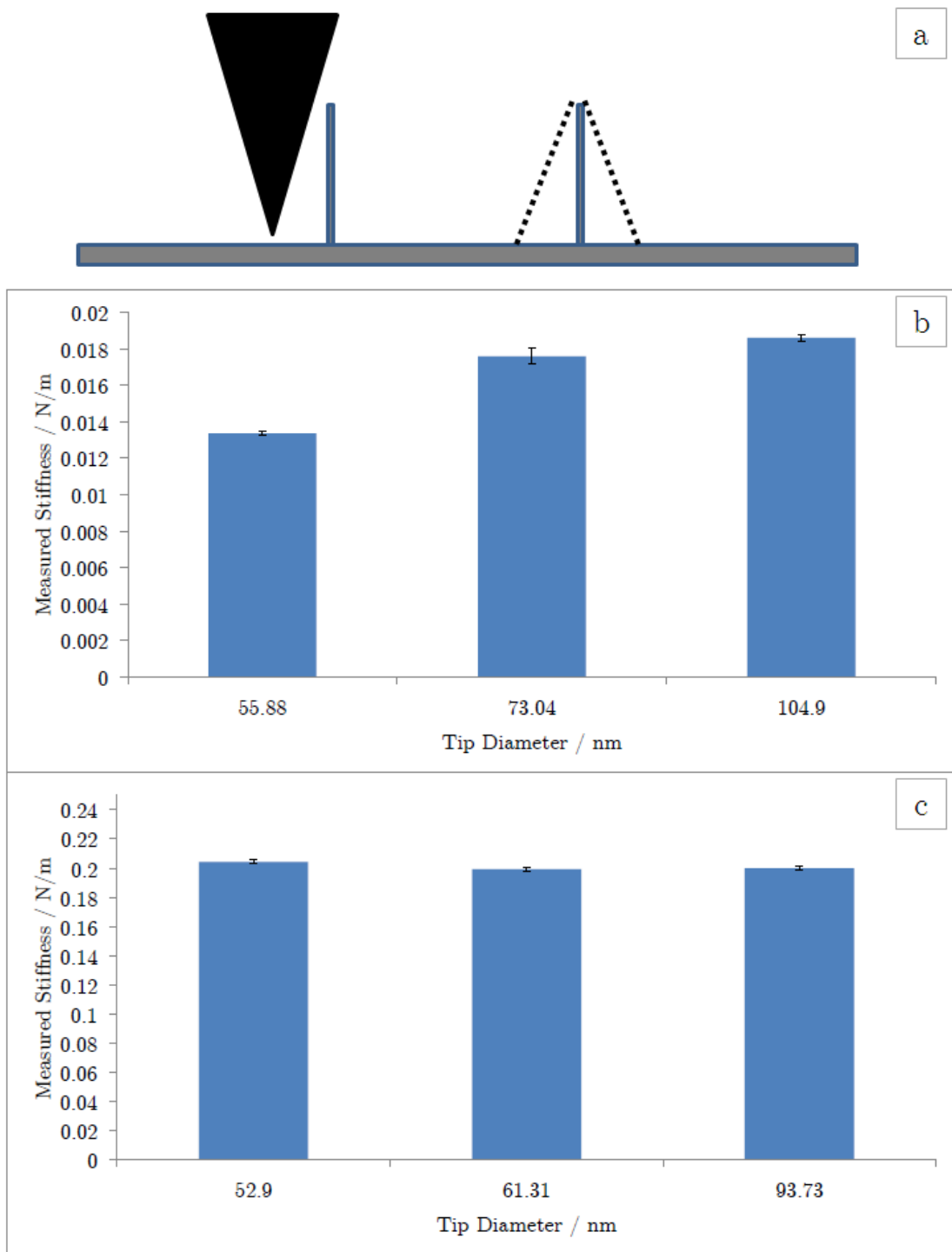


Figure 5.6: Using blunted tips characterised by using a TGT-1 grating (a) to investigate the effect of increased contact area on measured stiffness for 0.01 Nm⁻¹ (b) and 0.07 Nm⁻¹ (c) cantilevers.

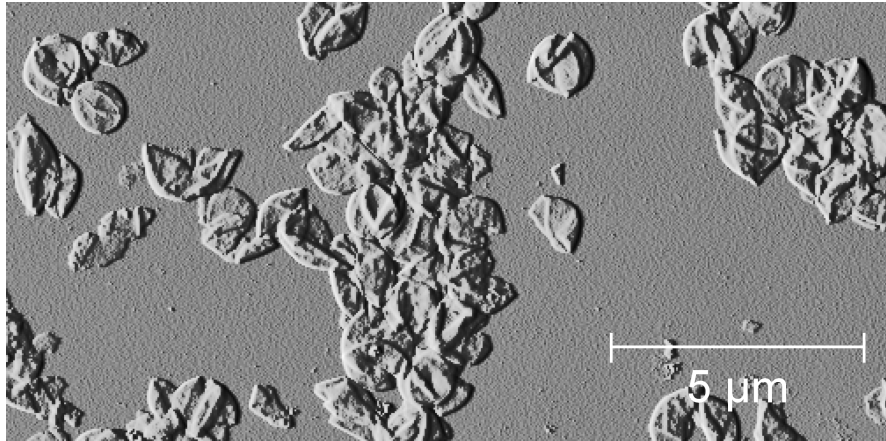


Figure 5.7: Contact mode vertical deflection image in air showing a field of SA cell walls.

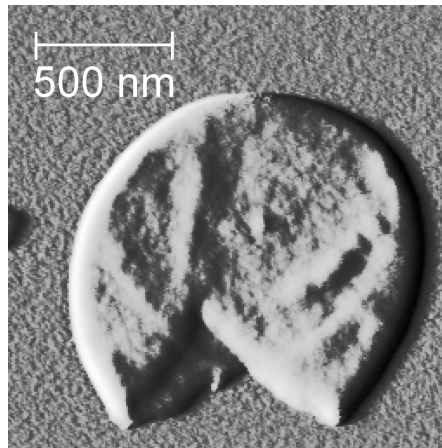


Figure 5.8: Contact mode vertical deflection image in air showing a single SA cell wall after removal of membrane and contents.

proposal and also to compare with the published values. Fragments that showed single and double layer areas, such as at the bottom left of Figure 5.8, were particularly useful for this as it gave measurements which could be confirmed as either one or two cell wall thickness from the image.

After taking measurements over a number of cell walls, a value of (27 ± 3) nm was obtained, which is in good agreement with the literature and reasonably close to the value obtained from the log - log plot of (21 ± 2) nm. The main reason for this

apparent difference in measured thickness is most likely due to the measurement from live cells actually measuring how much the cell wall can be indented before it becomes incompressible and the influence of the cells' turgor contributes to the force data, whereas the measurement of the extracted sacculi in air is a complete measurement of the total thickness.

When force measurements were taken on these fragments, they were taken on both individual fragments, and on areas where many had stacked together on the mica. All of these measurements were done with setpoints < 1.0 V, so that the tip did not go through the wall. This was to ensure that the thin cell walls were not affected by the very stiff mica beneath them when shallow indentations were taken on them [127], and indeed no differences between the two data sets were observed.

The values obtained from the fragment measurements gave a stiffness value of (0.0137 ± 0.0010) Nm^{-1} , which is very close to the value obtained on the live cells.

Cells were also prepared in almost the same way for a second part to this test. They were given the same treatment apart from the FastPrep part. This resulted in cells with no membrane and consequently no turgor pressure, but a completely intact cell wall. Measurements on these samples were taken on mica in air, as for the fragments, as they were very difficult to immobilise in fluid.

The result for the intact walls was (0.0136 ± 0.0010) Nm^{-1} , in very close agreement with both the fragments and the first region of the curves on the whole, regular cells. Performing Student's t-tests on these data sets gave the following results. Comparing the broken cell walls with the measurements on live cells gave $p = 0.60$;

comparing the whole, treated cells with the live ones gave $p = 0.42$; and comparing the broken walls with the whole, treated cells gave $p = 0.43$, all significantly greater than 0.05. Because all of these different measurements were in such good agreement with one another, it was concluded that the first part of the two - step force curve was indeed measuring the properties of the cell wall.

5.2.11 Testing Region 2:

Whole Cell Compression with Turgor Component

In order to test whether the second part of the force curves were measuring whole cell compression with a contribution from the turgor pressure, the pressure was modified within the cells and the measurements taken throughout the change. If there was a significant change in the measured stiffness during this process then it would indicate that the measurement contains a contribution from the turgor pressure. The turgor pressure was changed by filling the surrounding medium with a high concentration of three different solutes; NaCl, Sorbitol and SDS.

The NaCl and the Sorbitol created an osmotic pressure across the membrane, since the solute concentration outside the cell was initially made to be 1.0 M or higher, and the solute pressure inside the cell is approximately 0.1 M. This caused some of the water in the cell to leave through the membrane, resulting in a drop of turgor pressure.

The SDS also caused a drop in turgor pressure, but in a much more exaggerated way. SDS damages cell membranes, so the water and many of the smaller solutes from the cell will have been able to leave into the surrounding medium, causing the pressure to drop, potentially much more than for NaCl or Sorbitol.

The AFM was used to take force measurements on the cells throughout the addition of the solutes to the imaging media, looking for a drop in the measured stiffness. The values of the stiffness in these experiments are lower than they should be here due to a calibration error. As this is a systematic error, it only affects the values, so the changes in the measurements over time still stand. The whole cell compression with a contribution from the turgor pressure measurement here is around 0.11 Nm^{-1} rather than the corrected value of approximately 0.20 Nm^{-1} .

5.2.11.1 NaCl

NaCl was initially used at a target concentration of 1.0 M in PBS. Cells were imaged initially in PBS, until a suitable scan location was found. Force measurements were then taken on the cells as the NaCl was added to the medium to track any changes in the measurements. Figure 5.9 shows a plot of the measurements taken during this experiment. NaCl was added at time = 0 seconds, and a force curve was taken every 10 seconds.

After a short amount of time, approximately 50 - 150 seconds, the expected drop in measured stiffness is seen. The sudden drop was initially a little surprising, but agrees well with work by Pilizota and Shaevitz [69] who use fluorescence microscopy to observe a sudden drop in the volume of *Escherichia coli* cells when exposed to high NaCl concentrations. Slight differences in this time seen between repeat experiments are likely to be due to mixing effects as the NaCl is dissolving through the initial medium.

It is known that SA cells are unhappy at low turgor pressure, so use compatible

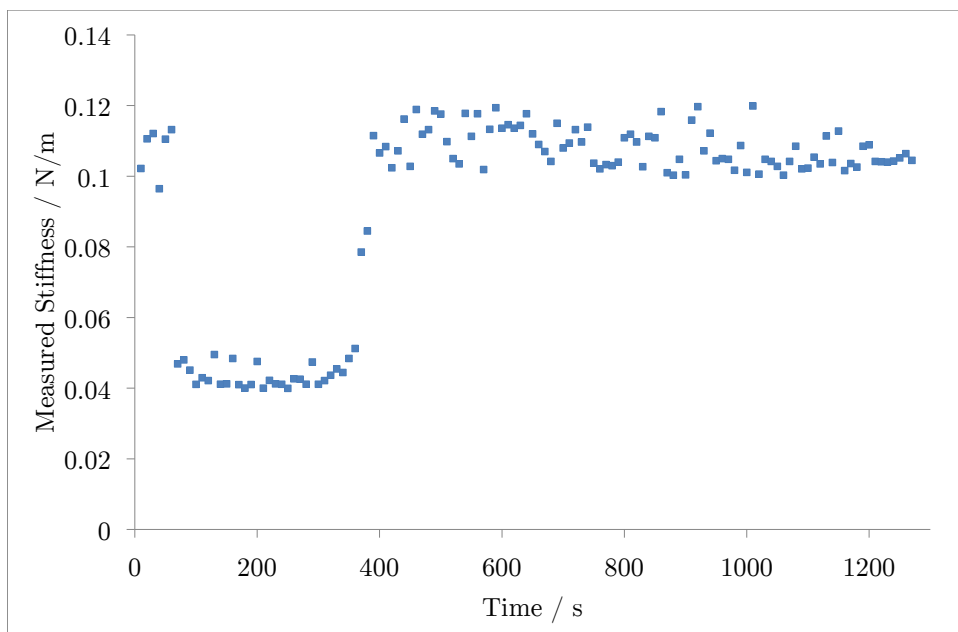


Figure 5.9: Adding 1.0 M NaCl to SA cells in PBS and monitoring the measured stiffness at high setpoint.

solutes to restore their pressure when it is reduced (see Chapter 2). This could explain the second part of Figure 5.9, where the measured stiffness rises back up to its original value. The same study by Pilizota and Shaevitz also shows a rise of the volume of their cells back to regular levels, although this is over a much larger timescale. It could be possible that the cells are restoring their pressure in order to slowly push the membrane back out, steadily expanding the volume.

This experiment was repeated using a range of NaCl concentrations, still with PBS as the buffer. The point at which the measured stiffness was lowest was recorded, and is shown in Figure 5.10. From this data, it appears that in environments up to and including 0.6 M NaCl, SA cells can deal with the osmotic pressure and do not lose any water to the surroundings. At concentrations above 1.0 M the minimum

was measured as being almost the same value, implying either that the cells are able to keep some turgor pressure no matter what the strength of the surrounding medium, or that this is the completely flaccid (but full) cell stiffness.

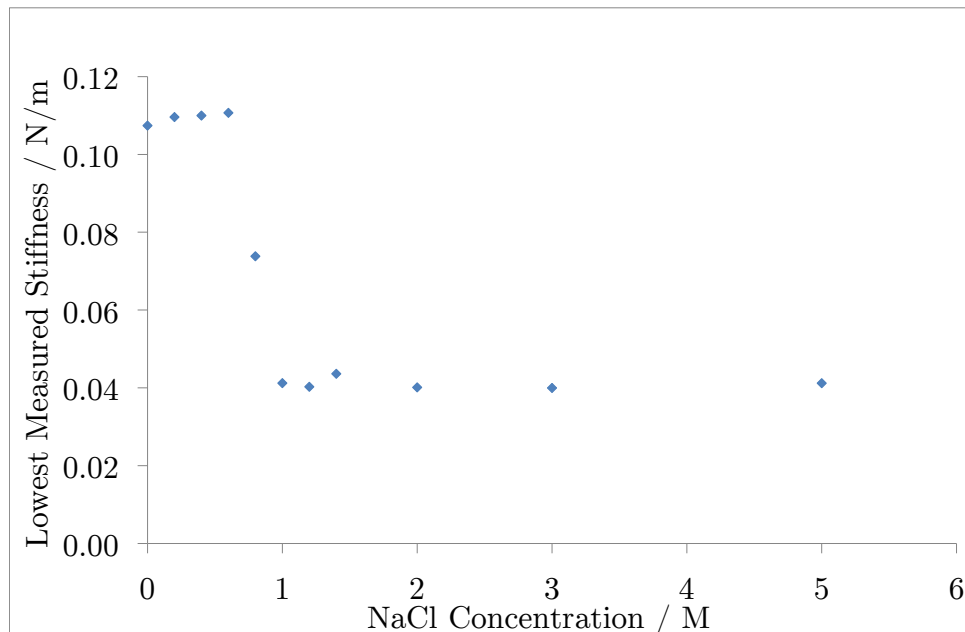


Figure 5.10: Change in the lowest measured stiffness depending on the concentration of NaCl in the medium.

Interestingly, all of the timescales for the drop and rise in measured stiffness were very similar, irrelevant of the NaCl concentration of the medium. The drop occurred between 50 - 150 seconds of the addition of the NaCl, with the rise back up taking between 380 - 450 seconds. It is currently unclear whether the initial delay is due to the cells temporarily resisting the change, or something to do with the cells not feeling the osmotic pressure for a short amount of time as the NaCl is added to the liquid. As the cells are sunk into the silicon wells they may be briefly shielded against the changing media.

The experiment was also repeated using different buffers, for comparison, with 1.0 M NaCl. HEPES and growth media (BHI) gave the same results as for PBS, with almost identical timescales and minimum values, indicating that the processes involved in the drop and rise of the measured stiffness of the cell is independent of the environment, only on the salt being there.

5.2.11.2 Sorbitol

To confirm that the changes in measured stiffness were due to the osmotic pressure and not some form of toxicity due to the use of NaCl, repeat experiments were performed using Sorbitol. This is a non - metabolisable sugar, so it would provide an osmotic pressure without being able to be taken up by the cells. Sorbitol was used at a final concentration of 1.0 M in PBS.

Sorbitol experiments gave the same result as for NaCl, with roughly similar timescales, as shown in Figure 5.11. This confirmed that the effect was due to the osmotic pressure across the membrane, as it was the same for both NaCl and Sorbitol.

5.2.11.3 Reversibility of Change

As the cells appear to be able to restore their pressure after exposure to high osmotic pressure, how would they react to a second exposure? Experiments were performed where the cells were initially exposed to a 1.0 M Sorbitol solution in PBS, and as soon as the measured stiffness dropped off, this medium was pipetted away and pure PBS was added. If the cells were able to restore their turgor here then a second batch of 1.0 M Sorbitol would be added to see if a second drop in

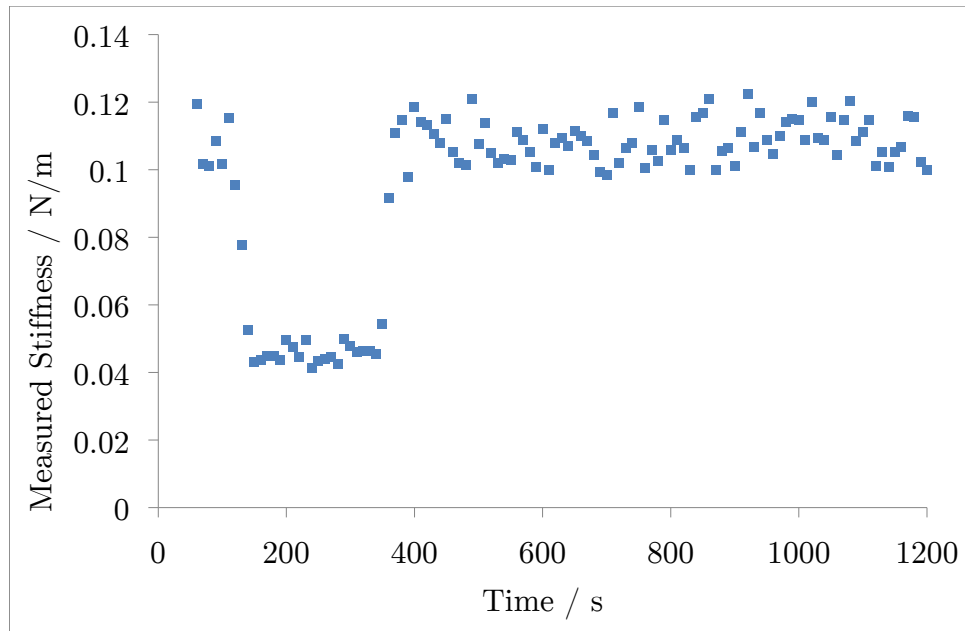


Figure 5.11: Graph showing the effect of adding 1.0 M Sorbitol to SA cells in PBS on the measured stiffness at high setpoint.

the measurement would be seen.

The results of one of these experiments can be seen in Figure 5.12. The vertical lines represent the time points at which the medium was changed, as indicated on the graph. The gaps after the lines are due to images being quickly taken after the change in medium to ensure that the force curve measurements would still be taken in the correct place.

The graph shows that on a second exposure to high solute concentration, the same drop in measured stiffness is seen, implying a second drop in the turgor pressure. The first time the cell is immersed in PBS it appears to recover quickly, whilst the second time the recovery takes much longer. This could be due to the cell having

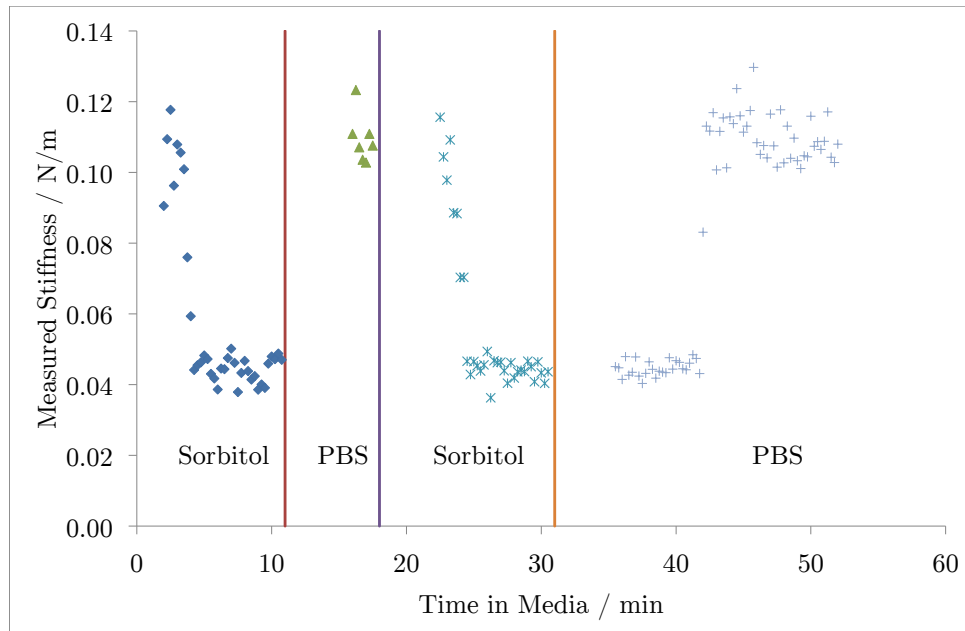


Figure 5.12: Monitoring the effect of repeatedly changing the media solute concentration from high to low molarity. Recovery takes much longer the second time around, perhaps because the cell has used up its reserves during the first recovery.

used up some of the components that it needs to recover from the exposure in the first case, so it needs to manufacture more the second time around.

5.2.11.4 SDS

The final part of testing these measurements was with the use of SDS. When this was added to the imaging medium it should have damaged the membrane, causing the cellular contents to leak out, reducing the turgor pressure. The measurements taken throughout this addition should therefore also show a reduction in the measured stiffness a short time after the SDS was added.

The example shown in Figure 5.13 is of measurements taken over three neighbouring cells simultaneously. The SDS was added to the PBS buffer at time = 0 seconds.

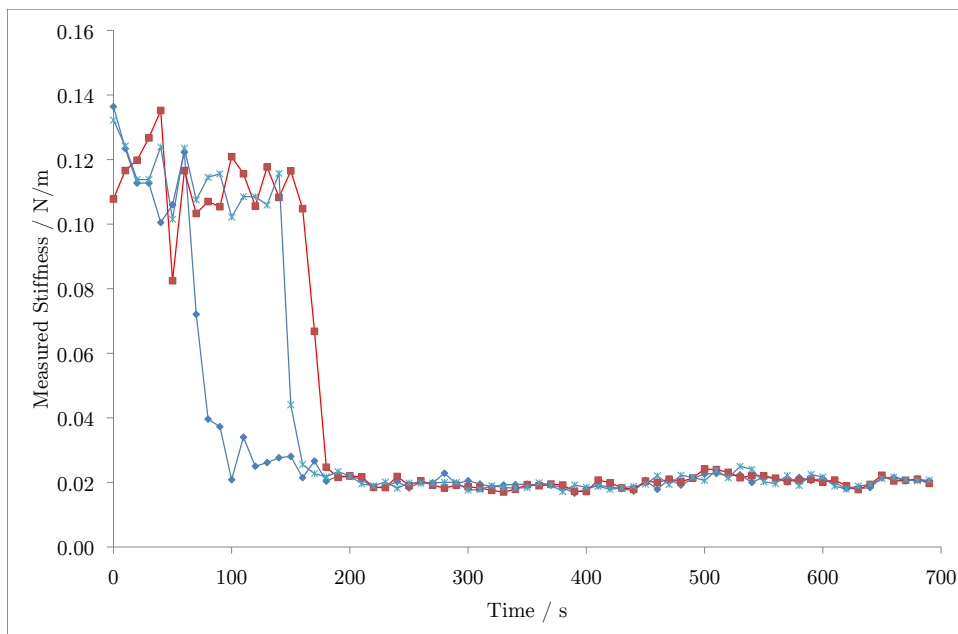


Figure 5.13: Effect of 1% SDS on the stiffness measurements of live cells.

The graph shows that after a short time the measured stiffness of the cells dropped to a value of approximately 0.02 Nm^{-1} , and unlike with the NaCl and Sorbitol there is no recovery. This is as expected since cells cannot survive with a compromised membrane.

The value that the stiffness drops to with the SDS is much lower than it was for either NaCl or Sorbitol. This is not too surprising since in the SDS case, the cell was losing a large amount of its internal material, not just some of its water, as was the case for NaCl / Sorbitol. However, as the SDS is damaging the membrane allowing the majority of the cellular components to escape, it would be

expected that the measured stiffness would have dropped to the value of the cell wall stiffness, at approximately 0.013 Nm^{-1} .

To check the significance of this measured 0.02 Nm^{-1} value, cells were incubated in PBS with added SDS for 1 hour, allowing the SDS to create similar damage to that caused in the experiments above. These damaged cells were then examined on mica in air, as it was very difficult to immobilise them in liquid once this damage had been done.

Figure 5.14 shows cells on mica imaged by contact mode in air before (left) and after (right) the SDS incubation. From a visual inspection of these cells it can be seen that after the incubation the cells do not look as healthy as before, as they appear much less 'full', more wrinkled due to the wall not being pushed out by the turgor pressure any more, and there is a lot more flattened wall material on the surface.

Force measurements taken on these cells again showed that the measurements targeting the whole cell compression with a contribution from the turgor pressure were giving readings of $(0.0208 \pm 0.0004) \text{ Nm}^{-1}$, as before. However when the softer cantilevers and lower setpoints were used in order to target the measurements at the cell wall, a very similar value of $(0.0207 \pm 0.0006) \text{ Nm}^{-1}$ was obtained.

One possible explanation for this is that the long exposure of the cells to SDS has had some effect, directly or otherwise, on the cell wall, stiffening it slightly. As the turgor pressure has dropped away to a very low value due to the damaged membrane, both sets of measurements are now only taking readings of the newly stiffened cell wall.

A study by Longo *et al* [128] found that ampicillin, another β -lactam antibiotic,

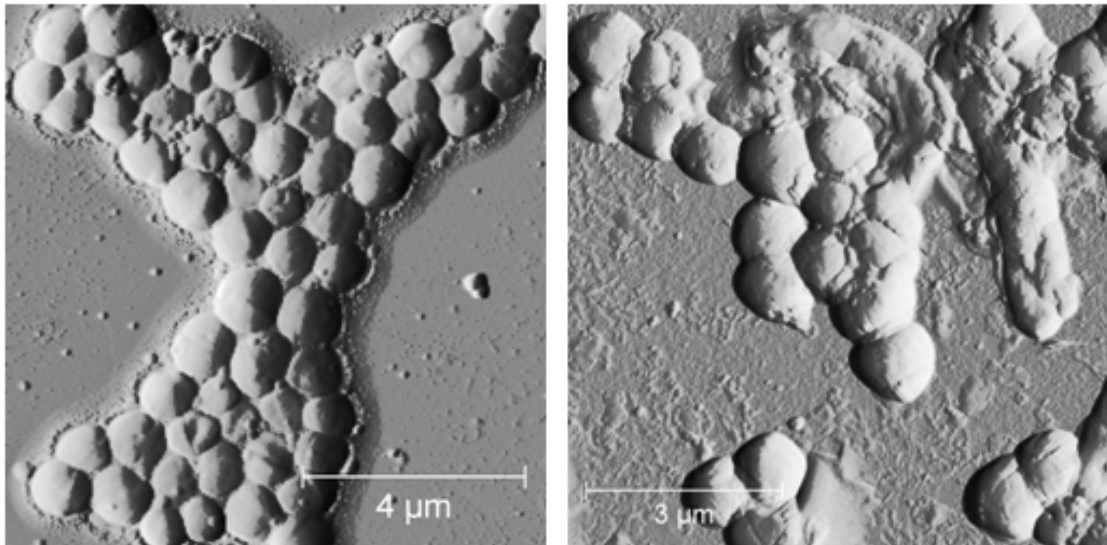


Figure 5.14: AFM vertical deflection images in air of cells before (left) and after (right) a 1 hour incubation in PBS with 1% SDS.

caused a stiffening of the membrane in areas where proteins inside the cell agglomerate on the inside of the wall after treatment. This potentially explains why these treated cells appear stiffened, and why the cell walls that were measured after boiling in SDS were not, as the proteins in the boiled cells were destroyed (and removed in the FastPrep).

5.2.11.5 Using Water as the Medium

The results when salt was added to the medium was relatively consistent in different media, with BHI, PBS and HEPES. However when pure water was used instead of a buffer the timescales changed dramatically. As shown in Figure 5.15, the time taken for the drop in pressure when the cells are in water is much longer than in PBS - and the drop itself is a shallower slope. The time taken for the pressure restoration is also increased, from approximately 10 - 15 minutes in PBS to somewhere in the region of 1 hour in water.

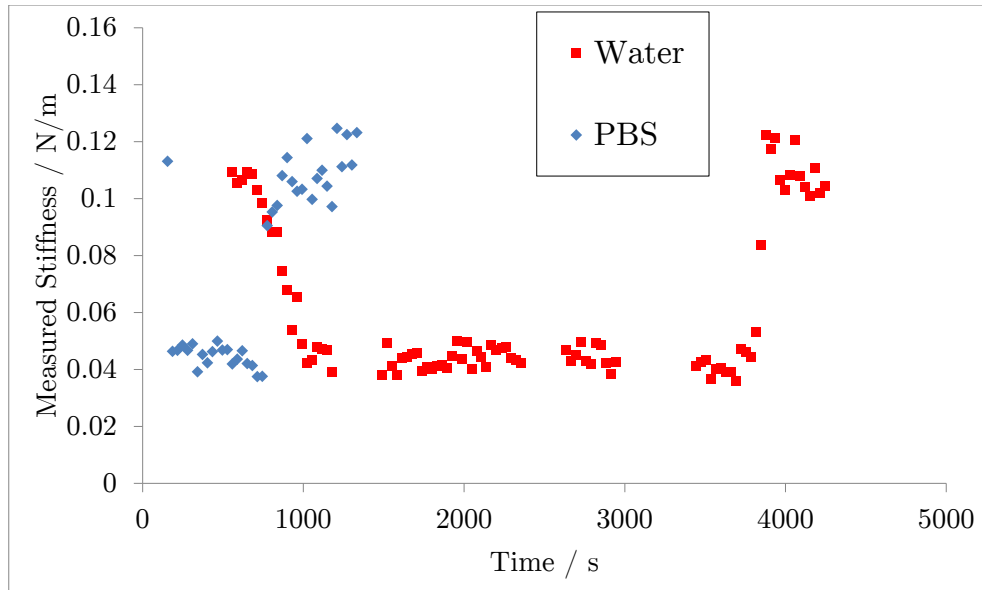


Figure 5.15: Comparing the use of water and PBS as the medium for the addition of NaCl.

The reasons for this shift are unclear, although it is understood that SA cells are in a stressed state in pure water due to the osmotic pressure across the membrane and wall. It is therefore a possibility that the cell has somehow shut down (or at least severely limited) movement across the membrane and wall, creating the initial delay. If the cell has gone into a shut down or dormant state, the active processes required to restore the turgor pressure would be expected to take longer, which would explain the large shift in recovery time.

5.2.11.6 Use of Chloramphenicol to Block Active Processes

Chloramphenicol is a bacteriostatic drug that blocks protein synthesis, and therefore stops any active processes being performed by a cell. It does this by binding

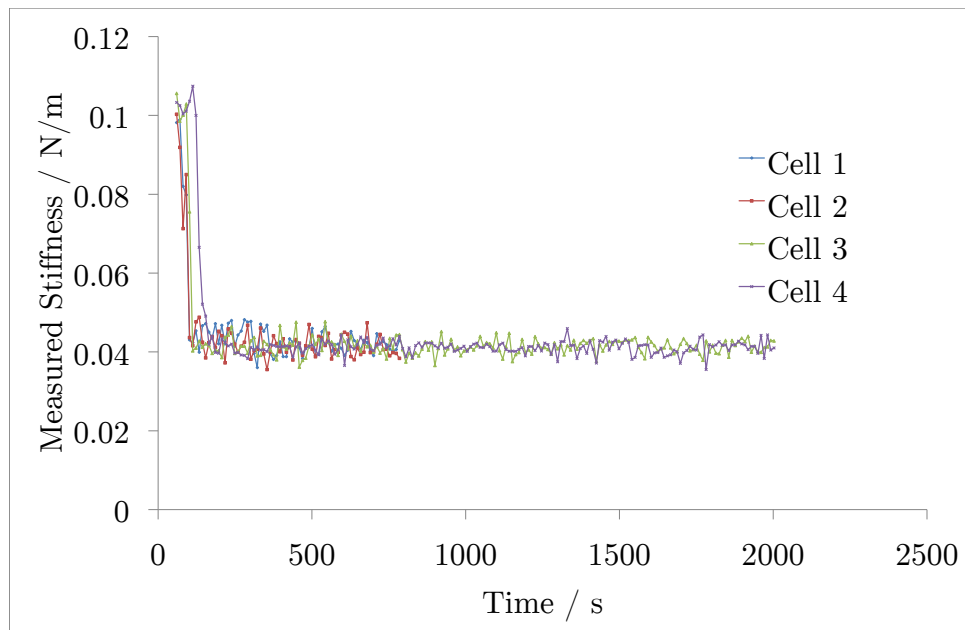


Figure 5.16: Measuring whole cell compression after the addition of both 1 M NaCl and 100 $\mu\text{g}/\text{ml}$ chloramphenicol to cells in PBS buffer, showing that the cell cannot restore its turgor pressure in this experiment.

to the ribosome, blocking the channels required for activity. Experiments were repeated for the addition of NaCl to live cells in both PBS buffer and water, but here also with the addition of 100 $\mu\text{g}/\text{ml}$ chloramphenicol at the same time. This was performed to see whether the loss and restoration of the cells' turgor pressure was due to active or passive processes, and may go some way towards explaining the unusual delay when water was used as the medium for these experiments. The results of monitoring the whole cell compression during these experiments are shown in Figures 5.16 (using PBS) and 5.17 (using water).

This data shows that in PBS the cells are unable to create the rise back to the initial value of the stiffness of the whole cell compression, as they had done in

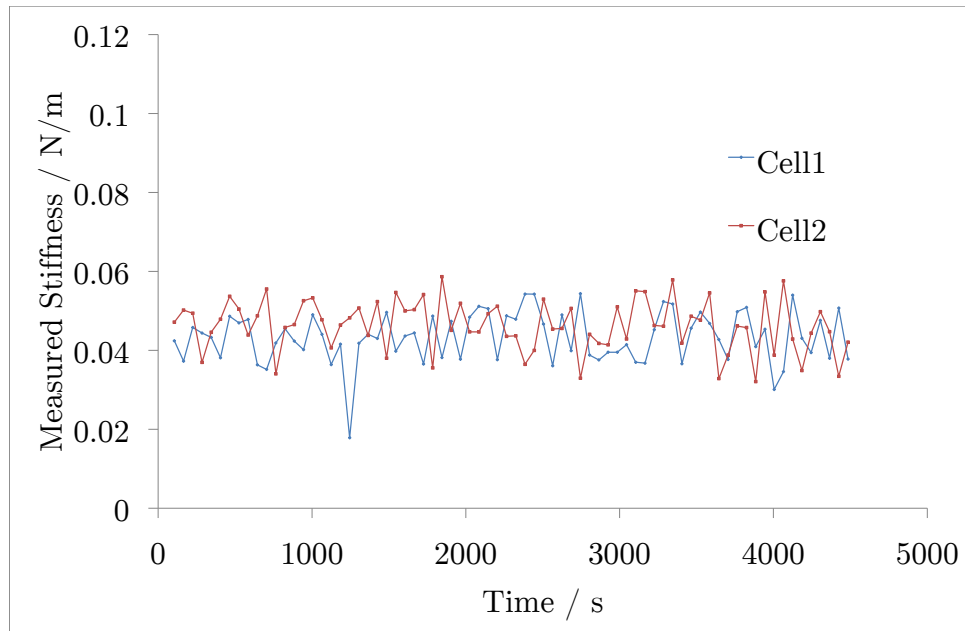


Figure 5.17: Measuring whole cell compression after the addition of both 1 M NaCl and 100 $\mu\text{g/ml}$ chloramphenicol to cells in water, showing that the cell cannot restore its turgor pressure in this experiment. Here it is also shown that the delay before the measurement dropped, as seen previously in water, does not exist.

just a few minutes previously (see Figure 5.9), which is also seen when the cells are in water. This indicates that the response seen previously was an active response, since the only difference here is the addition of the chloramphenicol to block the active processes. The second interesting feature of Figure 5.17 is that as the measurements are started, the cells have already lost their pressure and the measurements are at around 0.04 Nm^{-1} within 105 seconds, when the first data point was taken. It is difficult to start these measurements faster than this, as the first moments after the addition of the NaCl and chloramphenicol are used to quickly check that there has not been too much drift during the addition of the new material, ensuring that the force spectroscopy data is still being taken over a

cell surface and not elsewhere. This low measurement shows that the long delay during which the cell maintained the high value previously in water and NaCl (see Figure 5.15) indicates that this delay is also an active process, appearing to confirm the idea that the cell has somehow blocked transfer of material across its wall and membrane during the stressed conditions of living in pure water. This may not be a realistic assumption though, as there was probably not time for the cell to react to the change in osmolarity of the medium in order to synthesize anything or protect itself. The behaviour of these cells in water is still a little bit of a mystery, and is the subject of future work inspired by the data presented here.

5.2.11.7 TEM of Cells Exposed to NaCl

TEM images taken of thin sections of SA cells were taken before, during and after the drop in whole cell compression stiffness. The aim of this was to attempt to observe any changes in the internal structure of the cell, whether or not the cell membrane was still fully attached to the inside edge of the cell wall or whether the inside of the cell had shrunk and pulled the membrane away.

The resulting images from these data sets are shown in Figure 5.18. The cells in images 1 (a-c) in this figure have not been exposed to NaCl at all, so are used as a control and they appear as expected, with the cellular contents pushed up against the inside edge of the wall and appear to be dividing normally. The cells in images 2 (a-c) are taken at a time during which the cells studied by AFM were at their lowest measured stiffness, during the apparent drop in pressure seen within minutes of the exposure to NaCl. There is no indication from the appearance of these cells that they are under any stress or that their internal structure is

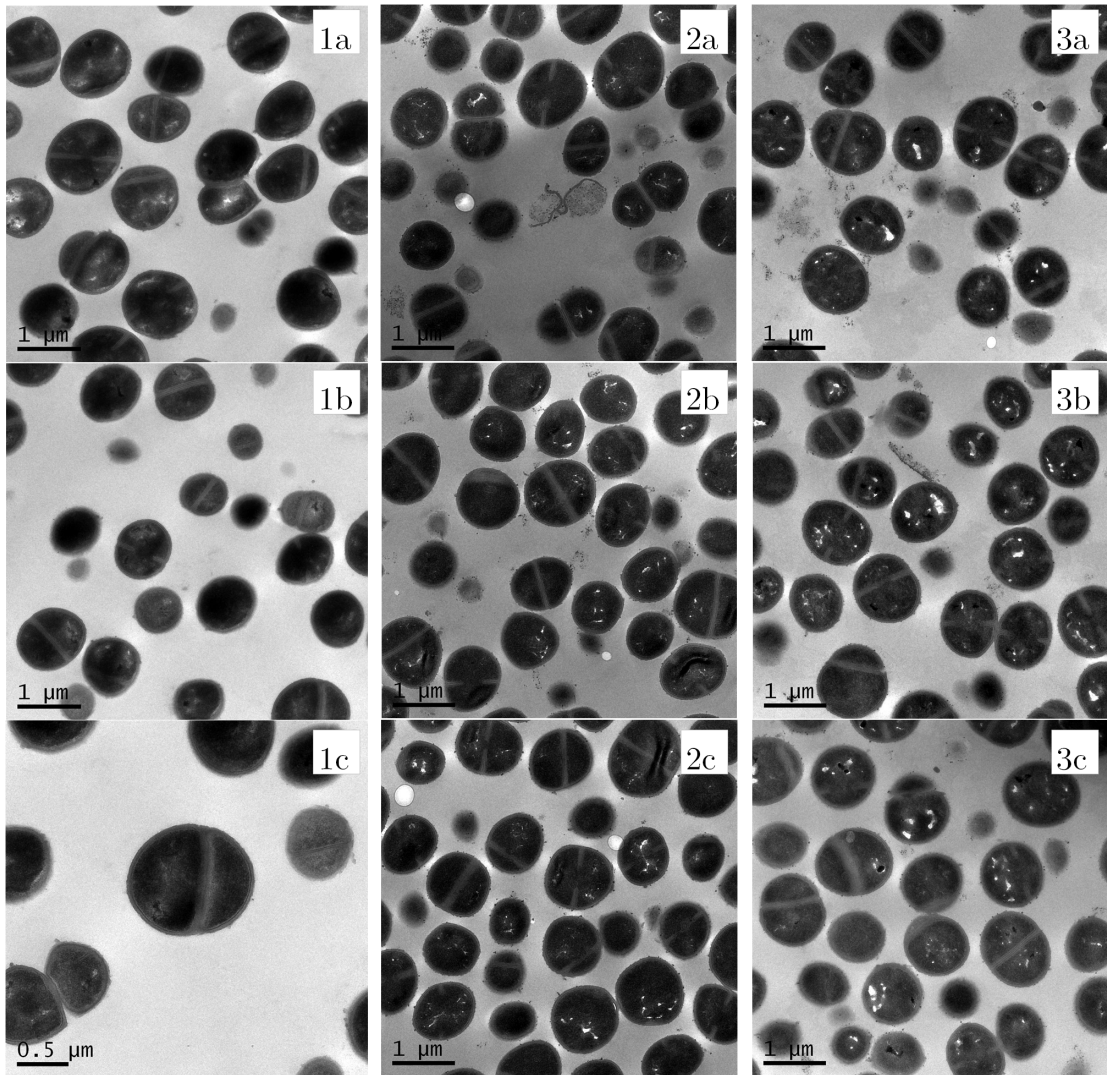


Figure 5.18: TEM images of cells before (1), during (2) and after (3) the drop in whole cell compression stiffness caused by the exposure to 1 M NaCl.

suffering, as they appear to also have their contents pushed up against the inside of the cell wall and there is no noticeable shrinkage of the cell membrane away from the inside edge of the wall. The situation is the same for the cells in images 3 (a-c), after the recovery of cells at the same stage observed by AFM. Again the membrane appears to be up against the inside edge of the cell wall. This is most likely due to the presence of lipoteichoic acids, which stitch the wall and membrane together, bridging the periplasmic space and binding to both components, ensuring that they do not become separated.

Throughout the entire process, there appears to be no noticeable change in the shape or the structure of the cells, indicating that although the AFM measurements indicate a change in pressure, there appear to be no visible changes to the shape or volume of the cellular contents. The bright white blotches visible on some of the images is due to the resin stain not reaching that particular part of the sample, and the reasons for this are unclear, although it is understood to be a reasonably common occurrence during TEM staining.

5.2.11.8 Stress Stiffening Test with Increasing Indentations

Cells were indented with setpoints from 1.0 to 7.0 V, at intervals of 0.5 V. The cells used for this experiment were those with a reduced measurement for the whole cell indentation, after exposure to both 1 M NaCl and 100 $\mu\text{g}/\text{ml}$ chloramphenicol, with the 0.07 Nm^{-1} tip. This was performed in order to see whether the measurement would increase with increasing indentation setpoint, due to either stress stiffening of the cell wall or an approach into a regime in which the cell was deformed to the point where the turgor pressure would be increased. The results from this experiment, for five averaged repeats, are shown in Figure 5.19.

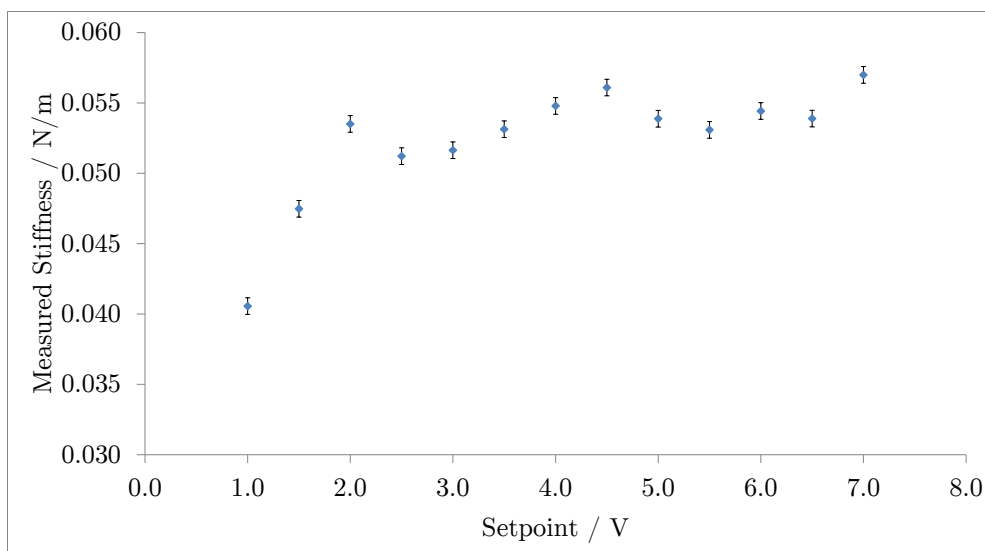


Figure 5.19: Measured stiffness on live SA cells when under stress due to exposure to NaCl, when indentation setpoint was increased in 0.5 V intervals. Error bars show 1 standard deviation over 5 repeat measurements.

The data shown on this graph indicates that the measured stiffness rises slightly for the first three data points, which is probably due to the tip indenting further into the cell, getting gradually more resistance. At an indentation setpoint of 2.0 V the measured stiffness levels off, and stays at approximately similar values right up to a setpoint of 7.0 V. This levelling off indicates that there is no stress stiffening of the cell wall during very deep indentation, as that would be seen as a constant increase in the stiffness at a small rate. Although this measurement is targeted at the whole cell compression and not at the cell wall itself, the stiffness of the cell wall will still be contributing to this measurement since the wall needs to be indented through in order to get this measurement. The indentation depth reached in this experiment, with a setpoint of 7.0 V for this tip, was (192 ± 4) nm ($n = 5$), a significant indentation considering that the diameter of the entire

cell is approximately 1 μm .

There also appears to be a repeating sinusoidal feature within this data. With peaks at 2.0, 4.5 and 7.0 V, and dips in between. This could suggest a rupture event, if the sharp tip is breaking through parts of the cell wall structure as it indents further and further into the cell.

5.2.11.9 Region 2 Conclusions

From the results of all of the experiments involving NaCl, Sorbitol and SDS to affect the turgor pressure within the cells, it appeared that the measurements taken were able to track and monitor the changes that were expected. It was therefore concluded that the second region of the two gradient force curves did have a component that was related to the turgor pressure.

5.2.12 Targeted Measurements

Once it was confirmed that the measurements taken appeared to be of two different properties, it was possible to target which of these properties was measured when taking force curves.

If the properties of the wall were required, then a soft cantilever, the 0.01 Nm^{-1} was used with a low setpoint of 1.0 V. This was tested and consistently found to give the correct measurements. Whilst it is in theory possible to just fit the initial part of one of the two gradient force curves to obtain this value, fitting to the whole of one of these softer curves was found to be much easier and much more accurate. Where the whole cell compression was the property of interest, the stiffer

cantilevers were used with a high setpoint. The 0.07 Nm^{-1} was the cantilever of choice, rather than the 0.1 Nm^{-1} , because it was easier to image the cells with this. 2.5 V was kept as the setpoint, and tests have found this to consistently give values close to the original for the second part of the force curves. In both cases the curves were fitted at the point of maximum indentation by fitting a tangent at this point. The indentation depths were approximately 10 nm for the cell wall indentations and 50 nm for the whole cell compression measurements.

5.3 Conclusions

In conclusion, live SA cells were immobilised on etched silicon wafer substrates for study in liquid by AFM. Mechanical measurements taken on these cells revealed force curves with two different gradients, and the change in between these two different parts was at an indentation depth roughly equivalent to the thickness of the cell wall. A proposal was therefore formed that the first part of the data was measuring the properties of the cell wall, before the tip experienced a second, higher stiffness due to indenting deep enough to feel the turgor pressure beneath the wall.

This proposal was tested initially by measuring cell walls that had no turgor pressure beneath them, as the contents of the cells were removed leaving fragments of cell wall that were studied and indented on a flat piece of mica. Small indentations on these cell walls revealed measurements in good agreement with the initial data. The proposal was secondly tested by forcing the cells to change their turgor pressure by adding different solutes to the surrounding medium, and monitoring any changes to the measurements at high indentation. These solutes caused either

an osmotic pressure across the membrane, or extensive damage to the membrane, in both cases causing the cells to lose water and consequently pressure. The cells that lost pressure due to the presence of NaCl or Sorbitol were able to recover their pressure after a short time, which is thought to be due to the accumulation of compatible solutes within the cell. Cells that were irreversibly damaged with SDS were unable to recover, and lost more pressure than those in NaCl or Sorbitol, due to the greater volume of water that would be expected to leave the cell when damaged. The choice of medium for the experiments with NaCl and Sorbitol had little effect if PBS, HEPES or BHI was used, but the timescales were much longer in water, possibly due to the cell employing some kind of shut down mechanism when in stressed conditions. The AFM measurements in all of these experiments were able to measure these changes, indicating that the turgor pressure was contributing to the data taken at high indentation forces. The use of chloramphenicol to block protein synthesis showed that both the recovery, and the delay observed when water was chosen as the medium, were due to active cellular processes as these only occurred when there was no chloramphenicol present. Transmission Electron Microscopy of thin sections through cells before, during and after the drop in measured stiffness revealed that the internal parts of the cell suffered no visible changes throughout this process, with the cell membrane remaining pushed up against the inside of the cell and the cytoplasm still filling the whole cell volume. This means that although the pressure is measured to change, the volume of the cell does not appear to change significantly.

Cells were indented up to approximately 20% of their diameter in order to see if there would be any stress stiffening of the cell wall during this large distortion. Despite a small rise during the first three data points, the measurement soon levelled off and stayed at a similar level throughout the next ten measurement

points.

Both parts of testing the proposal appeared to indicate that the initial idea was correct. This meant that at low forces, the properties of the wall were measured, and at high forces, the turgor pressure was contributing to the measurements, so it could be monitored. By knowing what force was being applied, and by selecting a suitable cantilever and indentation setpoint, it was possible to target measurements at the required property to be measured in a particular experiment. It is proposed that the low forces are creating small indentations into the cell wall, and at higher forces the tip starts to compress the whole cell. This conclusion is backed up by experiments with blunted tips, showing that increasing the contact area increases the measured stiffness of the cell wall but not of the whole cell compression, as expected for these indentation schemes.

Values for the two different regions were found to be $(0.0134 \pm 0.0068) \text{ Nm}^{-1}$ for the cell walls and $(0.2062 \pm 0.0039) \text{ Nm}^{-1}$ for the whole cell measurements, with the pyramidal silicon nitride tips used for this study.

6 | Mechanical Mapping

6.1 Introduction

Mechanical mapping is a very useful technique for studying the differences between different samples, or even different parts of the same sample. As a force curve is taken at each pixel of the map, the image is constructed from a colour scale of different quantities taken from the curves. The most commonly used of these are sample height, stiffness and adhesion.

In this study, the main emphasis is on the stiffness maps. These were used on cells in both stationary and exponential growth phases, to attempt to see differences both between the two stages, and also between different areas on the same cell.

As it was possible to target the measurements at either the cell wall of the whole cell compression with a contribution from the turgor pressure, maps of both of these properties were able to be taken separately. This allowed the search for differences to be performed on both sets of measurements.

For example, in exponential phase, is there a difference in the properties of the

new and old cell wall on a cell that has just split, revealing the new wall on the septum? In terms of the turgor pressure, is there a difference between a cell at stationary phase and a cell that is about to divide, and if there is, could this contribute to the separation of the two daughter cells?

Maps were therefore taken on cells in both growth phases, at various different stages of growth, with both wall and pressure measurements. These maps were then edited by setting the scales on all of the corresponding maps to the same value, allowing direct comparison.

To maximise the usable data from a force map, the maps were positioned and sized such that the cell filled as much of the map as possible, leaving minimal empty space around the edge. As the edges of the cells are difficult to measure accurately due to the angle of this part of the surface potentially creating artefacts, only a 6 x 6 grid from the very centre of each 32 x 32 grid was used to collect quantitative data.

In total over 20 cells were mapped under each condition, unless otherwise specified, giving a broad sample population.

Unless otherwise stated, this data was taken with the cells in PBS for cell wall measurements, and in BHI for the pressure measurements. This allowed measurements of the cell wall with living cells, but that there would be no active growth processes carrying on due to the lack of nutrients available to the cells. This allowed the measurement of various different stages of growth without the cell walls changing during the measurements. The whole cell compression measurements were taken in BHI in case the cells in PBS were not at 100% of their natural turgor pressure.

6.2 Results

6.2.1 Measurement Boundary

The first step when analysing a force map of a topographic surface such as these cells is to check how much of the map was actually usable. As the surface of a SA cell is so curved, measurements taken on the top of the cells should be fine, as this surface appeared relatively flat to the tip. However the closer to the edge of the cell that the tip got, the steeper the slope got. When the AFM tip attempts to indent a steeply sloping surface, it doesn't really indent at all, and rather slips on the edge or twists, instead of indenting as expected.

To do this, the height map over a cell was taken and an individual slice across the centre of the map was analysed. At each point on the map the stiffness was measured from the corresponding force curve. From this data it was easy to check at what point the curves started to become unusable. In the centre of the slice, the stiffness readings were all broadly similar, but at the edges the numbers started to drop off rapidly, giving almost random results, some even turning out negative. It was therefore easy to select a region from which the curves could be used.

An example of one of these slices is shown in Figure 6.1. This example is taken from a height map measuring the cell wall. The stiffness measurements corresponding to each point on the map are shown below the slice as a number and a point on a stiffness versus position graph.

It shows that in the centre of each slice, as indicated by the green stripe below the graph, the measurements are all within acceptable limits (i.e. within noise)



Figure 6.1: Example slice through the centre of a force map, showing a stiffness vs. position graph for the measurement from each point.

of the averaged value. Where the height slice image starts to fade towards black the readings become much more deviated, and there is no longer any consistency between neighbouring values, indicated by the red stripes. This is most likely to be due to the tip slipping and/or the cantilever twisting as it approaches a surface at an incline to the horizontal, so it does not indent the surface as expected.

To ensure that the readings taken from a map were of suitable quality, curves were only used from a 6 x 6 grid from the centre of a 32 x 32 grid. This meant that only 36 out of 1024 possible curves were used per force map, but it ensured the quality of the data, removing effects due to the topography of the edges of the cell surface.

It would have been possible to take force maps just over the centre of the cell, allowing all of the curves to be used in analysis, but it was useful to be able to see the whole cell on the map for a visual comparison of different regions of the cell, and also to compare the whole cell to other maps taken on other cells.

6.2.2 Stationary Phase

Maps were initially taken on cells in stationary phase. As with the initial force curves, stationary phase cells are not expressing any growth features, so in theory all cells should have more or less the same properties. Comparisons between different cells should therefore show minimal variation, and a good idea of the heterogeneity of the cell as a whole could be seen. These results could then be used later to compare against cells in exponential growth phase.

Maps were taken at both low indentation, to map the cell wall, and at high indentation, to map the whole cell compression, and the contributions of the turgor pressure.

6.2.2.1 Mapping with Low Force

Maps of the cell wall were taken with the 0.01 Nm^{-1} cantilever, with a setpoint of 1.0 V. As expected for stationary phase, there was little difference seen both across the surface of each cell, due to the relative homogeneity of the cell wall in stationary phase, and also between different cells, as they were all at the same growth stage.

Three example cell wall maps are shown in Figure 6.2. The slight variations that appear in the maps are likely to have been due to small amounts of noise in the data, as when the data was extracted numerically each cell had very similar overall values, within the experimental errors, and these values match very well with the data collected from the individual force curves in Chapter 6, with a result of $(0.0132 \pm 0.0021) \text{ Nm}^{-1}$. Student's t-tests comparing different cells to each other

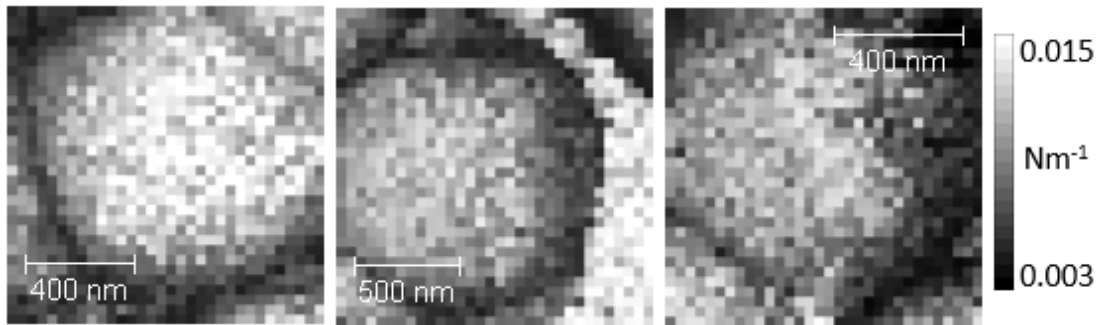


Figure 6.2: Three examples of cell wall stiffness maps showing little distinguishable variation on each cell, and between different cells.

and to the original measurements were in the range $p = 0.11 - 0.60$, showing that the data is likely to be from the same population.

These force maps, along with some of the others shown later, show cells that have taken on slightly irregular shapes, compared to the regular spheres that are expected from SA cells. This was seen many times during this study, and it appeared that the cells were taking on the shape of their container to a certain extent. This means that cells that were sunk into wells that were not round, or cells that were squashed tightly up to neighbours on the surface were changing shape slightly to better occupy the available space. This changing of shape depending on the cell's container was also noted by Kailas *et al* [41].

6.2.2.2 Mapping with High Force

High Force mapping was performed to look for variations in turgor pressure. These maps were taken with 0.07 Nm^{-1} tips at an indentation force of 2.5 V .

The results were visually very similar to the stationary phase cell wall maps when imaging cells in stationary phase with high forces, to indent into the turgor pressure. There was little variation seen between the cells, and also hardly any

difference in measurements across individual cells. The readings acquired from the force curves were also in good agreement with those obtained from individual force curves at high indentation force. Example force maps from this data set are shown in Figure 6.3.

These maps appear brighter than the cell wall ones due to the measured stiffness for the whole cell compression being much higher than that for the cell wall. Values taken from 20 of these maps gave a result of $(0.202 \pm 0.019) \text{ Nm}^{-1}$. Student's t-tests on these measurements, both between different cells and in comparison with the original force curves, gave p values in the range 0.14 - 0.67, again showing good agreement between these data sets.

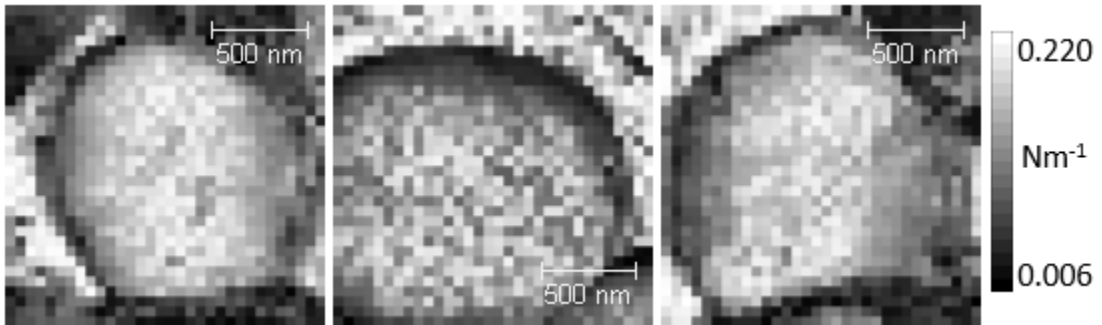


Figure 6.3: Three examples of whole cell compression maps on stationary phase cells showing little variation on each cell, and between different cells.

6.2.3 Exponential Phase

Cells were then mapped in exponential phase. As this covers a range of different growth stages, from the initial formation of the septum right up to the point where the two daughter cells are separated and fully expanded, data was collected across the entire range and the different stages could therefore be compared.

6.2.3.1 Mapping with Low Force

As cells were always imaged before force maps were taken, various different features of exponential phase could be recognised in the images, and the force data could consequently be linked to the feature that it was taken over.

Cells were seen at all stages of division, from the edge of the septal plane just becoming visible from the outside, up to the new cell wall being visibly starting to round up to form the spherical shape required. This allowed the comparison between different features at different growth stages, and between parts of the cell that visually appeared to stay the same throughout a single division, such as the cell wall around the rest of the cell, away from the specific division site.

6.2.3.2 Low Force Measurements During Stage 1 of Division: Septum Visible

The first external sign that a cell has started to undertake the division process is when the outer edge of the septum starts to become visible on the cell wall. This appears as a slightly indented ring around the edge of the cell. As the septum fully forms before there is any visible indication visible at the outside edge of the cell wall, cells at this stage of the division cycle are likely to already have fully formed septa, but this is the first point at which there is any external visible indication of division.

Force maps of the cell wall were taken of cells at this stage to compare the cell wall to that at stationary phase, so see if the stresses and strains of division were having any mechanical effect on the wall.

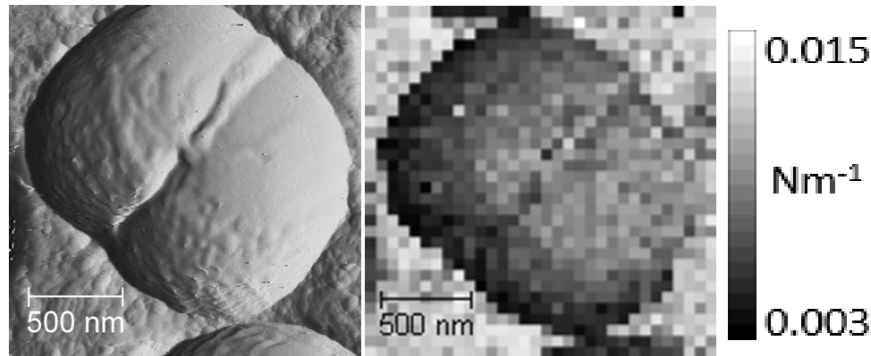


Figure 6.4: AFM vertical deflection image (left) and force map (right) of an SA cell as the septum shows on the outer wall.

An example of the data taken at this stage is shown in Figure 6.4. The vertical deflection image on the left shows the visible mark where the septum has started to break the outer cell wall, but has not caused the cell to separate yet.

Measurements taken on cells at this stage allow the properties of the wall around the cell to be taken. The majority of the wall should be the same as at stationary phase, as the only new wall made during the division process so far is still enclosed inside the cell. Values taken from the wall measurements at the growth stage were in the range $(0.0133 \pm 0.0019) \text{ Nm}^{-1}$, in good agreement with the stationary phase values. This indicates that the parts of the cell wall that are not directly located at the division site suffer no measurable change during the onset of division.

6.2.3.3 Low Force Measurements During Stage 2 of Division: Cells Rounding Up

The next easily visible part of the division cycle that was targeted was as the two halves of the dividing cell started to round up. This implied that the two daughter cells were parted by a completed septum, and they were starting to fully separate, beginning to expand into two fully formed spheres.

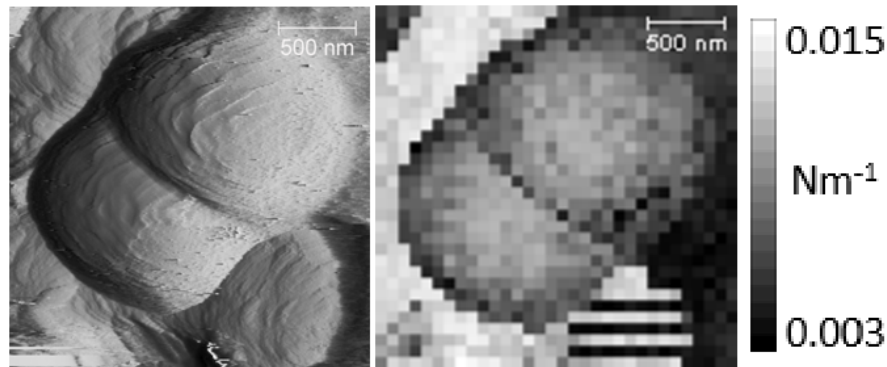


Figure 6.5: AFM vertical deflection image (left) and force map (right) of an SA cell as the cells start to round up after the septum has finished forming.

The confinement in the wells could be preventing the complete separation of the two daughter cells when the cell is sat with its division plane side - on to the substrate, keeping the pair immobilised together nicely for taking measurements. Data taken here would further be able to identify the properties of the cell wall away from the division site, adding to the data taken when the septum was just visible from the outside.

An example of a cell at this stage is shown in Figure 6.5. When the curves over the two halves of the dividing cell were extracted and analysed, it was found that there were no significant differences between the cell wall properties between the two sides of the same dividing cell. The measurements acquired here also showed that the measured stiffness was in very good agreement with all of the data taken previously, indicating that the properties of the wall had still not changed significantly. The values measured at this growth stage were (0.0134 ± 0.0012) Nm^{-1} .

6.2.3.4 Low Force Measurements During Stage 3 of Division: Exposed Septal Material

The final growth stage that was studied, before the cells became two fully formed daughter cells was when the cells had become separated. When this happened with the cells in a suitable position, the new cell wall of the septum was occasionally seen on the top surface, as viewed by the AFM.

When cells at this stage were found suitably orientated, it was possible to examine the newly formed cell wall material of the exposed septum. It is believed that once the septum is completed, the cell does not make any more wall to expand the septum into the fully rounded hemisphere that it becomes. This means that there should be enough material in the flat septum to expand into the hemisphere, so the septum should be more dense than the rest of the cell wall. The measurements taken on septal cell wall were therefore expected to show a higher measured stiffness, although the extent of the increase was unknown.

Figure 6.6 shows a cell that appears to have just separated, revealing a patch of new septal cell wall in the centre, indicated by the red circle. The deflection image on the left appears to show that the new wall has a different structure to the old wall, as it appears smoother.

The force map on the right also appears to show visually that this patch of new wall is brighter than the rest of the cell. This indicates a higher measured stiffness, as predicted, and when the measurements were quantified the values confirmed this. The curves over the new wall gave a value of $(0.0169 \pm 0.0013) \text{ Nm}^{-1}$, higher than the values of the older cell wall. Measurements were also taken on the old cell wall from this map, giving a value of $(0.0132 \pm 0.0027) \text{ Nm}^{-1}$, similar to the values

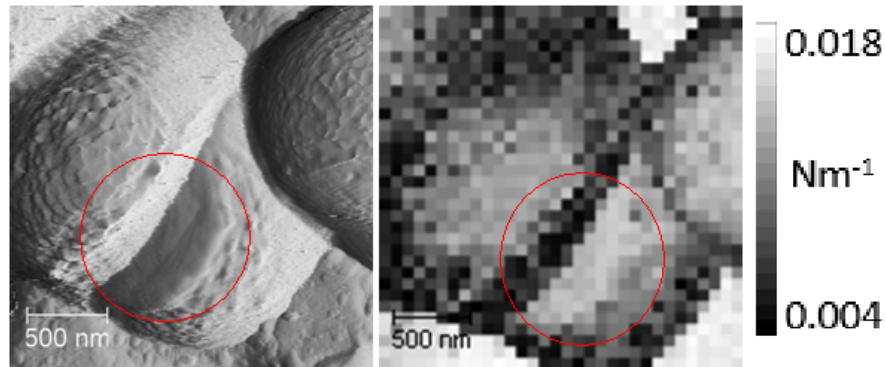


Figure 6.6: AFM vertical deflection image (left) and force map (right) of an SA cell showing new cell wall, indicated by the red circle.

obtained previously for the cell wall.

The data taken from this force map is not ideal, since there is only a small region from which the data could be collected, so a number of further cells were studied. It does however provide a nice clear difference between neighbouring regions of old and new cell wall, with the corresponding differences in measured stiffness. Adjacent to the brightly shaded new cell wall on the map is a region that is much darker, almost black (across the top right of the red circle). From the corresponding area on the image this part of the cell appears to be almost vertical, as shown by the arrows in Figure 6.7, so the tip is likely to be slipping or twisting as it makes contact here. Due to these factors, data to be fully analysed for this section was not taken from cells such as the example shown in Figures 6.6 and 6.7, but from cells with much larger areas of new cell wall that are roughly horizontal, providing much more reliable indentation data.

When cells were to be studied with the new cell wall at the top surface of the cell, it was not possible to identify them by the contrast between old and new such as in Figure 6.6, as the majority of the visible surface would all be new wall, giving little visual contrast between the two. Fortunately it was possible to identify the new

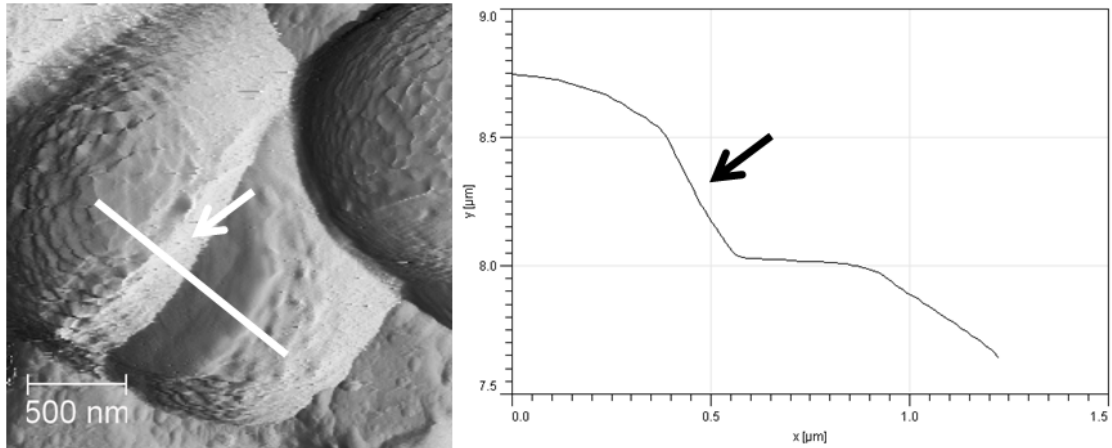


Figure 6.7: AFM vertical deflection image (left) showing corresponding height profile (right). Arrows indicate the steep region from which data would be unreliable.

wall by a particular characteristic feature of newly formed septal cell wall.

When the septum is formed, it grows steadily inwards, like the closing of a camera aperture [42]. As a consequence of this growth pattern, the septal material is formed of concentric rings [129], much like the rings on the cross section of a tree trunk. When a cell is imaged and part of the wall is displaying rings like these, it is a very strong indication that the cell wall being observed is that of a recently exposed septum. The images in Figure 6.8 show cells showing these rings on their surface.

Another feature that these images show quite nicely is the way in which consecutive divisions in SA occur. Tzagoloff and Novick [43] report on how consecutive division planes in SA are always perpendicular to each other. This is apparent in these images, as the line of little indentations visible on the surface of the cells indicates the location of the outer edge of a septum forming. As this is cutting across the surface of the cell which is showing the concentric rings, it implies that the newly forming division plane is at 90° to the previous one, which formed these

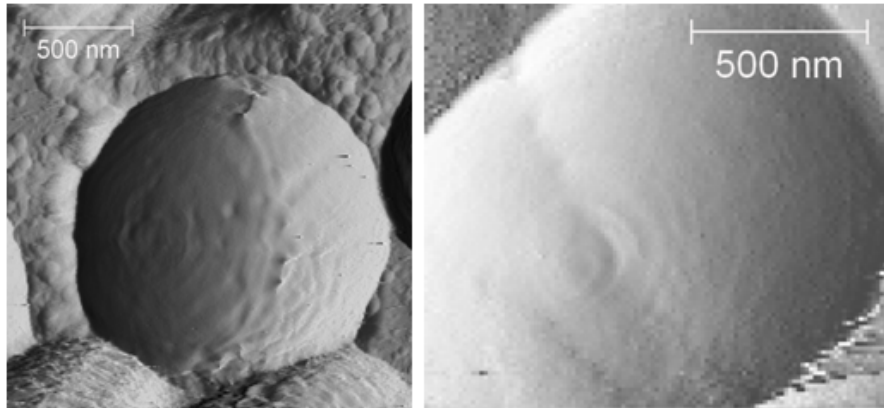


Figure 6.8: AFM vertical deflection images showing typical rings as seen on new septum surfaces.

rings.

It also demonstrates the speed with which these cells are dividing. The septum from the last division cycle is still new enough that it shows the concentric rings and has not yet fully expanded to make the cell a full sphere, and yet the first signs of the next division cycle are already in place. It is known that in ideal conditions SA divides approximately every 24 minutes, but this rapid formation of the next division plane was still a little surprising.

The values extracted from mapping these new areas of cell wall, indicated by the concentric ring pattern and measured on cells that were still roughly hemispherical in shape, was $(0.0157 \pm 0.0012) \text{ Nm}^{-1}$, close to the value taken from the map in Figure 6.6, and stiffer than the measurements of the older cell wall, as expected.

These results add weight to the theory that the material in the septa should be more dense than the older cell wall, due to its need to expand from the septum to the full hemisphere without making any new material.

The Student's t-test was again used to compare these sets of data, and gave p

values in the range 0.16 - 0.91 for the different areas of the old cell wall, showing very good agreement. When the old cell wall was compared to the new areas of the wall that appeared to be stiffer, the p values ranged between 4.25×10^{-6} and 1.41×10^{-23} , proving that there is a significant difference between the old and the new wall.

6.2.3.5 Mapping with High Force

Cells were also mapped with the 0.07 Nm^{-1} cantilever at a setpoint of 2.5 V to obtain data on the whole cell compression at various different stages of the growth cycle during exponential phase.

Cells were targeted at the same stages that were measured for their cell wall properties, to get a good comparison and to look for correlations between the different measurements at corresponding stages of division. Examples of these maps are shown in Figure 6.9, with force maps on three cells at different growth stages. The left hand cell was mapped just as the septum was starting to show on the outside of the cell wall. The centre cell was mapped after the cells had split and started to round up, but were still connected together. The right hand cell was mapped when the other daughter cell had come away and the septum with its concentric rings was visible on the top surface of the cell.

The measurements taken from 20 of these cells were found to all be very consistent with one another, and with the data from the initial two - gradient force curves, giving values in the range $(0.210 \pm 0.021) \text{ Nm}^{-1}$

Figure 6.10 shows a sample of this data. Each point on the graph is an average over the points taken from an individual cell, with the sample number indicating

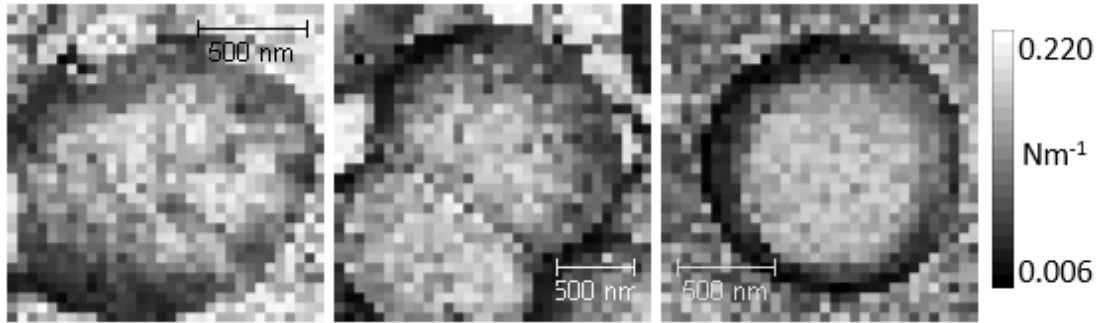


Figure 6.9: Three examples of whole cell compression maps taken on exponential phase, dividing cells, showing little variation on each cell, and between different cells.

the order of the division stage at which the cell was when the data was taken. The blue line, labelled ‘b’, is the average of this data, and the red line, labelled ‘c’, is the average of the data taken on cells at stationary phase.

Although the exponential phase cells appear to be slightly stiffer, this is not a particularly significant change from the stationary phase value. The new value is $(0.2084 \pm 0.0014) \text{ Nm}^{-1}$ compared with the stationary phase value of $(0.2062 \pm 0.0039) \text{ Nm}^{-1}$. A statistical t-test on these two data sets gave $p = 0.37$, so it is likely that the two data measurements are from the same population. There also does not appear to be any kind of pattern in the values from Figure 6.10.

With these considerations, it does not appear that the turgor pressure, as measured by this technique, changes significantly during the division process. This is not what was predicted, since the proposal involved an increase in the turgor pressure that could help to separate the daughter cells.

This proposal was an attempt to explain how the two daughter cells pull themselves apart once the septum has fully formed between them. The idea was that both daughter cells contain enough material to form two fully formed daughter cells, but at this stage they are only approximately 50% of that size. It was therefore

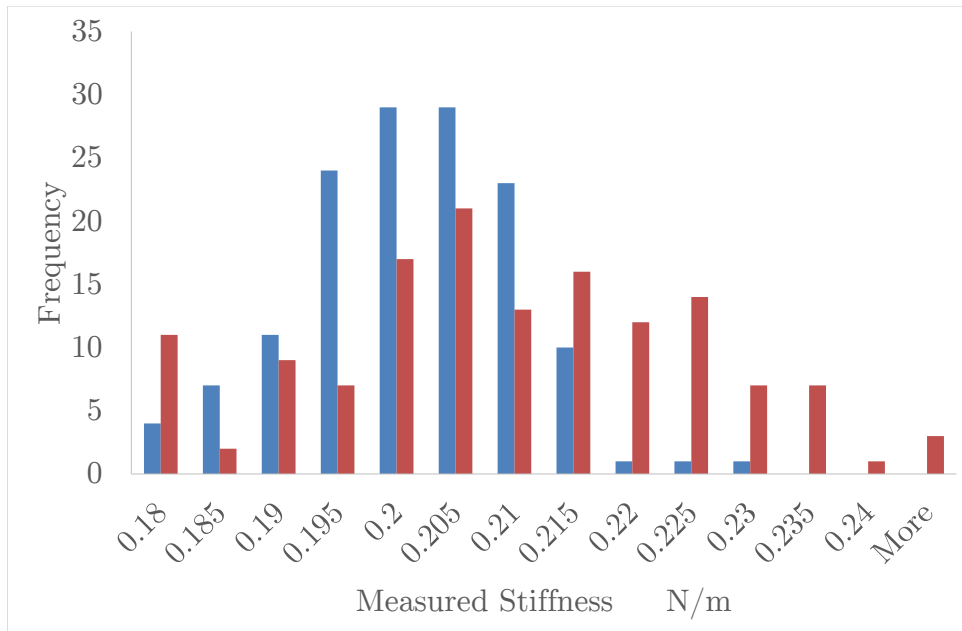


Figure 6.10: Measurements of the whole cell compression taken on cells at different stages of the division process. Key: Blue: Stationary phase data; Red: Exponential phase data.

proposed that there would be an increase in the turgor pressure in the cells, which would help to separate the cells as the pressure in each daughter cell is pushing the flat wall of the septum out, to form a more stable spherical shape.

However, as the data does not show a significant increase, which would be expected particularly towards the end of the division cycle, this proposal appeared to be incorrect.

6.2.3.6 The ‘Pie Crust’

In order to attempt to understand the separation stage of cell division better, the next set of experiments were performed taking force maps on very small regions of the cell wall, targeting the measurements at the point where the edge of the septum was visible at the outer surface. These measurements would target the part of the cell sometimes known as the ‘pie crust’. Turner *et al* [42] describe this feature in detail, which is also covered in Chapter 2. It is essentially the outer edge of the septum where it meets the cell wall.

If the properties of the pie crust are significantly different from the rest of the cell wall then it could contribute in some way to the daughter cell separation process. Since the part of the old cell wall that initially holds the two daughter cells together will be between two pie crust ridges, the pie crust itself may have a part to play in breaking open this connecting wall and separating the two daughter cells.

Figure 6.11 shows a vertical deflection image of a dividing cell showing the outer edge of the septum visible on the cell wall. The height profile of the line across the cell is also shown. The locations of the pie crusts on either side of the septum (indicated by the arrows) appear as ridges on the height profile, and the connecting wall between the two appears as a valley between the two peaks.

By taking small force maps over the centre of cells such as the one in this example, it was possible to compare the measured properties of the pie crust edges and the connecting wall between the two, and to compare these two features with the rest of the cell wall.

The force map taken on the above cell is shown in Figure 6.12. The box on the

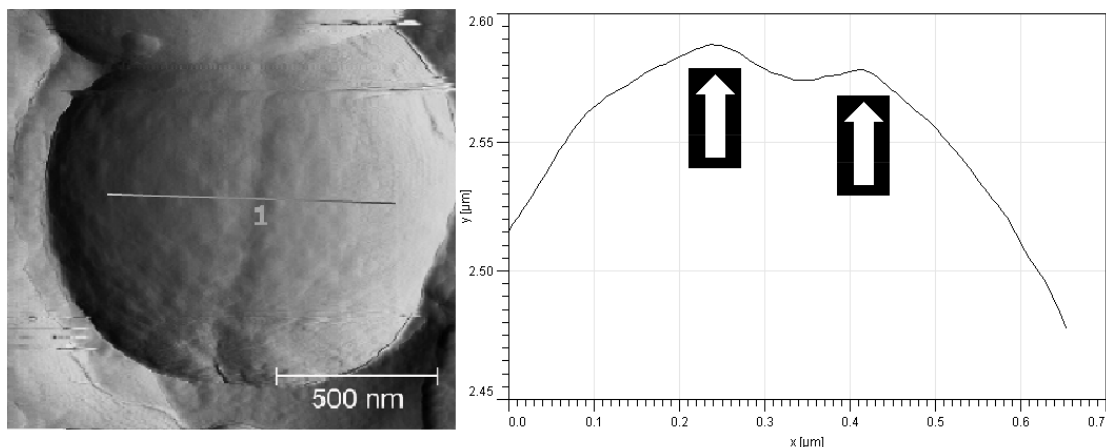


Figure 6.11: AFM vertical deflection image (left) and corresponding height profile (right) showing the pie crusts of a dividing cell, indicated by the arrows.

vertical deflection image on the left of the figure represents the area over which the force map, on the right, was taken. This area was 300 nm^2 , allowing the map to contain data on both pie crusts, the interconnecting region between them, and also a little of the rest of the cell wall, to the outside of the pie crust. There is only very little data on the outer cell wall in these maps, so values for this were taken from larger maps over the cell surface. These small maps were used to gather data on the pie crusts and the interconnecting material specifically. In total 10 pie crust maps were taken, on different cells, all of approximately the same size.

As the differences between the values for the different regions of these maps are very small, they can be difficult to distinguish by eye on some of the maps. However as with the one in Figure 6.12, it can be seen that the strip down the centre of the map is dark, indicating it is less stiff than other parts of the map. The two strips either side of this are much brighter, so the pie crusts are somewhat stiffer than the rest of the map. The small region of regular cell wall to the left also appears darker, so the pie crusts may not only be stiffer than the interconnecting material, but also stiffer than regular cell wall.

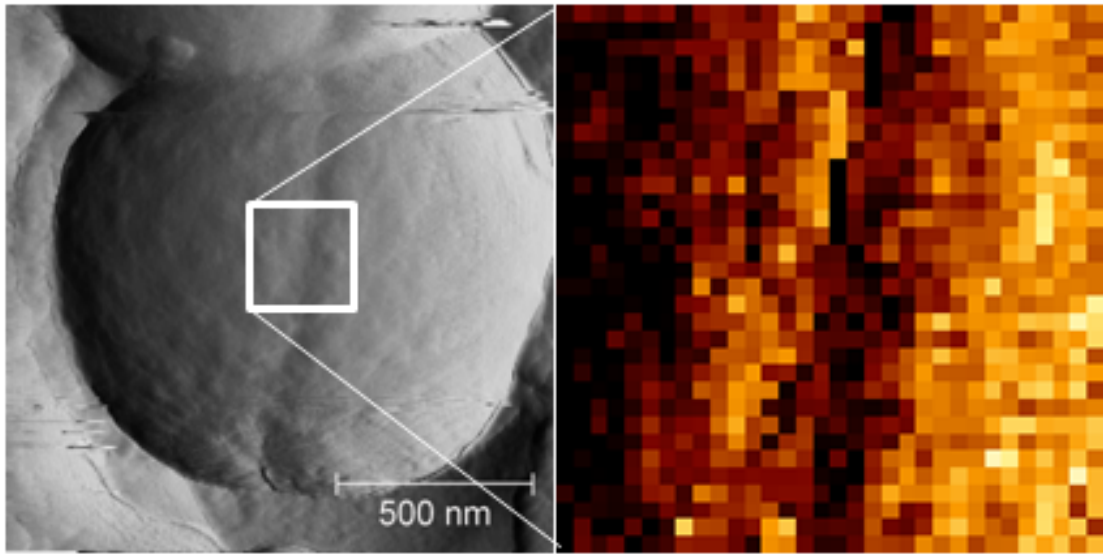
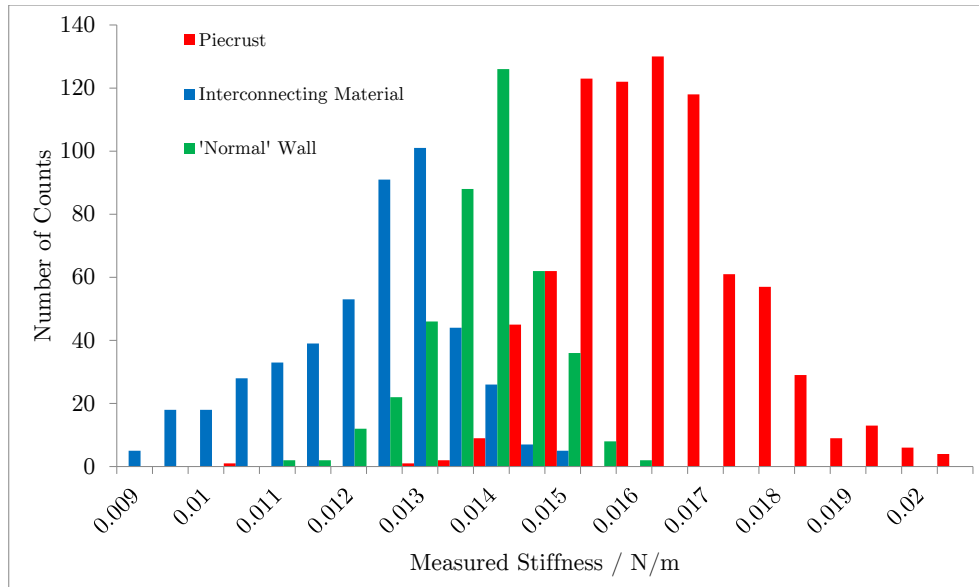


Figure 6.12: AFM vertical deflection image (left) and corresponding 300 nm² stiffness force map (right) showing the pie crusts as being stiffer than the central, septal cell wall. Force map Z scale from 0.003 - 0.015 Nm⁻¹.

Figure 6.13 shows a histogram containing the data taken from 10 of these maps, and values of the stiffness of the majority of the cell wall taken from larger maps over the same cells. The data confirms what was seen visually from the maps, although with very small differences between the data sets. The data indicates that the majority of the cell wall, green on the histogram, is at a very similar measured stiffness to at all other growth phases with a value of (0.0135 ± 0.0016) Nm⁻¹, as expected. The measurements taken over the pie crust however appear to have a wider spread, and the values are slightly higher than the regular wall, measured at (0.0162 ± 0.0025) Nm⁻¹. Finally the interconnecting material between the two pie crusts was measured at (0.0118 ± 0.0021) Nm⁻¹, slightly softer than the standard wall.

Although these changes in measured stiffness are only small, they could contribute to the separation of the two daughter cells. The stiff ridges around the pie crusts could help to break apart the interconnecting material between them, separating



The slight drop in stiffness of the interconnecting region of the wall between the two pie crusts can be explained using a current theory on the biology of cell division. It is understood that this part of the wall is digested by enzymes, called autolysins, when the cell is ready to divide [42, 39, 130], so as the wall is being degraded it will appear softer to indentation.

The sketch in Figure 6.14 shows a cross section of what is believed to be happening at this stage. In this sketch, the central strip is being digested by enzymes, making it appear soft to indentation. The strip either side of that is reinforced by the pie crust underneath the cell wall, which is supporting the weakened corners of the cell wall during the stressful separation process, appearing stiffer to indentation. Either side of the pie crust the cell wall is as normal.

6.3 Continuum Plate Theory

By using continuum plate theory [131], the stress in a cell wall can be described by modelling its shape. For an area of cell wall that is flat, homogeneous and circular, the maximum stress at the centre due to the turgor pressure p is of the order $p(R/t)^2$, where R and t are the radius and the thickness of the cell and cell wall, respectively. This flat cell wall is subject to a compressive stress in its inner surface and an equal magnitude tensile stress on its outer surface. A spherical area of cell wall is subject to a uniform tensile stress of the order of $p(R/t)$, which means that the ratio of the maximum stress between these two cases is of the order of R/t . This is only a simple analysis, but it reveals that the peak stress in a hemispherical cell is more than ten times higher than that of the spherical cell. Because of this, the stress in the flat cell wall causes some deformation towards the

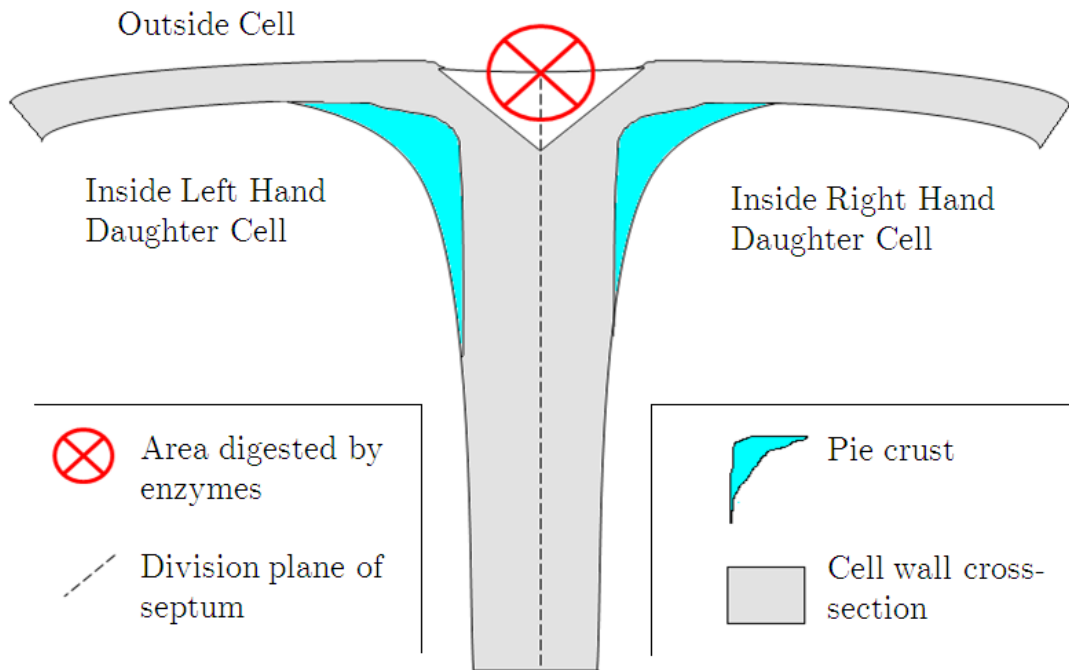


Figure 6.14: Sketch showing a cross section of the splitting edge of the septum at initial separation stages, showing a possible conformation of the pie crust and the area being digested by enzymes. This fits with the force data, as the central strip would be softer due to the digestion, and the strip either side of that would be stiffer due to the support of the pie crust under the remaining shallow cell wall at the new corner.

spherical shape, only stopping once it has reached a shape that can be maintained by the higher measured cell wall stiffness in these areas.

6.4 Conclusions

Force mapping of large numbers of SA cells at different stages of the growth cycle has provided a wealth of information on the mechanical properties of these cells, and allowed the study of changes to these properties as the cells grow and develop.

By carefully selecting a suitable cantilever and indentation setpoint it was possible to target the measurements at either the cell wall or the whole cell compression, and extensive testing has revealed that this system is very reliable.

6.4.1 The Cell Wall

The mechanical stiffness of the SA cell wall has been measured in stationary phase with little variation between different regions of the same cell, and also between different cells overall. This is not too surprising, since the Gram positive cell wall is relatively homogeneous and cells at the same growth stage should have very similar structures.

By studying cells at exponential phase, the cell wall was also studied at a range of different stages. These experiments indicated that the majority of the cell wall does not suffer any significant mechanical change during the division cycle, as all of the measured values were in good agreement with the stationary phase value.

The only part of the cell wall that displayed any difference in mechanical properties was the newly synthesised material of the septum, which was examined when it was still new, when the cell was still a hemisphere. This was identified by the characteristic concentric rings formed during the growth of the septum. This material was found to be stiffer than the older cell wall, which is expected, due to the growth pattern of the septum. Once the cell splits into two hemispherical daughter cells, it does not make any more cell wall material as the hemispheres become full spheres, so the septum must contain enough material to expand to complete the sphere required. The septum should therefore be more dense

than the rest of the wall, causing it to have a higher measured stiffness. These measurements, whilst they were as expected, lead to an adapted idea about the pressure inside the cell during division. If there were to be a rise in pressure then this would be more likely to push out on the softer, older wall than the stiffer, newer wall, so would not contribute to the separation and growth of the daughter cells. It was therefore thought that the pressure could not contribute to the division cycle.

The septum was also closely studied on the outer edge of cells that were close to splitting, so that the cell wall was showing signs of the location of the septum but the whole cell was still intact. These data indicated that the pie crusts, the ridges either side of the split, appeared stiffer than the majority of the wall. It also showed that the connecting material between the two pie crusts was softer, which makes sense as this material has to decay to allow the two daughter cells to become separated. It is possible that the increased stiffness of the pie crusts could contribute to this separation, but it could also be the case that the measurements in this area are just measuring the stiffness of the edge of the new septal material, since these two data sets show good agreement. The softer material between the two pie crusts could be due to this material being degraded by the activity of autolysins.

6.4.2 The Whole Cell Compression

Measurements of the whole cell compression with a contribution from the turgor pressure were initially taken on cells at stationary phase to establish a value of how the cells were when they were not part way through division. This value was then

compared to data taken from a large quantity of cells at various different stages of growth and division, and in all cases the values were in very good agreement.

These data indicates that the turgor pressure, as measured in this way, is consistent between different cells, and does not go through any significant change during the division cycle. This agrees well with the new cell wall being thicker than the old cell wall, as explained above.

6.4.3 Separation Questions

With all of this data combined, it appears that there is no pressure change to bring about a forced separation of the two daughter cells. This means that the separation must be down to something else, although it is unclear exactly what. It is possible that the pie crusts are stiffer than the surrounding material, as they appear from the measurements, and that contributes to the separation. It could also be that the digestion of the central strip between the two pie crusts by the activity of enzymes is sufficient. It is still unclear how the hemispherical daughter cells then expand into full spheres, which is likely to be controlled by enzymes which modify the dense peptidoglycan network of the septal wall to regular wall density, enlarging the area that the material covers.

7 | Mutant Strains

7.1 Introduction

As discussed in Section 2.4, the length of the peptidoglycan chains in the bacterial cell wall is controlled by a group of enzymes called the cell wall hydrolases. In SA there are four of these, labelled as a, A, B and H. Work in progress by Foster *et al* indicates that the hydrolase labelled B is the most significant, and that a cell can survive with up to three of these four enzymes genetically removed (currently unpublished). Therefore, the removal of these enzymes should inhibit the shortening of the peptidoglycan in the cell walls, leading to living cells with longer chains. As the B enzyme is currently believed to be the most significant and the other three have minimal effects, strains of SA were chosen in order to investigate the effect of this gene removal on the measured mechanical properties of the cell wall, with particular attention on the B hydrolase.

The experiments presented in this chapter feature mutant strains which were prepared in the same way as the standard strain used previously (apart from the antibiotics included in the growth media as described in Section 4.2.1). They were imaged in the same etched silicon wafer grids, in PBS, with the same AFM

techniques.

All of the genetic mutation to produce these mutant strains was performed by members of the Foster lab, and preprepared agar plates were used by the author.

Studying cells with mutated cell wall hydrolases is vital for understanding the methods involved in cell growth. It is currently not clearly understood how the newly formed hemispherical daughter cells grow to become fully grown spherical cells. By controlling the cells' ability to control their peptidoglycan chain length it should be possible to gain a greater insight into how the cell creates and uses new peptidoglycan throughout the growth and division process.

7.2 Strains

Six total strains were analysed in this section of the work, in addition to the standard wild type strain *SH1000* used previously. The first of these was *sagB*, where the only one of the four hydrolases removed was B, the one believed to have the most important role. The second was the complemented version of this strain, *sagB C*. In this case the removed genes for the B enzyme have been reinserted. This is a commonly used technique where specific genes have been removed, as the reintroduction of the same genes should reverse any effect that the initial removal had. This is an important control as it ensures that the removed gene(s) only removed the desired effect; if the re-introduction of the removed gene(s) does not restore the effect to that before the initial removal, then there must have been a knock on effect due to this removal. It therefore helps to ensure that the desired effect does not create any further undesirable and irreversible change to

the organism. The remaining strains were all ‘triples’, meaning that they all had three of the four hydrolases removed. These are labelled by the ones that they have had removed, so for example *ABH* has had the A, B and H hydrolases genetically removed, and so on for *aAB*, *aAH* and *aBH*.

7.3 Results

The results for all seven strains (including *SH1000*) are shown in the box and whisker plot in Figure 7.1, with the raw data displayed in the histogram in Figure 7.2 and Student’s T-Test calculated *p* values for each strain comparison are shown in Table 7.1. Upon initial inspection the plot appears to show the data in two populations, those below the dotted line and those above. This becomes significant when the presence or absence of the B hydrolase is considered, as those below the line still have the B genes (or have had them removed and then reintroduced), and those above have had it removed (and it remains absent). The grouping together of strains in terms of the presence of the B hydrolase agrees well with previous work in the area from which the B hydrolase appears to be the most significant (as mentioned previously).

	sagB	sagB C	ABH	aAB	aAH	aBH
SH1000	1.31e-115	0.16	1.76e-125	2.86e-110	1.37e-38	1.76e-125
sagB	-	5.84e-12	0.33	0.22	1.01e-83	0.33
sagB C	-	-	8.95e-13	5.12e-13	0.23	9.85e-16
ABH	-	-	-	9.16e-6	6.14e-51	0.0021
aAB	-	-	-	-	2.87e-62	0.05
aAH	-	-	-	-	-	8.57e-68

Table 7.1: Table showing Student’s T-Test *p* values for all strain comparisons.

As the hydrolases are associated with the length of the peptidoglycan chains,

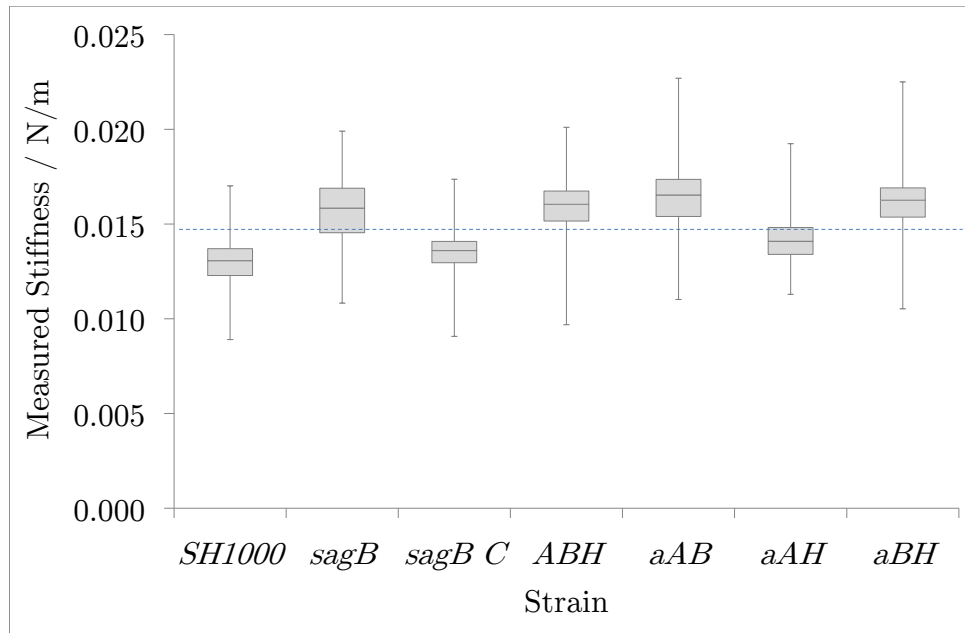


Figure 7.1: Box and whisker plot showing the measured stiffness for the cell walls of different strains of SA. There appear to be two populations; the first containing *SH1000*, *sagB C* and *aAH* (below the dotted line) and the second containing the other four.

removing them (and particularly the B hydrolase) inhibits their effect, leading to cells that have longer cell wall chains. The differences in the measured stiffness of the cell walls for these strains is therefore highly likely to be due to this chain elongation. From the data obtained here, all of the strains in which B is no longer present appear to have slightly stiffened cell walls. This is not entirely surprising, as longer chains in the cell wall create a denser mesh network and allow for the possibility of much more crosslinking, creating a stronger and more rigid framework. The results for each strain are discussed below, with particular attention to the presence or absence of the B hydrolase.

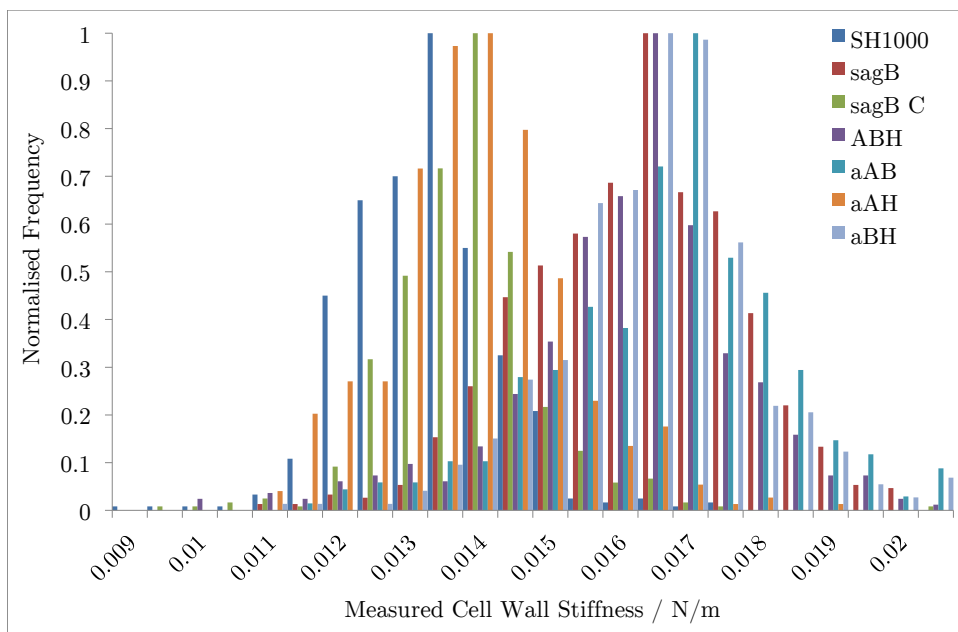


Figure 7.2: Histograms of raw data taken from different cell mutants, showing *SH1000*, *sagB C* and *aAH* grouped at lower stiffness, and the other mutants grouped at higher stiffness.

7.3.1 Discussion for *sagB* and *sagB C*

Removing only the B hydrolase caused a small but very significant ($p = 1.41\text{e-}115$) increase in the measured stiffness of the cell wall. This result indicates that the B hydrolase alone has an effect on the measured stiffness. As it is known that removing these genes results in cells with longer cell wall chains, the increase in stiffness can be attributed to this.

For the strain *sagB C*, called the complemented strain, the genes coding for the B hydrolase have been reintroduced to the *sagB* strain. In genetics this is a common practice to check that observed effects in the depleted strain are due specifically

to the removal of the desired genes and not related to another change caused as a secondary consequence of the removal. If complementing the strain restores the cell properties to the same as the wild type, then the depletion is considered to have been successful, if not then the observed changes cannot be linked directly to the specific genes removed.

As seen in Figure 7.1, the measured cell wall stiffness of the complemented strain is restored to being similar ($p = 0.16$) to the wild type again. This indicates that both the initial depletion and complementation of the B hydrolase genes were successful, and also that restoring the B hydrolase restores the cell wall stiffness, due to the re-established cell wall chain length.

7.3.2 Discussion for *ABH*, *aAB* and *aBH*

For these three strains, the genes encoding for the synthesis of three of the four hydrolases have been removed. The key feature of these three is that the B hydrolase is one of those no longer coded for. The box and whisker plot shows that all three of these strains had very similar measured stiffness values, all of which were stiffer than wild type and matched well with the data collected from the *sagB* strain.

These data agree well with the original theory that B is the most significant of the four hydrolases, as removing three including the B has the same effect as only removing the B, and the one that is left in the cell maintains the cell viability but cannot resist the increase in the measured stiffness. It also makes very little measurable difference whether the two removed alongside the B are the a, A or H; the fact that the B is removed is the dominating feature of these strains.

7.3.3 Discussion for *aAH*

The last remaining triple, the *aAH*, has all three of the hydrolases except the B removed. In the box and whisker plot it can be seen that the measured stiffness of these cell walls is only marginally increased, and remains very similar to the wild type and *sagB C* strains. This again indicates that the B is the most significant, as removing all of the other three does not have the effect of removing the B alone or with others. Removing all of the other three hydrolases and leaving behind only the B on its own gives a more similar stiffness to the wild type than removing the B alone.

This means that all these three of the studied strains which still contain the B hydrolase have a very similar cell wall stiffness, and the ones in which the B is removed, on its own or amongst others, also have very similar stiffness properties but at a higher value.

7.4 AFM Imaging Observations

When all of these strains were studied, they were first imaged in air on freshly cleaved mica, and the force maps taken in PBS, using the same etched silicon wafer substrates used for the wild type, were also used for visual analysis. From these scans the size and shape of the mutant strains was observed, along with any significant deviations from the regular spherical shape of the wild type.

From these observations, the size of the cells for all of the mutants was approximately the same as for the wild type. In air, on mica, the cells all appeared to be

of similar sizes and shape, and when force mapped in liquid the mutants often appeared spherical, though on occasion appearing to have slightly square shapes. This was not necessarily due to the depletion of any of the hydrolases, as this slight squareness was observed both in this study and by Kailas *et al* [41] for wild type cells when grown in a constrained well, where the cells appear to take on the shape of their container to a certain extent (and was not seen on the mutant cells imaged on mica).

The similarity of these mutants in appearance to the wild type cells indicate that the depletion of up to three of the four hydrolases does not significantly affect the size or shape in a way that can be observed by AFM, despite the longer chains and slightly stiffer cell walls.

7.5 Conclusion

SA contains four hydrolase enzymes that are used by the cell to degrade manufactured peptidoglycan in new areas of the cell wall, shortening the chains. These four hydrolases are denoted here with the letters a, A, B and H. It is currently believed that the B hydrolase is the most significant of the four, and does most of the work. It is also known that the cell can survive with up to three of these four removed.

Force measurements taken on SA mutants show that when the B hydrolase is removed, whether it is removed alone or as one of three, the cell wall stiffens, due to the longer cell wall chains that exist in the cell wall when the B hydrolase is removed, due to the lack of degradation. Re-introducing the B hydrolase reverses

this effect, as seen with the complemented strain. When the B hydrolase is kept in the cell and the other three (a, A and H) are all removed there is very little stiffening of the cell wall, as these three have little effect when compared with B. In summary, if the B hydrolase is present, the cell wall stiffness is very close to that measured on wild type, and if B is absent, the cell wall stiffness increases slightly but significantly. The effect due to the presence or absence of the B hydrolase is dominant over the effect of each or all of the other three.

When imaged, all of the mutants studied here appeared to have no significant difference with respect to their size or shape, compared both to each other and to the wild type. This indicates that the cells can grow relatively healthily with only one of the four hydrolases present.

This is a very significant result since it leads towards a whole new model of bacterial growth. Here it is strongly indicated that the cells grow by degradation; the initial cell wall of the septum is manufactured with much longer chains, higher crosslinking and density than the final composition, and this flat area of new septal wall material expands to become the new hemispherical half of a finished sphere by the enzymatic degradation of these long chains into shorter ones, allowing the cell wall to reduce its crosslinking density and increase its surface area. This means that the cells go from a hemisphere to a full sphere without the manufacture of any new peptidoglycan, with the expansion provided by a combination of the enzymatic degradation of the long septal cell wall chains, the stress in the flat wall being higher than the hemispherical wall (see Continuum Plate Theory), and not a rise in internal pressure (see Chapter 6) as had originally been predicted.

8 | Oxacillin

8.1 Introduction

Oxacillin is a β -lactam antibiotic that is often used in the clinical treatment of SA infection, since it is resistant to penicillinase enzymes that are produced by penicillin resistant SA. It was also selected for this study due to its higher stability in water than penicillin, so that experiments could be run for longer without the worry of the antibiotic breaking down or becoming damaged after too long an exposure to the imaging buffer medium.

Since oxacillin's mode of action is believed to prevent the manufacture of new cell wall, consequently causing dividing cells to lyse, it is therefore believed that only actively growing cells would be killed by the introduction of the drug. Cells were therefore incubated initially in both growth medium (so these would be actively growing) and in PBS buffer (so these cells would be alive but not actively growing). This would provide evidence as to whether or not live cells were killed by the drug only when they were actively dividing, or whether this idea needs to be adapted for live but not active cells. Cells used for these experiments were never allowed to completely dry during the settling stage, as that would have dessicated the cells

and provided a range of complications.

For the main emphasis of this chapter, live cells were prepared as normal for imaging in growth medium by AFM, after which oxacillin was added to the chamber and any effects brought on by this were observed. Since this needed the cells to be active and growing, all of the experiments in this part of the study were performed with the Linkam heating stage present, with a target liquid temperature of 37 °C.

8.2 Results

8.2.1 Linkam Heating Stage Testing

Where cells were being studied with active processes required, the Linkam Stage was used to provide a heat source to keep the cells at as close to the optimal temperature of 37 °C as possible. The sample holder used here was designed specifically for this set up, and was tested before using with cells to check for any temperature lag and stability.

Due to the arrangement of the sample holder on the Linkam stage, there was a high probability of there being a temperature lag between the value set on the stage and the actual temperature of the liquid. This was tested by setting the stage to a range of temperatures around the target value and measuring the temperature of the liquid using a thermocouple. This was done both with and without the AFM head present in the set up, and the results of this are shown in Figure 8.1.

This data shows that the presence of the AFM head increases the temperature of

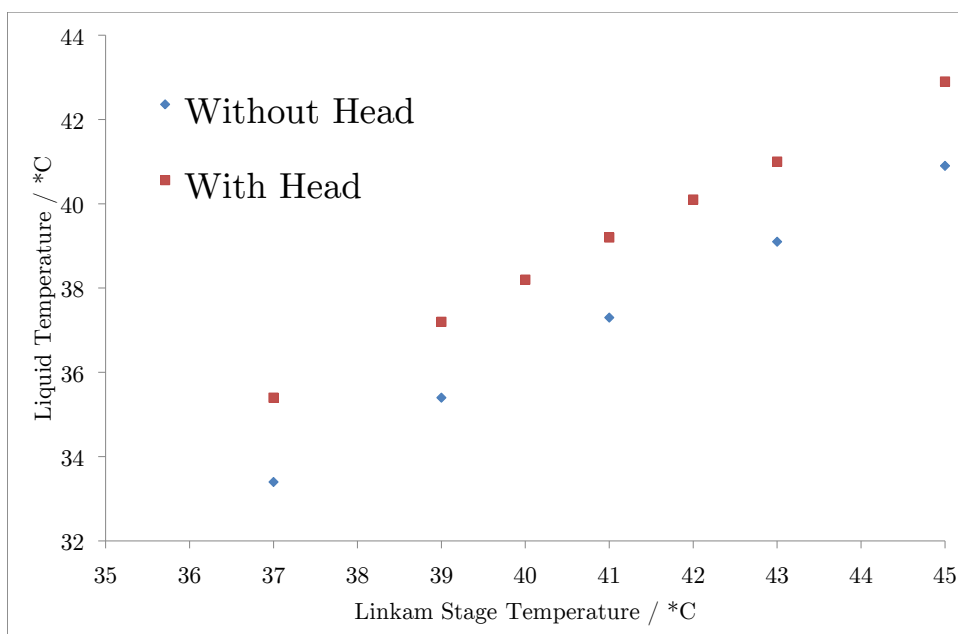


Figure 8.1: Graph showing the temperature measured for the liquid in the Linkam Stage holder compared to the set stage temperature, both with and without the AFM head present.

the liquid slightly, which is likely to be due to the insulation it provides against the heat lost from the liquid surface. With the head present, the temperature lag between the set value and the measured value is consistently approximately 2 °C. The stage was therefore set at 39 °C for all experiments.

The set up was also tested for stability over time. The stage was set to 39 °C and measurements of the temperature of the liquid were taken at regular intervals for 2 hours. The results of this are shown in Figure 8.2. This shows that there were some fluctuations in the temperature, but it stayed within 0.1 °C of the average value over time. These minor fluctuations are not a problem as they stay within a very small margin of the ideal target temperature and there is no decay or increase

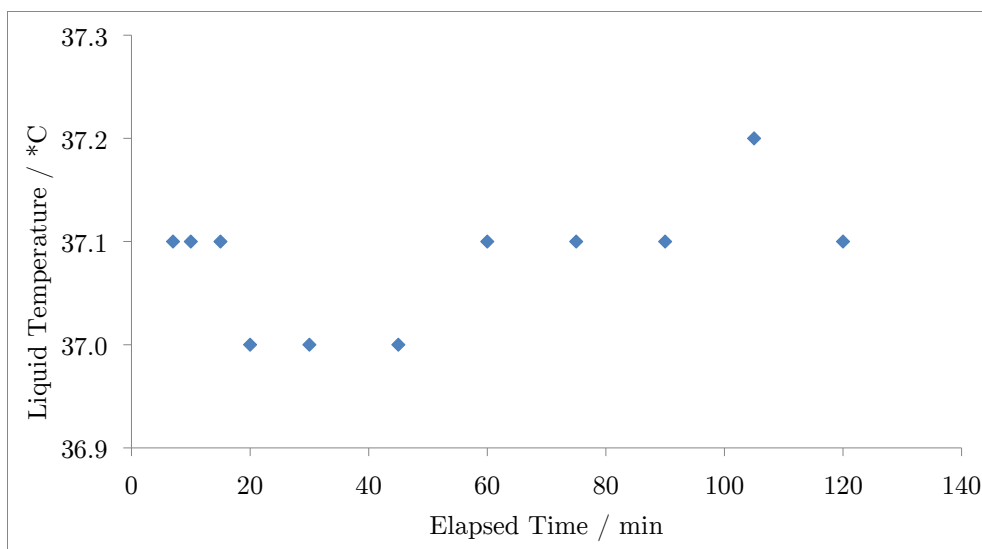


Figure 8.2: Graph showing the temperature measured for the liquid in the Linkam Stage holder over a total of 2 hours, to check the stability when set to the desired temperature.

over time, showing good stability of the system.

8.2.2 Results from Incubations

Cells were studied and measured after a 1 hour incubation in PBS and BHI (both with and without 5 $\mu\text{g}/\text{ml}$ oxacillin), after being grown to mid exponential phase in pure BHI. 1 hour was chosen as the time for the incubation as SA cells divide on average every 24 minutes, so the hour ensures that all of the cells in the population will have had the chance for at least one division during the incubation. When the cells that had been incubated in PBS and oxacillin were studied they appeared to be healthy and their measurements matched well with those cells that had not been exposed to the oxacillin (green and blue data in Figure 8.4). This indicated

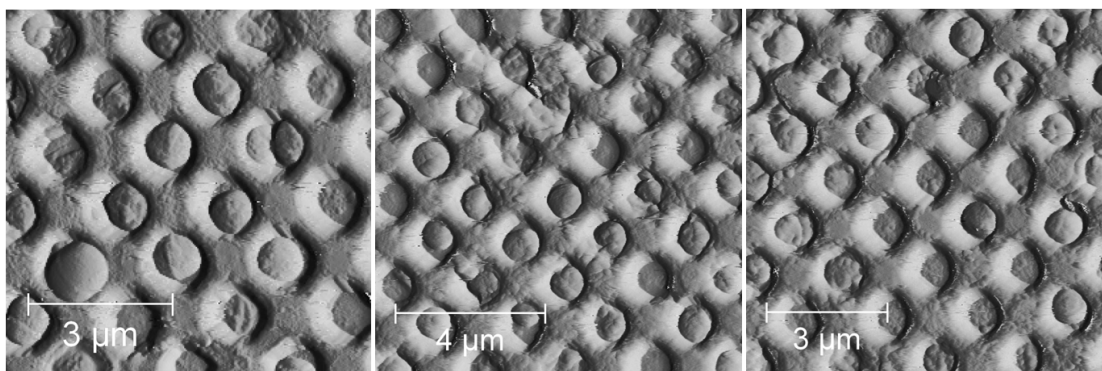


Figure 8.3: Three AFM vertical deflection images in air showing SA cells after a 1 hour incubation with 5 $\mu\text{g}/\text{ml}$ oxacillin in growth medium (BHI). All the cells appear shrivelled and died during the treatment.

that the cells in PBS were not affected by the presence of the oxacillin, which is as expected due to the nature of the mode of action of β -lactam antibiotics.

Cells that had been incubated in BHI and oxacillin are shown in Figure 8.3. These images are vertical deflection AFM contact mode images taken in air. The cells have been imaged in the original etched silicon wafers to give a sense of perspective, as it is easy to see that the cells in these images are not as large as the healthy cells usually imaged in these grids. These cells were unable to be imaged in liquid as they did not remain immobilised on the surface due to their diminished size. The shrunken size and the shrivelled appearance of these cells is indicative of their death due to the exposure to the drug in an environment promoting their activity and growth.

Figure 8.4 shows a comparison of cell diameter measurements for these groups of cells - those incubated in PBS and BHI, both with oxacillin, and those that were not exposed to the oxacillin at all. This data confirms what was indicated by the images, that there was no significant difference between the cells in PBS and oxacillin to those cells which remained untreated, and the cells that had been

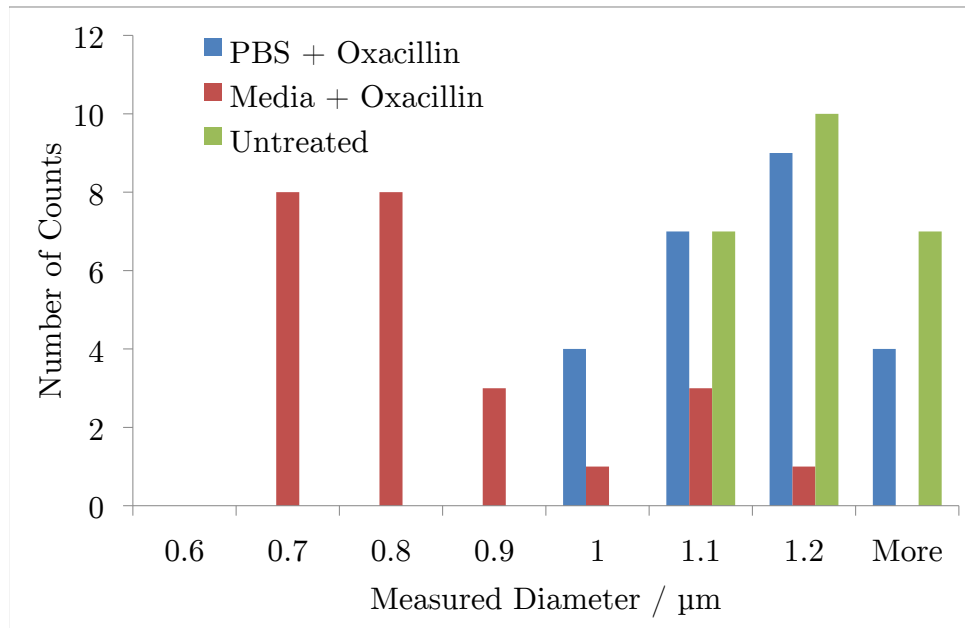


Figure 8.4: Graph showing the measured diameter of cells that were grown for 1 hour in PBS and oxacillin, BHI and oxacillin, and untreated cells (measurements were taken from cells in both PBS and BHI to check for consistency between the two).

incubated in BHI and oxacillin showed a drastic reduction in size. These smaller cells also had a greatly reduced whole cell compression measurement, as shown in Figure 8.5. As these cells have lysed due to the oxacillin action the turgor pressure will have dropped to zero. It is likely that the measurement of the whole cell compression for these cells is indenting into the damaged and ruptured cell wall far enough to be affected by the solid silicon substrate beneath, leading to a higher measurement than the one expected in this situation.

In this section it has been shown that oxacillin is only able to act on cells when they are actively growing and dividing, as expected, as those cells incubated with PBS buffer in place of BHI were unaffected. Those cells incubated with the oxacillin

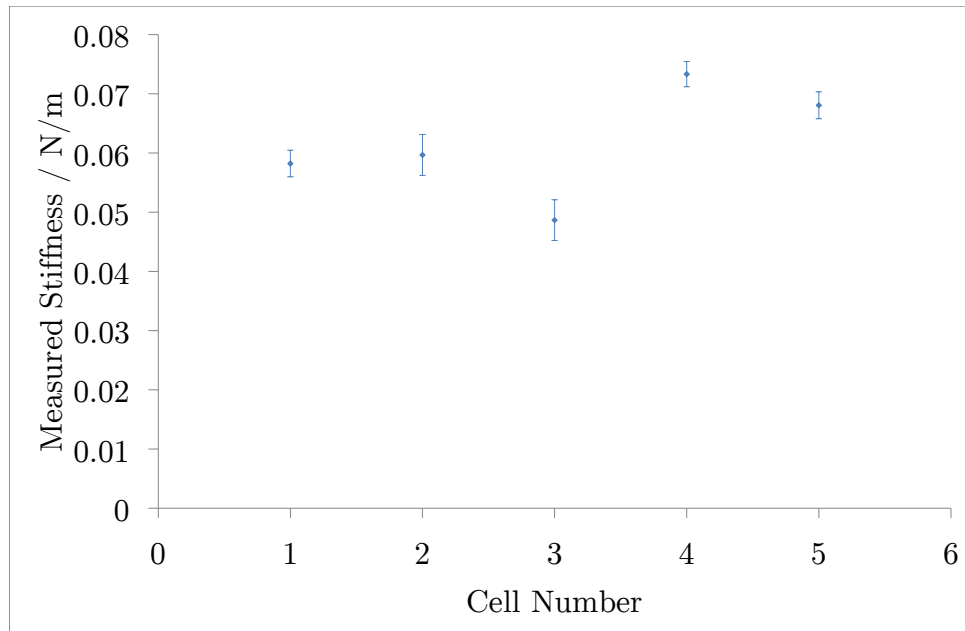


Figure 8.5: Graph showing the measured whole cell compression stiffness for cells after a 1 hour incubation in 5 $\mu\text{g}/\text{ml}$ oxacillin in growth medium (BHI), much lower than that for healthy cells.

and BHI appeared much smaller and visually looked wrinkled and unhealthy in comparison to healthy and untreated cell groups. The whole cell compression measurement was also greatly reduced, due to the lack of turgor pressure in the lysed cells.

8.2.3 Live AFM Imaging

Cells were prepared as normal for AFM imaging in BHI, and then oxacillin was added in order to attempt to view the effects of this drug on the cells directly. For several of the initial experiments using this technique there was no activity seen on the observed cells, and the reasons for this are unclear. It is possible that the

cells are not happy enough to be growing quickly in the etched holes, or they could be using them as shelter against the effects of the drug, as it is understood that cells in biofilms can protect themselves against threats such as this to a certain extent.

Although the majority of the cells in a sample would not appear to be showing much activity, there were some that were found to be growing after repeatedly scanning the same area for a number of hours. These cells were then scanned with time periods of approximately ten minutes, as any faster and there would be an increased risk of the cells detaching during the session. An example of the events seen for one of the successfully affected cells is shown in Figure 8.6. The scale bar in this figure represents 1 μm . At the point indicated by the white arrow labelled (a), the highlighted cell appears to suddenly expand, whilst all of the other cells in the image stay the same size. For the next thirteen images the cell does not appear to show any clear external changes, until the white arrow labelled (b). At this point the cell appears to burst, leaving a residue behind on the surface. It is unlikely that the cell has just detached and drifted away, as this would leave behind a clean surface such as in Figure 4.5. In this case the cell leaves behind a residue, which remains stuck to the surface and moves about under the scanning forces of the tip, indicating loosely bound, soft material.

From these images it would appear that the indicated cell has lysed due to the antibiotic. As this is only possible if the cell is actively dividing, the cell must have been dividing in a plane parallel to the plane of the view, so that the division septum is not visible as the cell is viewed from above. This also explains why the other cells are not lysing, as they have visible septa so it can be seen that they are not actively dividing during the scan. The reason for the inactivity of these

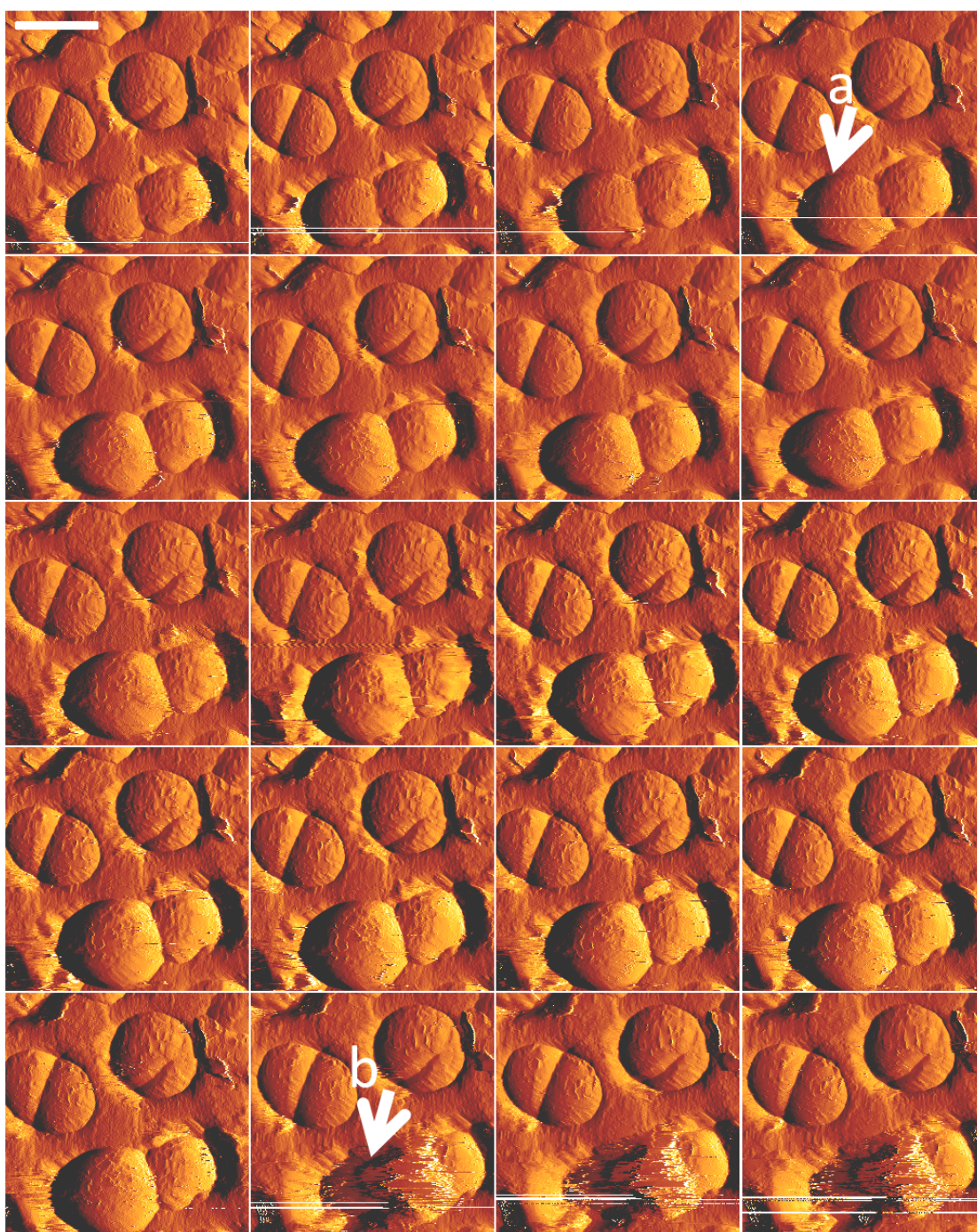


Figure 8.6: Series of AFM vertical deflection images taken at time intervals of approximately ten minutes of live SA cells showing a cell expanding (a) and then appearing to burst (b) under the effect of oxacillin. The scale bar represents 1 μm .

other cells is unclear, although it could be due to the conditions not being ideal, causing the majority of the cells to be inactive (and this also provides the reason for the amount of time taken for the lysing cell to burst).

Although it was rare to see this kind of activity in these experiments, it was seen a total of three times, indicating that the effects seen were likely to be a consequence of the oxacillin and not just a random cell collapse. Effects like this were never seen in the entire study where oxacillin was not being used.

8.3 Conclusions

Cells were grown to mid exponential phase in BHI, then transferred to both PBS buffer and BHI both containing 100 $\mu\text{g}/\text{ml}$ oxacillin. Incubating these cultures for 1 hour allowed the active cells in the BHI and oxacillin solution to progress through the time required for at least one full division cycle, whilst the cells in PBS and oxacillin would remain alive but not be active. The results when these cells were observed at the end of the hour showed that the cells from the BHI culture were dead and lysed, where the cells from the PBS culture were not. This experiment showed that the β -lactam method of action only works on cells that are actively growing, agreeing with the theory that they work by preventing the cells creating any new cell wall during the division process, lysing the cells as they attempt to split.

Oxacillin was also added to live cells imaged by AFM in BHI growth medium, in order to image the effects of the drug on the cells as it was happening. Whilst many of the cells observed during a run of these experiments did not appear to grow

at all during several hours of scanning, those that did appeared to lyse instead of being able to successfully divide. The reasons that some of these cells were not growing are unclear, although it is most likely due to the conditions not being ideal for growth (for example the confinement in a silicon well, and the lack of recovery after the cells have been prepared, during which time the temperature was below desired and the cells were in buffer rather than growth medium). Although the temperature is as close as possible to ideal, using a Linkam heating stage, the cells have been washed and spun down in a centrifuge in between their exposure to growth medium and warm temperatures, which could have stunted their growth rate significantly.

For those cells that did lyse during these scans, the key feature observed is the speed with which the cells burst, as in Figure 8.6. There is no visible gradual decay of the cell wall, the cell stays in more or less the same state for a significant amount of time after the addition of the oxacillin, until it lyses in the time taken for one frame, approximately ten minutes. This again agrees with the theory, in that the cell will be alive and well until it attempts to separate into two daughter cells, at which point it will suddenly rupture due to the absence of the division septum.

As this chapter was intended mainly as a tool for further study, proving that the substrates created for the rest of the work presented in this thesis could be used for this application, there is a great deal of scope for future work from this chapter's data. This mostly begins with further data collection on cells lysing as shown here, and there is the opportunity to collect force data on these in order to further study the mechanism of action this antibiotic. There is also the scope for other antibiotics to be used on cells studied by this technique.

9 | *Bacillus subtilis*

9.1 Introduction

Bacillus subtilis (BS) was used as a second species for a source of comparison for the data acquired from SA. As both of these species are Gram positive, the composition and general structure of their cell walls is broadly similar, although it is currently understood that the peptidoglycan layer is arranged slightly differently (see Chapter 2).

The experiments performed on the BS cells were executed in the same way as for SA, to keep the measurements as comparable as possible. The cells were deposited onto a silicon wafer, allowed to settle for a short amount of time before being scanned in Nutrient Broth (NB) growth medium by contact mode AFM. Fluorescence measurements were taken on the cells after being prepared in this way to ensure that the BS cells could survive the preparation procedure as they have never been imaged in this way before. Attempts were made to take the same measurements, of cell wall stiffness and the whole cell compression with a contribution from the turgor pressure, as for SA.

As BS is a self motile rod shaped cell, it is much more difficult to immobilise in liquid for measurements by AFM than non motile spherical cells, such as SA. This chapter describes the method development for a technique to perform measurements on live BS cells in liquid, and discusses some preliminary data that has been taken using the immobilisation method created. This data covers a range of preliminary force measurements on the cell wall and whole cell compression of live cells, as well as the ability to view cells appearing to grow and divide under the AFM tip.

9.2 Results

9.2.1 Silicon Wafers

Initial attempts to immobilise BS were unsuccessful, involving the use of wafers etched to contain gutters, or micron wide channels, designed to trap the cells along their length but keeping the ends of the cells free.

When these samples were imaged in liquid there were no cells seen at all. It is thought that as the imaging liquid was added to the substrate it washed along the surface and down the channels, causing the cells to move with the flow. As logs floating down a river align themselves perpendicular to the direction of the river's movement, the cells could be doing something similar. Therefore as the liquid moves down the gutters the cells will line themselves up perpendicular to this, meaning they cannot be immobilised by this technique. Figure 9.1 shows a contact mode height image of a section of the gutter substrate, with a cross section taken across the sample. The gutters are approximately 1 μm wide and

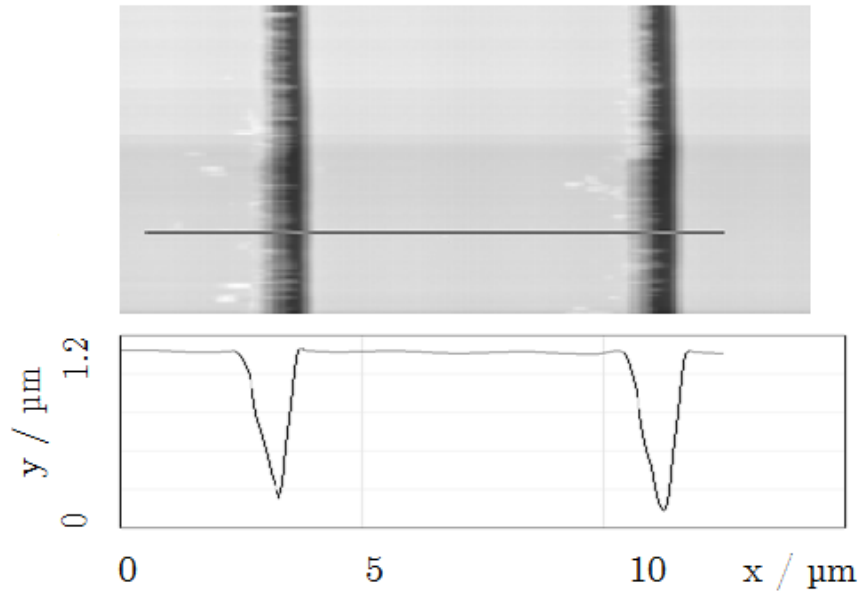


Figure 9.1: AFM contact mode height image showing the initial gutter substrates (top) with cross section from marked line (bottom).

deep, matched to the dimensions of the BS cells. Although the cross section shows the gutters to be v - shaped, this almost certainly a tip artefact as the gutters were formed by etching straight down into the surface so they should be more u - shaped than they appear here.

The design of the wafers was then modified into a bed-of-nails style design of regular arrays of pillars. This would prevent the added liquid from all travelling along channels with the cells aligned parallel to the flow, as the more open surface would not encourage any specific flow direction.

A contact mode AFM image in air of a finished pillar wafer is shown in Figure 9.2. This design allows the cells to align themselves in either the x or the y direction, held in place by the support from the pillars at various points along their length. As BS often forms long chains of connected cells, the length is left unlimited to allow these chains to lie uninterrupted yet immobilised.

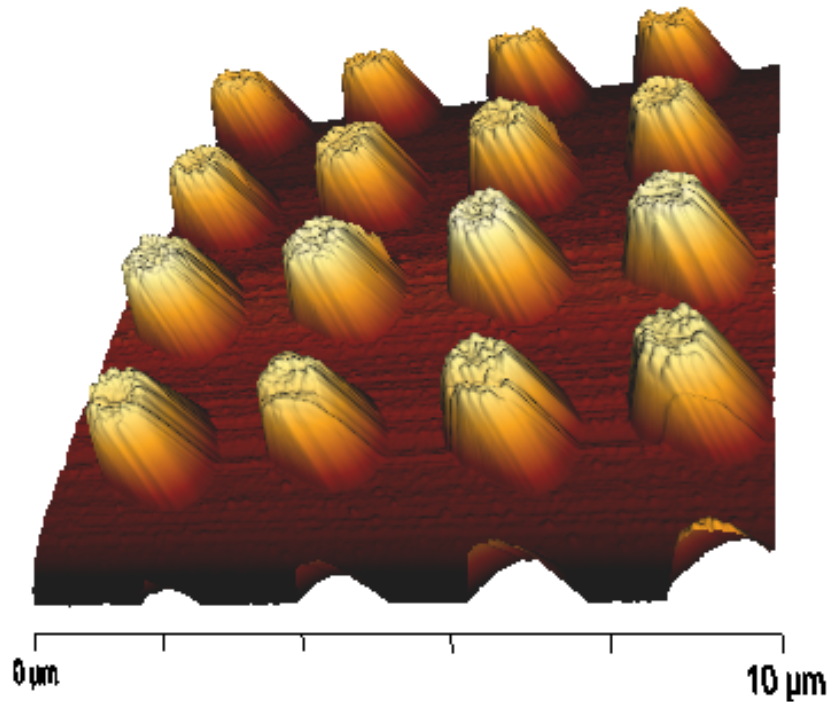


Figure 9.2: 3D rendered AFM contact mode height image of etched pillar wafer in air. The height of the pillars is approximately 1.2 μm .

9.2.2 Fluorescence

Fluorescence measurements were taken with BS on the pillar wafers, prepared by the same technique as they would have been for AFM (and the same technique that was used for SA). DAPI stain was initially used to check that the technique worked with the cells on the silicon rather than the glass slides that are more conventionally used for fluorescence imaging, before the live / dead staining was used to check for cell viability.

9.2.2.1 DAPI stain

Initial images taken with the DAPI stain were not very clear, but managed to show what was required from them. As shown in Figure 9.3, it was easy to locate the stained cells and the method appeared to work well. The cells also did not appear to move around in between different images taken at the same location, which implied that they were immobilised, at least a little, on the wafer surface.

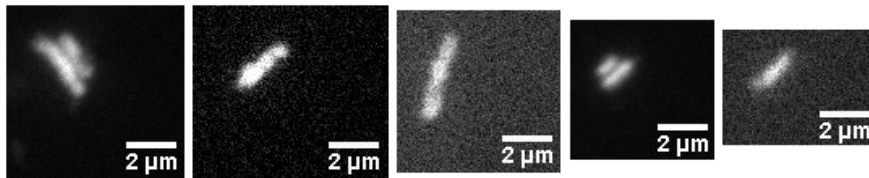


Figure 9.3: Fluorescence image of BS cells mounted on silicon pillar wafers using the DAPI stain.

9.2.2.2 BacLight™ Live / Dead Stain

Once it had been established that it was possible to use staining with the cells on the silicon wafers, the next step was to use a live / dead stain. Three total experiments were performed with this; a first control with live cells imaged on a glass slide immobilised in agarose (positive control, cells alive); a second control with cells prepared in the same way via a short exposure to ethanol (negative control, cells dead); and finally the sample with the cells imaged on the silicon wafers.

Images taken from the control samples are shown in Figure 9.4. The left hand image is of the negative control, with the cells that were killed in ethanol. All of

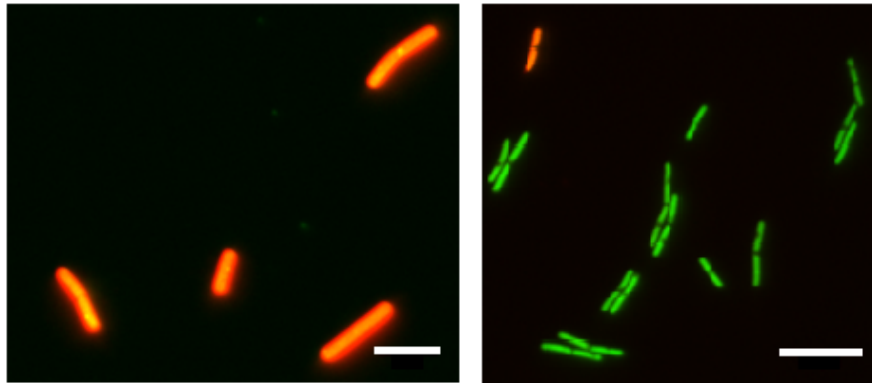


Figure 9.4: Fluorescence images of BS cells mounted on agarose using the live / dead stain. Left: Negative control, dead cells, scale bar is 5 μm ; Right: Positive control, live cells, scale bar is 10 μm .

the cells that were seen on this sample were stained red, indicating a compromised membrane and a dead cell, as expected.

The right hand image shows the positive control, with the live cells. There is a red, dead pair of cells in the top left of the image, but it can easily be seen that the majority of the cells in this sample were stained green, showing that they were alive. From all of the images taken on this sample, 92% of the cells appeared alive.

Once it was apparent that the stain was working well and the controls were done, cells were stained and imaged whilst immobilised on the silicon pillar wafers. Resulting images taken from this are shown in Figure 9.5.

The first thing noticed from these images was the mixture of live and dead cells, the ratio between which varies across the sample. Upon closer inspection it becomes apparent that the live green cells are larger, longer and wider than the dead red ones, with the live ones often connected in long chains, unlike the usually single dead ones. It is unclear why so many of the cells appear to have died, and whether

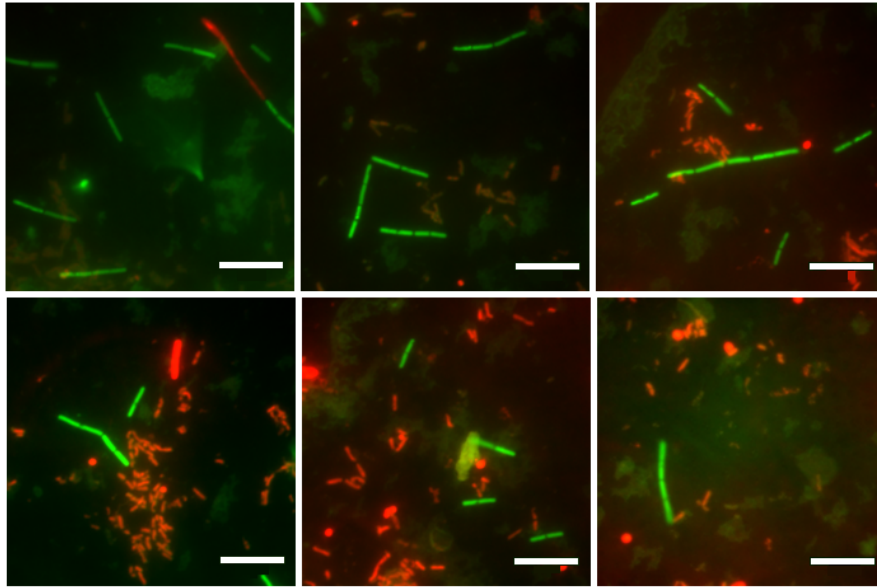


Figure 9.5: Fluorescence images of BS cells mounted on silicon pillar wafers using the live / dead stain. Each scale bar represents 10 μm .

the reduction in size caused them to die or vice versa.

The live / dead stain therefore shows that around 40 - 50% of the cells in a sample survived the preparation procedure for this experiment. As the same preparation is used for AFM, and the experiments would be preferentially performed on live cells, the target would be the plumper cells connected in chains rather than the small, shrivelled up cells that appear to have died. It was thought at the time that this difference would be relatively easy to spot during AFM imaging, and as shown later, it was.

9.2.3 Initial AFM Imaging

9.2.3.1 Images in Air

BS cells were initially imaged in air, on freshly cleaved mica, as shown in Figure 9.6. This allowed the dimensions of a large number of cells to be measured (data not shown), in order to ensure that the measurements of the grids would be suitable. It also allowed a check on the way in which the cells appear when dried onto a substrate. The images showed that the cells had a tendency to clump together, and many long chains were found where dividing cells had not fully separated. This was promising, as long chains were expected to align themselves along the rows of pins on the imaging grid, increasing their chances for immobilisation during scanning.

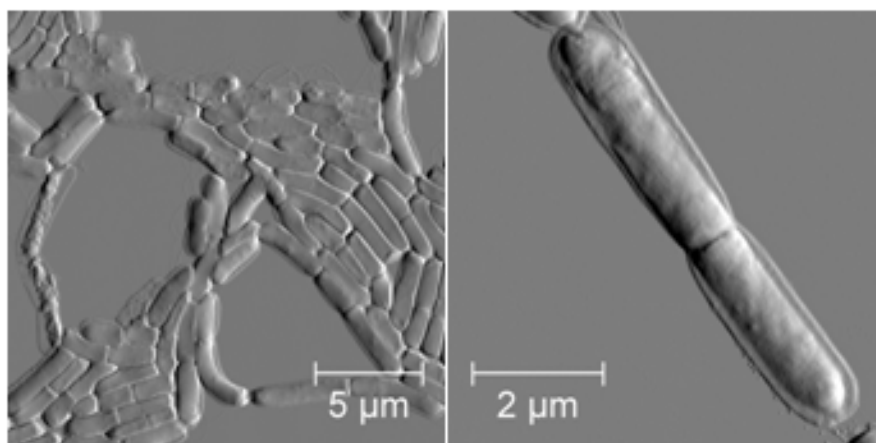


Figure 9.6: Contact mode vertical deflection image of *Bacillus subtilis* cells imaged in air on freshly cleaved mica.

9.2.3.2 Images in Liquid

When the cells were prepared on the imaging grids and scanned in liquid, it was relatively easy to find small clusters of immobilised cells on the surface. However most of these cells appeared small and very wrinkly, as shown by the majority of the cells on the left hand image of Figure 9.7. The cell in this image indicated by the white arrow appears larger and less wrinkled than the others. From the data acquired in the fluorescence experiments above, it is possible that the small, wrinkly cells are the dead ones and the larger, smoother one is one of the few that remained alive during the preparation.

The issue surrounding these larger cells is that as they are larger and more cylindrical, they are not as well immobilised during the AFM scan, as shown on the right hand side of Figure 9.7. Here the white arrow indicates the location of the same cell which has become detached during the scan (tip scanning from top to bottom). However the long chain of cells in this right hand image does not appear to be too wrinkled, so these cells could potentially be alive. Imaging this long chain for several scans did not detach any of the cells in the chain, so it is possible that the combined immobilisation experienced by these long chains is enough to allow scanning of live cells.

Both of these images were taken in contact mode, and as for the SA cells in the previous chapters, scanning in tapping mode led to all of the cells on the substrate being lost.

Two different techniques were used in order to locate cells for force measurements. The first of these involved scanning in contact mode, and as soon as a healthy looking cell was located, the tip was retracted before it had chance to detach the

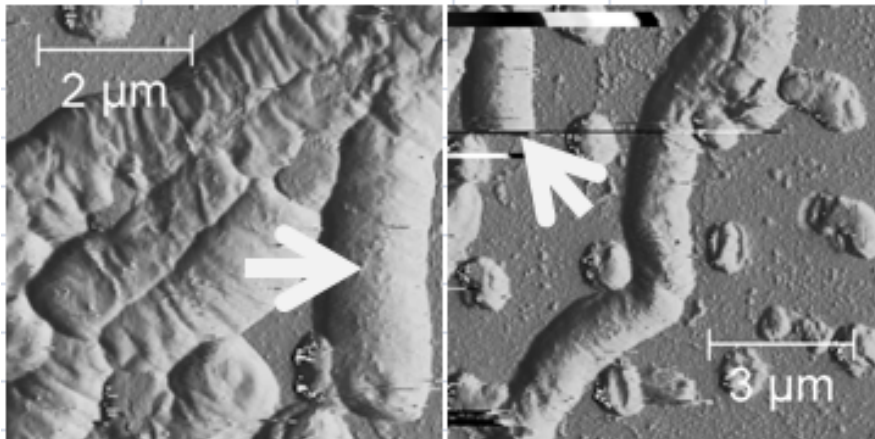


Figure 9.7: Contact mode vertical deflection image of *Bacillus subtilis* cells imaged in liquid on etched silicon wafer. The white arrow indicates one of the larger, healthier looking cells, which detached in the right hand image.

cell, and force measurements could therefore be performed on an area in which the cell was known to be. The second technique avoided the use of contact mode imaging, and just involved the use of force mapping to locate the cells, as this exerts almost no lateral force on the sample, so does not detach the cells. The issue with this technique was that the resolution is relatively poor, so it was difficult to tell whether or not the cells are small and wrinkled or large and smooth. Initially all of the measurements were taken on cells that had been at least partially imaged, so that the data from these could be used as a benchmark for the data collected from cells that had only been force mapped.

9.2.4 Initial AFM Force Measurements

Cells that appeared healthy in the contact mode image were force mapped, and the mechanical properties of both the cell wall and the whole cell compression were extracted, in the same way as for SA cells in previous chapters. BS cells were always scanned in nutrient broth growth medium. Two example force maps are

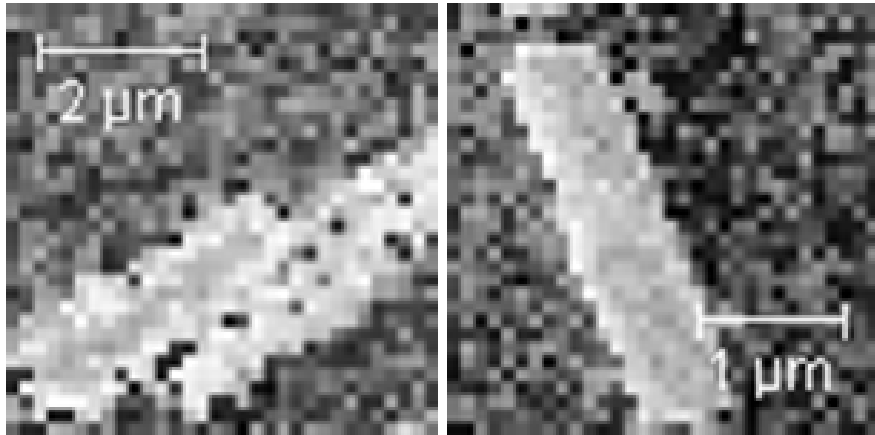


Figure 9.8: Slope force maps of *Bacillus subtilis* cells in growth medium. Z scales from $0.002 - 0.016 \text{ Nm}^{-1}$.

shown in Figure 9.8. The first feature of these maps to note is that, as with SA, the cells appear to have relatively homogeneous measurements across their whole surface. This is likely to be due to the resolution available in these images, as any features of the cell wall that would lead to heterogeneity are far too small to be visible at this stage. The turgor pressure is expected to be relatively homogeneous across the cell body, as with SA.

The results obtained from these measurements gave the stiffness of the cell wall as $(0.016 \pm 0.002) \text{ Nm}^{-1}$ and the measured whole cell compression as $(0.201 \pm 0.033) \text{ Nm}^{-1}$. The cell wall measurements were confirmed by measuring extracted cell walls, which gave stiffness values of $(0.018 \pm 0.005) \text{ Nm}^{-1}$, in good agreement with those obtained on live cells, by the same technique as for SA. When the measurements for BS and SA are compared, there is a significant difference ($p = 7.8 \times 10^{-11}$) between the cell wall stiffness, but not between the turgor measurements ($p = 0.51$). The distributions of the measurements are shown in Figure 9.9.

The higher stiffness measured on the BS cell walls can potentially be explained by the structure of the cell wall. Whilst the exact structures of these walls are still

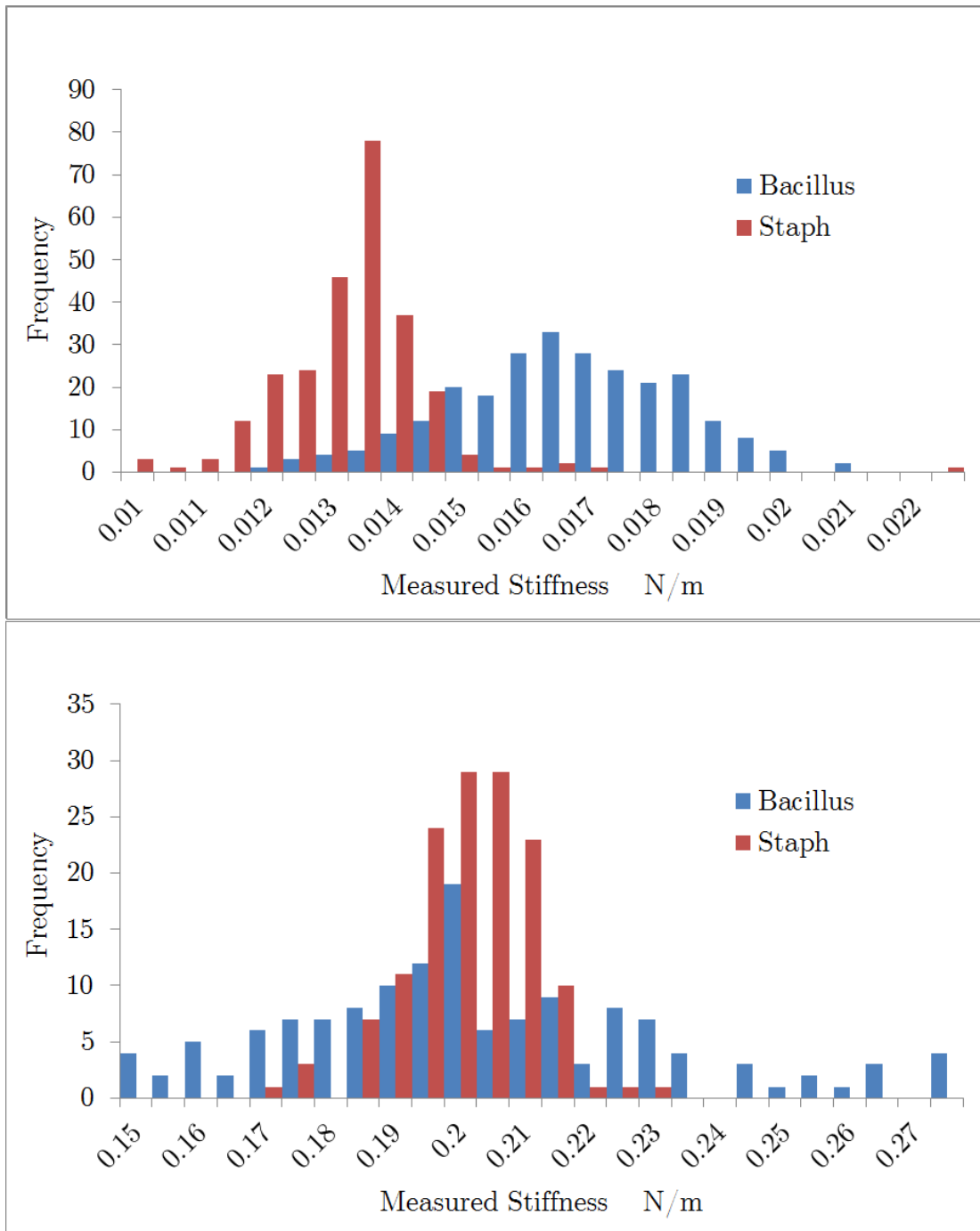


Figure 9.9: Histograms comparing the measured stiffness of the cell wall (top) and the whole cell compression (bottom) for BS and SA cells.

not completely known, it is understood that SA has short peptidoglycan chains whereas BS has much longer chains. The organisation of these longer chains, and the increased crosslinking between them, could be the reason for this increased measured stiffness. This idea is backed up by the experiments shown in Chapter 7, where mutants of SA with longer cell wall polymer chains were examined. These SA mutants also showed an increase in the measured cell wall stiffness, indicating that the increase in the length of their cell wall chains caused an increase in their measured stiffness. Despite this SA is understood to have greater crosslinking than BS, but the shorter chains would mean SA has many more free ends than BS. The dominating feature though is likely to be the chain length, as longer chains give stiffer cell walls consistently throughout this study. Secondly, as BS is a rod shaped cell and SA is spherical, BS needs an internal scaffold (MreB) to help maintain its shape, which could also contribute to this measurement.

Whilst the distribution of the BS whole cell compression measurements is much wider than for SA, both sets of data appear to centre around very similar values. This is not perhaps entirely surprising, since the internal organisation of the two different species is believed to be very similar.

9.2.5 Consecutive Force Mapping

Where it was possible to target measurements at the large, unwrinkled cells, force maps were taken repeatedly on the same cell in order to attempt to see the cells grow. It has not been possible to achieve this with imaging, since the cells detach after just a couple of scans at most, but force mapping allows the cells to remain on the surface for extended periods of time. The disadvantage is that this can only

be achieved with very low resolution at the timescales required, approximately 15 minutes per force map. The data presented in this section used the Linkam heating stage to keep the cells at 37 °C.

9.2.5.1 Viewing Cell Growth

During a small number of experiments during which consecutive force maps were taken on the same cell, it was possible to see the cell appearing to grow. This was monitored by measuring the tip to tip length of the rod over time. The measured properties of these cells could then be monitored throughout the cells' growth. Data was collected on both the cell wall and the measured whole cell compression with a contribution from the turgor pressure. Figure 9.10 shows five maps taken over the same cell with a time resolution of 15 minutes. This was found to be the best trade off between scanning fast enough to collect a reasonable number of maps during the cell growth, the pixel resolution of the maps, and the quality of the force curves as the tip moves rapidly through the surrounding liquid medium.

From series of force maps such as this example, it was possible to extract mechanical measurements at each timepoint. The measured stiffness and the overall cell length were plotted against the image number as shown in Figure 9.11. The top graph shows measurements of the cell wall and the bottom one of the measured whole cell compression. The drop in measured length on the bottom graph is due to the cell appearing to divide (data not shown), so the final two measurements shown on the graph are from one of the two daughter cells, which each had very similar and comparable values to one another.

In both of these cases, the increase in cell length indicates that the cells are

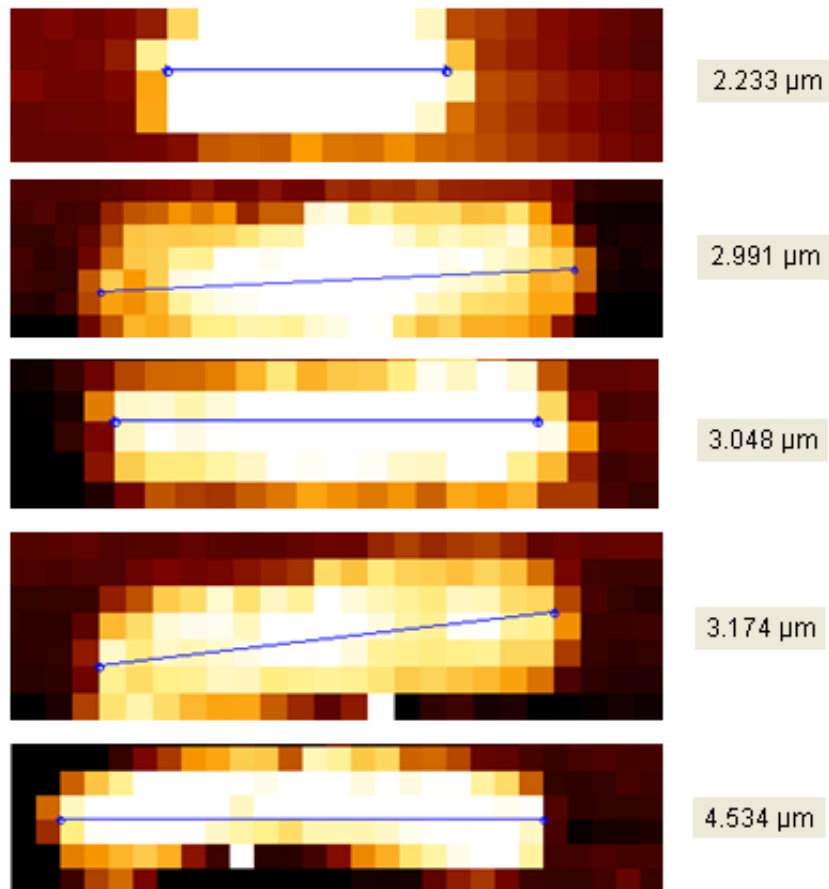


Figure 9.10: AFM force maps showing a BS cell elongating during growth, the quoted length is the measurement along the blue line. Time between scans is approximately fifteen minutes.

elongating and growing. This is shown to be happening at a much longer timescale than it would in ideal conditions, due to the cells not being completely happy as they are attached to the surface and cannot move to find new nutrients. As the cells are elongating, the measurements of both the cell wall and the measured whole cell compression stiffness do not show any significant signs of change, and there is no visible pattern to the measurements, indicating that any minor differences that can be seen are likely due to noise rather than any actual changes on the cells.

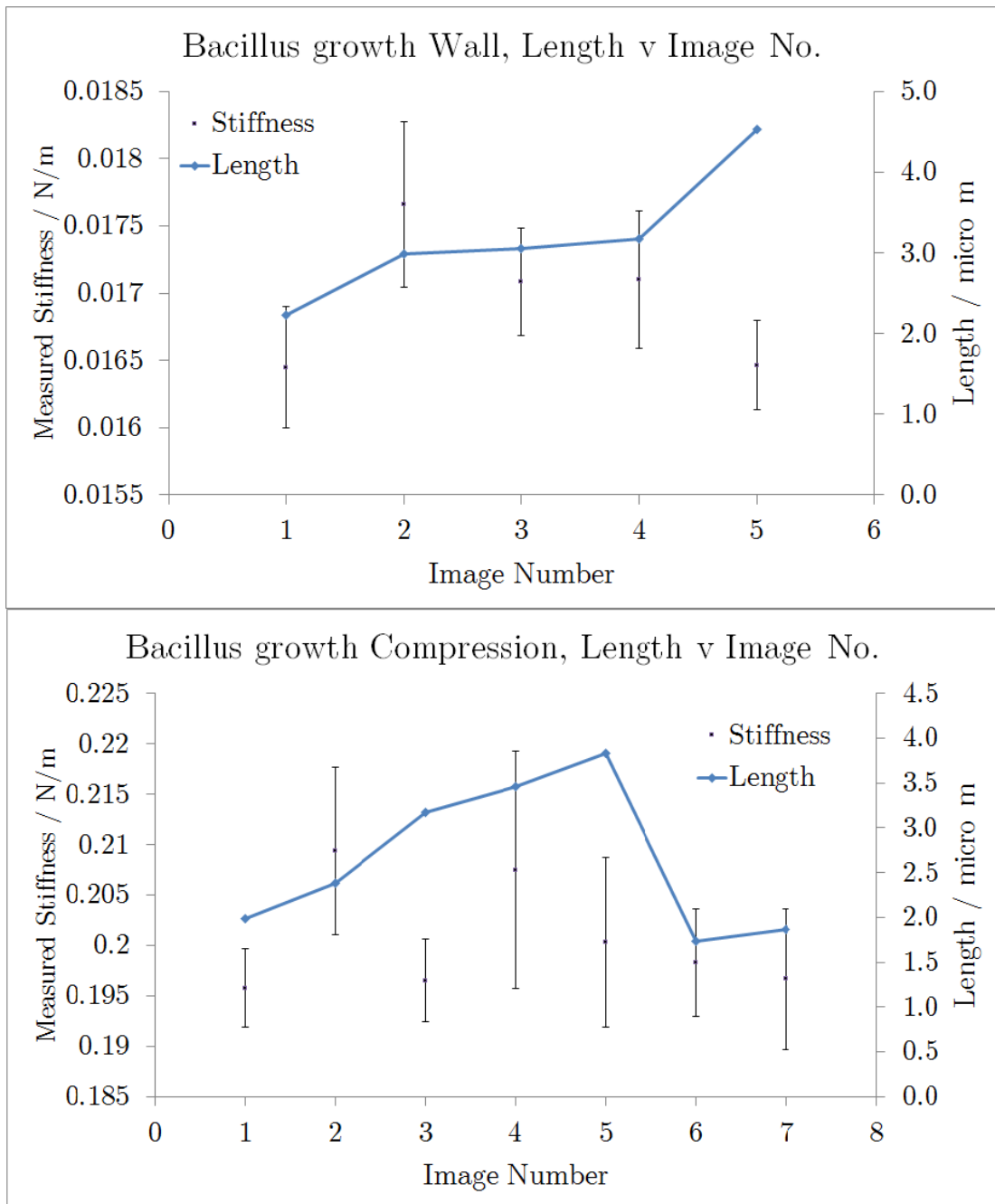


Figure 9.11: Measuring the length and stiffness for growing BS cells; Top: Cell wall, Bottom: Measured whole cell compression. Time between measurements is approximately fifteen minutes.

Although SA and BS have different growth and division mechanisms (see Chapter 2), the results of these force measurements show good agreement between the two. In both cases the outer, older cell wall and the measured whole cell compression do not show any measurable changes during the growth and division process. It has not been possible to make any measurements on the new septal cell wall of BS, since this is only found on the very end of the rods and this is inaccessible to the AFM tip.

9.2.5.2 Small Scale Force Maps and Adhesion Features

As BS is understood to grow by inserting patches of new material into the existing cell wall, small scale force maps (300 nm^2) were taken over the surface of live cells. This was in an attempt to view any changes to the height or the stiffness of the cell wall, which could be due to this insertion of new material. Figure 9.12 shows examples of these force maps, with images 1-3 taken on the surface of three different cells. (a) shows the height map, (b) shows the slope and (c) shows the adhesion, which is discussed in more detail later. Each scale bar in this figure represents 100 nm. In some areas of the height maps, there appears to be small regions of material at different heights to the neighbouring area, which is particularly noticeable in image 3(a). These small areas of higher material are of a suitable size to be considered candidates for pockets of new wall material, although they are not as clearly visible in some maps as they are in others. Looking at the stiffness maps (labelled (b)), it is difficult to see any ordered variation over the surface, and appears to be more noise than any discernible features. The only part of the stiffness maps that matches with the height is seen at the bottom of images 2(a) and (b), where the large high area on the height map appears to be located

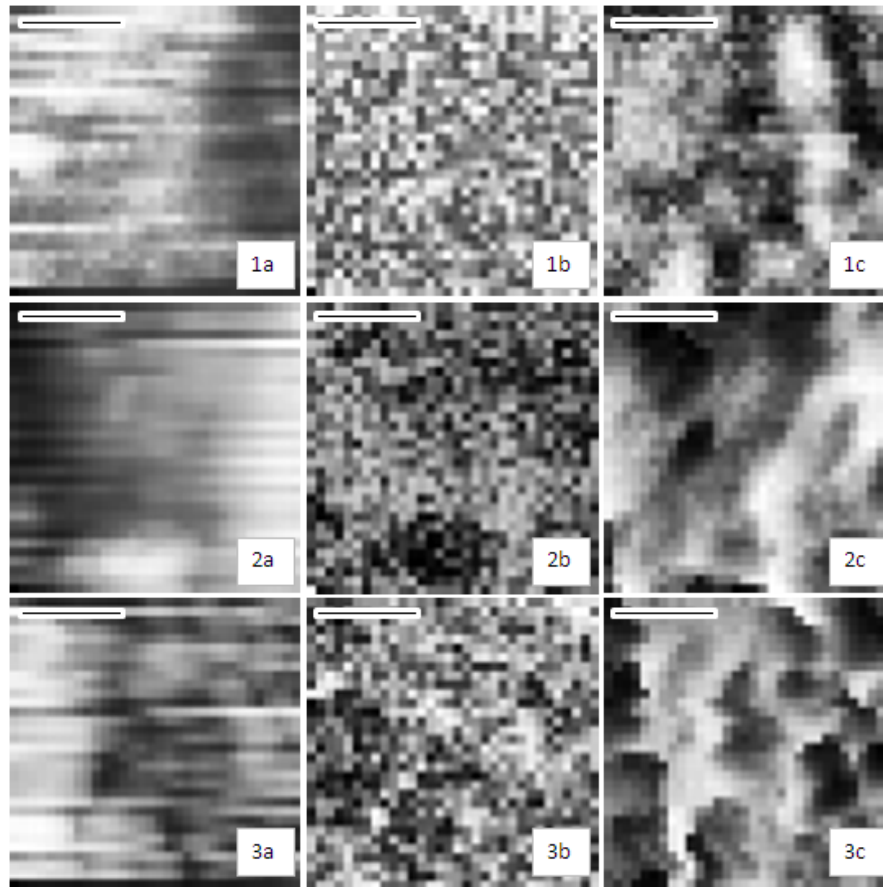


Figure 9.12: 300 nm^2 force maps of a small surface area of three different BS cells (1-3) showing (a) height, (b) slope and (c) adhesion. Each scale bar represents 100 nm.

in the same area as the similar dark (soft) area on the stiffness map. However, as none of the other high regions in the other images appear to have corresponding features on the stiffness maps, so it is difficult to take anything conclusive from these stiffness maps.

Previously in this study, whilst analysing force maps of cells, only the height and the stiffness force maps were studied. The software automatically also records the adhesion data, upon which stickier areas of the surface appear brighter than the areas on which the tip does not adhere. Figure 9.13 shows two retract curves taken over adhesive (blue) and non adhesive (orange) areas of a BS cell surface. The

adhesion measurement is the area under the x axis, contained within the adhesion 'spike'. In Figure 9.12 the final column, labelled (c), shows the corresponding adhesion maps for areas 1-3. These have been included in this instance as they show interesting features that do not appear on either the height or the stiffness maps. Features such as these were also never seen when SA was studied, even at lengthscales as small as the ones shown here. This was therefore interesting, as it was a feature that was only observed on BS and not on SA, despite the similarity in the composition of their cell walls. The adhesion force maps taken on the surface of live SA cells (data not shown) does not show any significant variation, only that which can be attributed to noise in the system.

In order to attempt to see whether or not these adhesion patterns were an artefact or a real feature, live cells were again mapped with the same size scan (300 nm^2) with maps taken consecutively on the same area with a time interval of fifteen minutes. Nine of the resulting adhesion maps from this experiment are shown in Figure 9.14. In these images, the dark band running across the top of the image is likely to be the edge of the cell, with the cell body filling the lower part of the scan below this band. In the first image (a) there is a clear difference between the bright, more adhesive majority and the dark, less adhesive patchy areas. In the following images the large dark cluster on the right hand side of (a) appears to move slowly to the left, although this is most likely to be due to slight drift in the system (due to the use of the heating stage and the temperature gradients that this can cause in the environment) and not due to the patch actually moving along the cell wall. Despite the slight drift, there is an observable change in the shape and size of these darker areas as they appear to be remodelling themselves and changing something about the cell wall adhesiveness as the cell grows and maintains its cell wall.

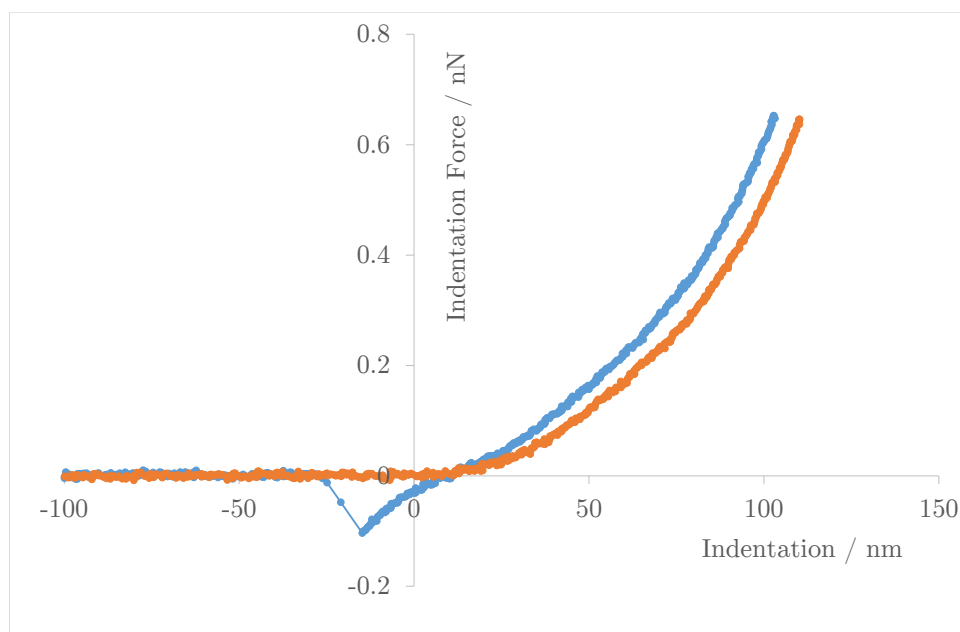


Figure 9.13: Plot of two retract force curves taken on adhesive (blue) and non adhesive (orange) areas of the same BS cell. The adhesion is quantified by measuring the area below the x axis, within the adhesion ‘spike’. Please note, the contact point on these curves has intentionally been chosen marginally incorrectly to visualise the contact part of the two curves without overlap, leading to a larger apparent indentation than in reality.

It is unclear exactly what caused these features to appear on these adhesion maps, as the tips used for these experiments were not treated or prepared in any way to bind to any surface agents of the bacterial cell wall. These were performed with standard silicon nitride tips, so the adhesion was not due to any specific binding, such as that used in single molecule force spectroscopy [116, 120, 132]. Because of the non specificity of the attraction it is impossible to say what is causing the adhesion between the bare silicon nitride and specific areas of the cell wall surface. The only ways in which there would be a chance to identify the parts responsible for this would be either AFM tip chemistry (in which the AFM tip

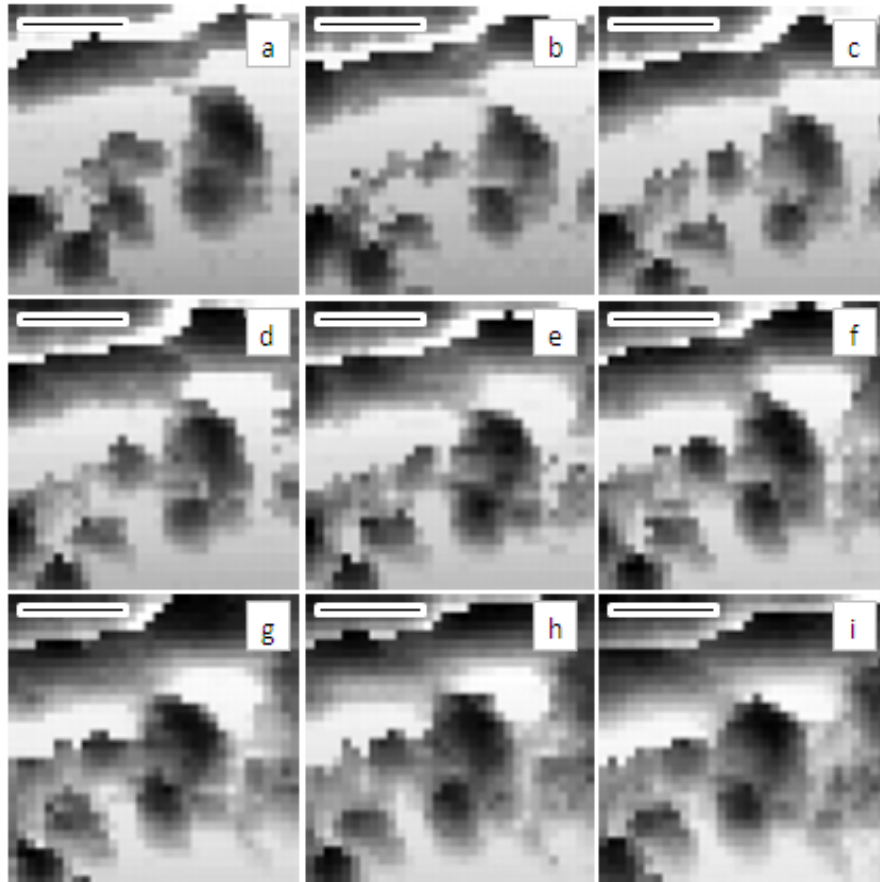


Figure 9.14: 300 nm^2 adhesion force maps of the surface of BS, taken repeatedly over the same area at 15 minute intervals. Each scale bar represents 100 nm.

is coated with a specific binding agent to attempt to target certain cell surface molecules), or to start working with the genetics of the bacteria to delete surface molecules one by one (to see at what point the adhesive patterns disappear). It could also be possible to make the tips hydrophobic by coating with a thin carbon film via scanning electron microscopy, and observing any effect this may have on the measurements. The issue here is that there is no guarantee that any of these techniques would yield a conclusive result, and that these techniques are incredibly difficult and time consuming. What these adhesion maps show though is that there is some heterogeneity in the cell wall surface structure, even if it would be very difficult to work out exactly what is causing it.

One possible explanation for the inhomogeneity of the adhesion maps is the distribution of charge across the cell surface, due to the distribution of different surface features.

9.3 Conclusions

A silicon wafer was etched to provide a surface with a series of pillars with such dimensions that they were able to trap and immobilise live BS cells for AFM analysis under liquid. Although these cells were frequently detached during imaging it was possible to scan them repeatedly by force mapping, which exerts far less lateral force on the sample, leaving the cells successfully immobilised.

The mechanical properties of the cells were quantified by force spectroscopy, yielding a value of cell wall stiffness significantly higher than that for wild type SA and only slightly higher than that of the cell wall mutants of SA described in Chapter 7. This rise in the measured stiffness of the cell wall is therefore likely to be due to the increase in the length of the cell wall chains, as the cells with the longer chains have the stiffer cell walls. The second mechanical measurement of the BS cells was the whole cell compression with a contribution from the turgor pressure, which was measured as being in the same population as that measured on SA cells, indicating that this measurement is approximately the same for the two different cell species, although it is difficult to elaborate on the relevance of this particular measurement since it is unclear exactly what this measurement is quantifying.

Force mapping the live BS cells allowed the continuous imaging of a single cell

without detachment by the AFM tip. Using this technique in growth media gave consecutive images of growing cells, in which the length of the cells was measured to be extending as the cells grew. Unfortunately due to the growth timescale and limitations of immobilisation these have only been achieved with very low resolution at this time.

Taking small force maps on the surface of live, active cells showed small deviations in the height of different regions within the cell wall, which could be attributed to the cell wall turnover method of growth, as explained previously, although it is difficult to confirm exactly what these small areas are as they are usually not seen on the slope graphs, which show very little variation across the small areas of cell wall studied in this way. The adhesion force maps taken at this scale showed regions of different adhesiveness over the surface which were shown to change over time, possibly due to some cell wall turnover or remodelling, although it cannot be said what is causing this difference in surface adhesion as the tips used for these experiments were bare silicon nitride, so should not have selectively bound to anything specific on the cell surface.

10 | Conclusions

10.1 Overall Conclusions

Staphylococcus aureus (SA) cells were successfully immobilised for study by Atomic Force Microscopy (AFM) in liquid by trapping the cells in holes etched into the surface of a silicon wafer. This immobilisation technique proved sufficient to allow several hours of scanning over the same area, with only minimal chance of cell detachment during an experiment.

Force curves taken on these live cells revealed two discrete stiffness measurements, with a change in behaviour at an indentation depth of around 21 nm, which correlates well with the thickness of the cell wall both from the literature and as measured in this study. The two different behaviours were both seen on the same force curve, as confirmed by plotting the force curve on a log - log scale, where two straight lines of non zero gradient indicate two different power laws on the original curves. Because of this change in behaviour, it was not practical to use an existing contact mechanics model, so all results have been given as raw stiffness data in units of Nm^{-1} .

The measured stiffness of the first part of these force curves matched well with that measured on extracted cell wall sacculi, so it was suggested that the first stiffness is that of an initial indentation into the cell wall. The stiffness of the second measurement dropped significantly when a detergent was introduced in order to greatly reduce the turgor pressure in a dying cell, indicating that this measurement includes a contribution from the cells' internal turgor pressure. This second measured stiffness was therefore associated with a compression of the whole cell, containing a turgor contribution. Through this method it was possible to separate the measured stiffness of the cell wall and the whole cell.

Changing the solute concentration in the surrounding medium by adding salt (NaCl) or sorbitol, a non - metabolisable sugar, also causes the expected drop in measured whole cell compression due to a drop in turgor pressure, however the cell is able to recover after a short timescale. This is most likely due to the SA's ability to restore its turgor pressure by the acquisition of compatible solutes, and the addition of chloramphenicol showed that this recovery was an active process. When water is used as the medium, instead of buffer or growth medium, the time for both the drop and recovery of the whole cell compression stiffness is much delayed, and the reasons for this remains a mystery. Transmission electron microscopy images of sections through cells at different stages of the drop and recovery in the presence of high external osmolarity do not show any visible change to the internal shape and structure of the cells.

Mechanical mapping allowed a visualisation of the mechanical properties of the cell, and a comparison between different cells and different areas of the same cell. Using this technique it was shown that measurements of the whole cell compression stiffness were consistent across a cell, between different cells at the same growth

stage and also throughout the cell cycle, indicating that there is no measurable change in the cells' overall properties. Taking the same measurements of the cell wall, again there was no measurable variation across cells and between different cells, except for the areas where newly formed septal cell wall was visible on the cell surface, indicated by its characteristic concentric ring pattern formed during the growth of the septum. This new cell wall was found to be stiffer than the older material, due to the longer chains and denser material present in these regions. This dense material is then degraded into shorter strands as it expands to form a fully spherical daughter cell.

Small mechanical maps taken over the outer edge of dividing septa showed that the central strip was softer than normal cell wall, with a stiff band running either side of this, surrounded on the outside by normal stiffness cell wall. This implied the central strip was being enzymatically degraded, causing it to be softer, with a reinforced stiffer ridge, or piecrust, on the corner of the newly formed septal material. These data sets lead to a new model of bacterial cell growth by degradation.

Mutant strains with cell wall hydrolases removed were studied in order to examine the difference that chain length would have on the measured stiffness of the cell wall. Data acquired on these cells showed that removing particularly one of the four hydrolases, denoted as B, significantly increased the measured stiffness, again leading to the conclusion that longer chains in the cell wall stiffen the structure, as found with the newly formed septal material on the wild type cells.

Oxacillin, a β -lactam antibiotic, was added to live cells whilst being imaged by AFM in order to attempt to view cell death by antibiotic induced lysis. The cells were not in ideal conditions during scanning, so this was difficult to achieve, but

a small number of cells did appear to burst after an extended exposure. The soft, loosely bound material left behind by these lysing cells indicated a violent death during which parts of the cell were left behind attached to the substrate, whilst the remaining parts were lost into the surrounding environment.

Bacillus subtilis (BS) was immobilised on etched silicon substrates for the first time, and was able to be either imaged for a short time or mechanically mapped for a longer time. This technique is currently insufficient to immobilise BS cells for repeated imaging scans. However via the mechanical mapping technique data was taken for comparison with that for SA cells, and BS was measured as having a slightly (but significantly) higher cell wall stiffness, but a similar whole cell compression stiffness. The measurement on the cell wall is important as again it shows that a cell wall with longer peptidoglycan chains has a higher mechanical stiffness when measured by this technique, in agreement with both the new septal cell wall on wild type SA, and also the mutant strains with depleted hydrolases.

Finally the mechanical mapping technique was used to view BS cells over time and it was possible to view cell growth in this way, although at very low resolution due to the limits of the mapping technique and the growth rate of the cells. During the growth process there was no observed change in either the measured cell wall stiffness or the whole cell compression data. An interesting feature observed on BS cells that was not seen on SA cells was a patchy pattern in the adhesion data, which changed over time as the cell grew and manufactured new cell wall. This could be due to the cell wall turnover method of growth, but it would be very difficult to examine exactly what is causing this surface heterogeneity.

10.2 Future Work

There are a number of unanswered questions remaining from this study, which provide opportunity for future work. The key part of this arises from the experiments concerning the addition of salt to the external medium. The exact nature of the sharp rise in measured whole cell compression as the cell recovers still needs further investigation. A second part of this experiment's further work is to understand the reasons for the delay when water is used as the medium. This could be started by genetically removing some of the membrane proteins and porins in an attempt to understand what is crossing the membrane (if anything) during this period. It could also be possible to examine the chemical components inside the cells, and see if the cells are taking up or losing anything specific.

Whilst in this study it has been assumed that the second part of the indentation force curve is measuring the whole cell compression with a contribution from the turgor pressure, a mathematical model would be useful in determining the exact way in which the cells are deformed during these relatively large indentations.

A key unanswered question on the cell walls of *Staphylococcus aureus* (SA) is still the exact structure of the peptidoglycan. As mentioned, there are a number of plausible models including the layered and the scaffold models, but it is still not fully understood how the peptidoglycan is arranged within the cell wall.

The measurements undertaken on live *Bacillus subtilis* (BS) cells are currently at a very early stage as it has only recently been possible to immobilise these cells for AFM analysis. There is scope for future work increasing the resolution of the force maps taken within the limited time frame provided by the growth rate of the cells,

perhaps with the use of newly developing techniques such as PeakForce Tapping or by improving the immobilisation technique to allow simultaneous imaging and force mapping of cell division.

The nature of the features seen on the small scale mechanical maps of BS cells are unknown, and by the use of tip chemistry and/or genetic manipulation of the cell wall components of the cells it could be possible to try to determine what is responsible for this heterogeneity.

Finally, the largest opportunity for future work stemming from this study is the possibility to characterise other bacterial species in the way that has been shown here for SA and BS. Modifications to the design of the etched wafers should allow the opportunity to immobilise a range of sizes of the shapes that have currently been successfully immobilised, but also for species of different shapes that have not yet been attempted, for example the crescent shaped *Caulobacter crescentus* and *Vibrio cholerae*, or rugby ball shaped cells (known as coccobacilli, halfway between spheres [cocci] and rods [bacilli]) such as *Haemophilus influenzae* and *Chlamydia trachomatis*.

Bibliography

- [1] K. O. Stetter, “Extremophiles and their adaptation to hot environments,” *FEBS letters*, vol. 452, no. 1-2, pp. 22–25, 1999.
- [2] C. Kato, L. Li, Y. Nogi, Y. Nakamura, and J. I. N. Tamaoka, “Extremely Barophilic Bacteria Isolated from the Mariana Trench, Challenger Deep, at a Depth of 11,000 Meters,” *Applied and environmental microbiology*, vol. 64, no. 4, pp. 1510–1513, 1998.
- [3] J. Xu, M. A. Mahowald, R. E. Ley, C. A. Lozupone, M. Hamady, E. C. Martens, B. Henrissat, P. M. Coutinho, P. Minx, P. Latreille, H. Cordum, A. Van Brunt, K. Kim, R. S. Fulton, L. A. Fulton, S. W. Clifton, R. K. Wilson, R. D. Knight, and J. I. Gordon, “Evolution of symbiotic bacteria in the distal human intestine,” *PLoS biology*, vol. 5, no. 7, pp. 1574–1586, 2007.
- [4] J. R. Porter, “Antony van Leeuwenhoek: Tercentenary of His Discovery of Bacteria,” *Bacteriological Reviews*, vol. 40, no. 2, pp. 260–269, 1976.
- [5] R. M. Macnab, “The Bacterial Flagellum: Reversible Rotary Propellor and Type III Export Apparatus,” *Journal of bacteriology*, vol. 181, no. 23, pp. 7149–7153, 1999.
- [6] R. S. Schwartz, “Paul Ehrlich’s magic bullets,” *The New England Journal of Medicine*, vol. 350, no. 11, pp. 1079–1080, 2004.
- [7] M. T. G. Holden, E. J. Feil, J. A. Lindsay, S. J. Peacock, N. P. J. Day, M. C. Enright, T. J. Foster, C. E. Moore, L. Hurst, R. Atkin, A. Barron, N. Bason, S. D. Bentley, C. Chillingworth, T. Chillingworth, C. Churcher, L. Clark, C. Corton, A. Cronin, J. Doggett, L. Dowd, T. Feltwell, Z. Hance, B. Harris, H. Hauser, S. Holroyd, K. Jagels, K. D. James, N. Lennard, A. Line, R. Mayes, S. Moule, K. Mungall, D. Ormond, M. A. Quail, E. Rabinowitsch, K. Rutherford, M. Sanders, S. Sharp, M. Simmonds,

- K. Stevens, S. Whitehead, B. G. Barrell, B. G. Spratt, and J. Parkhill, "Complete genomes of two clinical *Staphylococcus aureus* strains: evidence for the rapid evolution of virulence and drug resistance," *Proceedings of the National Academy of Sciences of the United States of America*, vol. 101, no. 26, pp. 9786–9791, 2004.
- [8] F. Kunst, N. Ogasawara, I. Moszer, A. M. Albertini, G. Alloni, V. Azevedo, M. G. Bertero, P. Bessières, A. Bolotin, S. Borchert, R. Borriss, L. Boursier, A. Brans, M. Braun, S. C. Brignell, S. Bron, S. Brouillet, C. V. Bruschi, B. Caldwell, V. Capuano, N. M. Carter, S. K. Choi, J. J. Codani, I. F. Connerton, and A. Danchin, "The complete genome sequence of the gram-positive bacterium *Bacillus subtilis*," *Nature*, vol. 390, no. 6657, pp. 249–256, 1997.
- [9] A. Ogston, "On Abscesses," *Clinical Infectious Diseases*, vol. 6, no. 1, pp. 122–128, 1984.
- [10] K. J. Miller, S. C. Zelt, and J.-h. Bae, "Glycine Betaine and Proline are the Principal Compatible Solutes of *Staphylococcus aureus*," *Current microbiology*, vol. 23, pp. 131–137, 1991.
- [11] Y. Gillet, B. Issartel, P. Vanhems, J.-c. Fournet, G. Lina, M. Bes, F. Vandenesch, Y. Piémont, N. Brousse, D. Floret, and J. Etienne, "Mechanisms of disease association between *Staphylococcus aureus* strains carrying gene for Panton-Valentine leukocidin and highly lethal necrotising pneumonia in young immunocompetent patients," *Mechanisms of Disease*, vol. 359, pp. 753–759, 2002.
- [12] J. J. Gordon, D. H. Harter, and J. P. Phair, "Meningitis Due to *Staphylococcus aureus*," *The American Journal of Medicine*, vol. 78, pp. 965–970, 1985.
- [13] G. M. Garrity, J. A. Bell, T. G. Lilburn, and E. Lansing, "Taxonomic Outline of the Prokaryotes," *Bergey's Manual of Systematic Bacteriology*, vol. 2, pp. 1–399, 2004.
- [14] J. W. Bartholomew and T. O. D. Mittwer, "The Gram Stain," *Bacteriology Reviews*, vol. 16, no. 1, pp. 1–29, 1952.
- [15] R. F. Matias, A. Al-amoudi, J. Dubochet, and T. J. Beveridge, "Cryo-Transmission Electron Microscopy of Frozen-Hydrated Sections of *Escherichia coli* and *Pseudomonas aeruginosa*," *Journal of bacteriology*, vol. 185, no. 20, pp. 6112–6118, 2003.

- [16] W. Vollmer, D. Blanot, and M. A. de Pedro, "Peptidoglycan structure and architecture," *FEMS microbiology reviews*, vol. 32, no. 2, pp. 149–167, 2008.
- [17] W. Vollmer and S. J. Seligman, "Architecture of peptidoglycan: more data and more models," *Trends in microbiology*, vol. 18, no. 2, pp. 59–66, 2010.
- [18] B. Dmitriev, F. Toukach, and S. Ehlers, "Towards a comprehensive view of the bacterial cell wall," *Trends in microbiology*, vol. 13, no. 12, pp. 569–574, 2005.
- [19] W. Vollmer and J.-v. Ho, "The Architecture of the Murein (Peptidoglycan) in Gram-Negative Bacteria: Vertical Scaffold or Horizontal Layer(s)?" *Journal of bacteriology*, vol. 186, no. 18, pp. 5978–5987, 2004.
- [20] D. Pink, J. Moeller, B. Quinn, M. Jericho, and T. Beveridge, "On the architecture of the gram-negative bacterial murein sacculus," *Journal of bacteriology*, vol. 182, no. 20, pp. 5925–5930, 2000.
- [21] V. Braun, H. Gnrke, U. Henning, and K. Rehn, "Model for the structure of the shape-maintaining layer of the *Escherichia coli* cell envelope," *Journal of bacteriology*, vol. 114, no. 3, pp. 1264–1270, 1973.
- [22] L. Gan, S. Chen, and G. J. Jensen, "Molecular organization of Gram-negative peptidoglycan," *Proceedings of the National Academy of Sciences of the United States of America*, vol. 105, no. 48, pp. 18953–18957, 2008.
- [23] M. Beeby, J. C. Gumbart, B. Roux, and G. J. Jensen, "Architecture and assembly of the Gram-positive cell wall," *Molecular microbiology*, vol. 88, no. 4, pp. 664–72, 2013.
- [24] B. A. Dmitriev, F. V. Toukach, O. Holst, E. T. Rietschel, and S. Ehlers, "Tertiary Structure of *Staphylococcus aureus* Cell Wall Murein," *Journal of bacteriology*, vol. 186, no. 21, pp. 7141–7148, 2004.
- [25] S. O. Meroueh, K. Z. Bencze, D. Heseck, M. Lee, J. F. Fisher, T. L. Stemmler, and S. Mobashery, "Three-dimensional structure of the bacterial cell wall peptidoglycan," *Proceedings of the National Academy of Sciences of the United States of America*, vol. 103, no. 12, pp. 4404–4409, 2006.
- [26] B. A. Dmitriev, F. V. Toukach, K.-j. Schaper, O. Holst, E. T. Rietschel, and S. Ehlers, "Tertiary Structure of Bacterial Murein: the Scaffold Model," *Journal of bacteriology*, vol. 185, no. 11, pp. 3458–3468, 2003.

- [27] E. J. Hayhurst, L. Kailas, J. K. Hobbs, and S. J. Foster, “Cell wall peptidoglycan architecture in *Bacillus subtilis*,” *Proceedings of the National Academy of Sciences of the United States of America*, vol. 105, no. 38, pp. 14603–14608, 2008.
- [28] G. Andre, S. Kulakauskas, M.-P. Chapot-Chartier, B. Navet, M. Deghorain, E. Bernard, P. Hols, and Y. F. Dufrêne, “Imaging the nanoscale organization of peptidoglycan in living *Lactococcus lactis* cells,” *Nature communications*, vol. 1, p. 27, 2010.
- [29] V. R. F. Matias and T. J. Beveridge, “Cryo-electron microscopy reveals native polymeric cell wall structure in *Bacillus subtilis* 168 and the existence of a periplasmic space,” *Molecular microbiology*, vol. 56, no. 1, pp. 240–251, 2005.
- [30] V. R. F. Matias and T. J. Beveridge, “Lipoteichoic acid is a major component of the *Bacillus subtilis* periplasm,” *Journal of bacteriology*, vol. 190, no. 22, pp. 7414–7418, 2008.
- [31] V. R. F. Matias and T. J. Beveridge, “Native Cell Wall Organization Shown by Cryo-Electron Microscopy Confirms the Existence of a Periplasmic Space in *Staphylococcus aureus*,” *Journal of bacteriology*, vol. 188, no. 3, pp. 1011–1021, 2006.
- [32] V. R. F. Matias and T. J. Beveridge, “Cryo-electron microscopy of cell division in *Staphylococcus aureus* reveals a mid-zone between nascent cross walls,” *Molecular microbiology*, vol. 64, no. 1, pp. 195–206, 2007.
- [33] G. Andre, M. Deghorain, P. A. Bron, I. I. V. Swam, M. Kleerebezem, P. Hols, and Y. F. Dufrene, “Fluorescence and Atomic Force Microscopy Imaging of Wall Teichoic Acids in *Lactobacillus plantarum*,” *ACS Chemical Biology*, 2011.
- [34] K. Schirner, J. Marles-Wright, R. J. Lewis, and J. Errington, “Distinct and essential morphogenic functions for wall- and lipo-teichoic acids in *Bacillus subtilis*,” *The EMBO journal*, vol. 28, no. 7, pp. 830–842, 2009.
- [35] J. M. Skerker and H. C. Berg, “Direct observation of extension and retraction of type IV pili,” *Proceedings of the National Academy of Sciences of the United States of America*, vol. 98, no. 12, pp. 6901–6904, 2001.
- [36] E. Sauvage, F. Kerff, M. Terrak, J. A. Ayala, and P. Charlier, “The penicillin-binding proteins: structure and role in peptidoglycan biosynthesis,” *FEMS microbiology reviews*, vol. 32, no. 2, pp. 234–258, 2008.

- [37] W. Margolin, "Sculpting the bacterial cell," *Current biology*, vol. 19, no. 17, pp. R812–r822, 2009.
- [38] W. Vollmer, B. Joris, P. Charlier, and S. Foster, "Bacterial peptidoglycan (murein) hydrolases," *FEMS microbiology reviews*, vol. 32, pp. 259–286, Mar. 2008.
- [39] T. Uehara and T. G. Bernhardt, "More than just lysins: peptidoglycan hydrolases tailor the cell wall," *Current opinion in microbiology*, vol. 14, no. 6, pp. 698–703, 2011.
- [40] A. Touhami, M. H. Jericho, and T. J. Beveridge, "Atomic Force Microscopy of Cell Growth and Division in *Staphylococcus aureus*," *Journal of bacteriology*, vol. 186, no. 11, pp. 3286–3295, 2004.
- [41] L. Kailas, E. C. Ratcliffe, E. J. Hayhurst, M. G. Walker, S. J. Foster, and J. K. Hobbs, "Immobilizing live bacteria for AFM imaging of cellular processes," *Ultramicroscopy*, vol. 109, no. 7, pp. 775–780, 2009.
- [42] R. D. Turner, N. H. Thomson, J. Kirkham, and D. Devine, "Improvement of the pore trapping method to immobilize vital coccoid bacteria for high-resolution AFM: a study of *Staphylococcus aureus*," *Journal of microscopy*, vol. 238, no. 2, pp. 102–110, 2010.
- [43] H. Tzagoloff and R. Novick, "Geometry of cell division in *Staphylococcus aureus*," *Journal of bacteriology*, vol. 129, no. 1, pp. 343–350, 1977.
- [44] T. Koyama, M. Yamada, and M. Matsuhashi, "Formation of Regular Packets of *Staphylococcus aureus* Cells," *Journal of bacteriology*, vol. 129, no. 3, pp. 1518–1523, 1977.
- [45] K. Tiyanont, T. Doan, M. B. Lazarus, X. Fang, D. Z. Rudner, and S. Walker, "Imaging peptidoglycan biosynthesis in *Bacillus subtilis* with fluorescent antibiotics," *Proceedings of the National Academy of Sciences of the United States of America*, vol. 103, no. 29, pp. 11033–11038, 2006.
- [46] M. A. De Pedro, "Patchiness of murein insertion into the sidewall of *Escherichia coli*," *Microbiology*, vol. 149, no. 7, pp. 1753–1761, 2003.
- [47] R. D. Turner, A. F. Hurd, A. Cadby, J. K. Hobbs, and S. J. Foster, "Cell wall elongation mode in Gram-negative bacteria is determined by peptidoglycan architecture," *Nature communications*, vol. 4, p. 1496, 2013.

- [48] N. Nanninga and L. J. H. Koppes, “The Cell Cycle of *Bacillus subtilis* as Studied by Electron Microscopy,” *Archives of Microbiology*, vol. 181, pp. 173–181, 1979.
- [49] D. W. Adams and J. Errington, “Bacterial cell division: assembly, maintenance and disassembly of the Z ring,” *Nature reviews. Microbiology*, vol. 7, no. 9, pp. 642–653, 2009.
- [50] D. S. Weiss, “Bacterial cell division and the septal ring,” *Molecular microbiology*, vol. 54, no. 3, pp. 588–597, 2004.
- [51] M. T. Cabeen and C. Jacobs-Wagner, “Bacterial cell shape,” *Nature reviews. Microbiology*, vol. 3, no. 8, pp. 601–610, 2005.
- [52] M. Osawa, D. E. Anderson, and H. P. Erickson, “Reconstitution of contractile FtsZ rings in liposomes,” *Science*, vol. 320, no. 5877, pp. 792–794, 2008.
- [53] Z. Li, M. J. Trimble, Y. V. Brun, and G. J. Jensen, “The structure of FtsZ filaments in vivo suggests a force-generating role in cell division,” *The EMBO journal*, vol. 26, no. 22, pp. 4694–4708, 2007.
- [54] S. A. Proctor, N. Minc, A. Boudaoud, and F. Chang, “Contributions of turgor pressure, the contractile ring, and septum assembly to forces in cytokinesis in fission yeast,” *Current biology*, vol. 22, no. 17, pp. 1601–1608, 2012.
- [55] G. Fu, T. Huang, J. Buss, C. Coltharp, Z. Hensel, and J. Xiao, “In vivo structure of the *E. coli* FtsZ-ring revealed by photoactivated localization microscopy (PALM),” *PloS one*, vol. 5, no. 9, pp. 1–16, 2010.
- [56] H. P. Erickson, D. E. Anderson, and M. Osawa, “FtsZ in bacterial cytokinesis: cytoskeleton and force generator all in one,” *Microbiology and molecular biology reviews*, vol. 74, no. 4, pp. 504–528, 2010.
- [57] E. Callaway, “Bacterias New Bones,” *Nature*, vol. 451, pp. 124–126, 2008.
- [58] L. J. Jones, R. Carballido-López, and J. Errington, “Control of cell shape in bacteria: helical, actin-like filaments in *Bacillus subtilis*,” *Cell*, vol. 104, no. 6, pp. 913–922, 2001.
- [59] K. D. Young, “Bacterial shape,” *Molecular Microbiology*, vol. 49, no. 3, pp. 571–580, 2004.

- [60] S. van Teeffelen, S. Wang, L. Furchtgott, K. C. Huang, N. S. Wingreen, J. W. Shaevitz, and Z. Gitai, “The bacterial actin MreB rotates, and rotation depends on cell-wall assembly,” *Proceedings of the National Academy of Sciences of the United States of America*, vol. 108, no. 38, pp. 15822–15827, 2011.
- [61] R. A. Daniel and J. Errington, “Control of cell morphogenesis in bacteria: two distinct ways to make a rod-shaped cell,” *Cell*, vol. 113, no. 6, pp. 767–776, 2003.
- [62] C. B. Anderson and L. D. Witter, “Glutamine and Proline Accumulation by *Staphylococcus aureus* with Reduction in Water Activity,” *Applied and environmental microbiology*, vol. 43, no. 6, pp. 1501–1503, 1982.
- [63] J. H. Christian and J. a. Waltho, “The Composition of *Staphylococcus aureus* in Relation To the Water Activity of the Growth Medium,” *Journal of general microbiology*, vol. 35, pp. 205–213, 1964.
- [64] J. F. Imhoff, “Osmoregulation and compatible solutes in eubacteria,” *FEMS Microbiology Reviews*, vol. 39, pp. 57–66, 1986.
- [65] J. E. Graham and B. J. Wilkinson, “*Staphylococcus aureus* osmoregulation: roles for choline, glycine betaine, proline, and taurine,” *Journal of bacteriology*, vol. 174, no. 8, pp. 2711–2716, 1992.
- [66] B. Pourkomialian and I. R. Booth, “Glycine betaine transport by *Staphylococcus aureus*: evidence for two transport systems and for their possible roles in osmoregulation,” *Journal of general microbiology*, vol. 138, no. 12, pp. 2515–2518, 1992.
- [67] U. Vijaranakul, M. J. Nadakavukaren, B. L. d. Jonge, B. J. Wilkinson, U. Vijaranakul, M. J. Nadakavukaren, L. M. Boudewijn, B. J. Wilkinson, and R. K. Jayaswal, “Increased Cell Size and Shortened Peptidoglycan Interpeptide Bridge of NaCl-Stressed *Staphylococcus aureus* and Their Reversal by Glycine Betaine,” *Journal of bacteriology*, vol. 177, no. 17, pp. 5116–5121, 1995.
- [68] I. Koujima, H. Hayashi, K. Tomochika, and Y. Kanemasa, “Adaptational Change in Proline and Water Content of *Staphylococcus aureus* After Alteration of Environmental Salt Concentration,” *Applied and environmental microbiology*, vol. 35, no. 3, pp. 467–470, 1978.
- [69] T. Pilizota and J. W. Shaevitz, “Fast, multiphase volume adaptation to hyperosmotic shock by *Escherichia coli*,” *PloS one*, vol. 7, no. 4, pp. 1–10, 2012.

- [70] P. C. Braga and D. Ricci, "Atomic force microscopy: application to investigation of *Escherichia coli* morphology before and after exposure to cefodizime," *Antimicrobial agents and chemotherapy*, vol. 42, no. 1, pp. 18–22, 1998.
- [71] T. R. Paul, A. Venter, L. C. Blaszcak, T. O. M. R. Parr, H. Labischinski, and T. J. Beveridge, "Localization of Penicillin-Binding Proteins to the Splitting System of *Staphylococcus aureus* Septa by Using a Mercury-Penicillin V Derivative," *Journal of bacteriology*, vol. 177, no. 13, pp. 3631–3640, 1995.
- [72] G. Binnig, C. F. Quate, and C. Gerber, "Atomic Force Microscope," *Physical review letters*, vol. 56, no. 9, pp. 930–933, 1986.
- [73] S. Magonov, V. Elings, and V. Papkov, "AFM study of thermotropic structural transitions in poly(diethylsiloxane)," *Polymer*, vol. 38, no. 2, pp. 297–307, 1997.
- [74] R. L. Meyer, X. Zhou, L. Tang, A. Arpanaei, P. Kingshott, and F. Besenbacher, "Immobilisation of living bacteria for AFM imaging under physiological conditions," *Ultramicroscopy*, vol. 110, no. 11, pp. 1349–1357, 2010.
- [75] M. J. Doktycz, C. J. Sullivan, P. R. Hoyt, D. A. Pelletier, S. Wu, and D. P. Allison, "AFM imaging of bacteria in liquid media immobilized on gelatin coated mica surfaces," *Ultramicroscopy*, vol. 97, no. 1-4, pp. 209–216, 2003.
- [76] M. Rangl, R. Nevo, I. Liashkovich, V. Shahin, Z. Reich, A. Ebner, and P. Hinterdorfer, "Stable, non-destructive immobilization of native nuclear membranes to micro-structured PDMS for single-molecule force spectroscopy," *Chemphyschem*, vol. 10, no. 9-10, pp. 1553–1558, 2009.
- [77] E. Dague, E. Jauvert, L. Laplatine, B. Viallet, C. Thibault, and L. Rossier, "Assembly of live micro-organisms on microstructured PDMS stamps by convective/capillary deposition for AFM bio-experiments," *Nanotechnology*, vol. 22, no. 39, pp. 1–7, 2011.
- [78] S. Kasas and A. Ikai, "A method for anchoring round shaped cells for atomic force microscope imaging," *Biophysical journal*, vol. 68, no. 5, pp. 1678–1780, 1995.
- [79] A. Méndez-Vilas, A. M. Gallardo-Moreno, and M. L. González-Martín, "Atomic force microscopy of mechanically trapped bacterial cells," *Microscopy and microanalysis*, vol. 13, no. 1, pp. 55–64, 2007.

- [80] C. Verbelen, V. Dupres, F. D. Menozzi, D. Raze, A. R. Baulard, P. Hols, and Y. F. Dufrêne, “Ethambutol-induced alterations in *Mycobacterium bovis* BCG imaged by atomic force microscopy,” *FEMS microbiology letters*, vol. 264, no. 2, pp. 192–197, 2006.
- [81] K. A. Whitehead, D. Rogers, J. Colligon, C. Wright, and J. Verran, “Use of the atomic force microscope to determine the effect of substratum surface topography on the ease of bacterial removal,” *Colloids and surfaces. B, Biointerfaces*, vol. 51, no. 1, pp. 44–53, 2006.
- [82] A. L. Weisenhorn, B. Drake, C. B. Prater, S. A. Gould, P. K. Hansma, F. Ohnesorge, M. Egger, S. P. Heyn, and H. E. Gaub, “Immobilized proteins in buffer imaged at molecular resolution by atomic force microscopy,” *Biophysical journal*, vol. 58, no. 5, pp. 1251–1258, 1990.
- [83] V. Dupres, D. Alsteens, G. Andre, and Y. F. Dufrêne, “Microbial nanoscopy: a closer look at microbial cell surfaces,” *Trends in microbiology*, vol. 18, no. 9, pp. 397–405, 2010.
- [84] S. Bahatyrova, R. N. Frese, C. A. Siebert, J. D. Olsen, K. O. Van Der Werf, R. Van Grondelle, R. A. Niederman, P. A. Bullough, C. Otto, and C. N. Hunter, “The native architecture of a photosynthetic membrane,” *Nature*, vol. 430, no. 7003, pp. 1058–1062, 2004.
- [85] R. Del Sol, I. Armstrong, C. Wright, and P. Dyson, “Characterization of changes to the cell surface during the life cycle of *Streptomyces coelicolor*: atomic force microscopy of living cells,” *Journal of bacteriology*, vol. 189, no. 6, pp. 2219–2225, 2007.
- [86] D. Yamamoto, A. Taoka, T. Uchihashi, H. Sasaki, H. Watanabe, and T. Ando, “Visualization and structural analysis of the bacterial magnetic organelle magnetosome using atomic force microscopy,” *PNAS*, vol. 107, no. 20, pp. 9382–9387, 2010.
- [87] A. E. Pelling, Y. Li, W. Shi, and J. K. Gimzewski, “Nanoscale visualization and characterization of *Myxococcus xanthus* cells with atomic force microscopy,” *Proceedings of the National Academy of Sciences of the United States of America*, vol. 102, no. 18, pp. 6484–6489, 2005.
- [88] C. Díaz, P. L. Schilardi, R. C. Salvarezza, and M. Fernández Lorenzo de Mele, “Have flagella a preferred orientation during early stages of biofilm formation?: AFM study using patterned substrates,” *Colloids and surfaces. B, Biointerfaces*, vol. 82, no. 2, pp. 536–542, 2011.

- [89] A. Gillis, V. Dupres, G. Delestrait, J. Mahillon, and Y. F. Dufrêne, “Nanoscale imaging of *Bacillus thuringiensis* flagella using atomic force microscopy,” *Nanoscale*, vol. 4, no. 5, pp. 1585–1591, 2012.
- [90] T. Schmid, J. Burkhard, B.-S. Yeo, W. Zhang, and R. Zenobi, “Towards chemical analysis of nanostructures in biofilms I: imaging of biological nanostructures,” *Analytical and bioanalytical chemistry*, vol. 391, no. 5, pp. 1899–1905, 2008.
- [91] T. A. Camesano, M. J. Natan, and B. E. Logan, “Observation of Changes in Bacterial Cell Morphology Using Tapping Mode Atomic Force Microscopy,” *Langmuir*, vol. 16, no. 10, pp. 4563–4572, 2000.
- [92] A. V. Bolshakova, O. I. Kiselyova, A. S. Filonov, O. Y. Frolova, Y. L. Lyubchenko, and I. V. Yaminsky, “Comparative studies of bacteria with an atomic force microscopy operating in different modes,” *Ultramicroscopy*, vol. 86, no. 1-2, pp. 121–128, 2001.
- [93] G. Francius, O. Domenech, M. P. Mingeot-Leclercq, and Y. F. Dufrêne, “Direct observation of *Staphylococcus aureus* cell wall digestion by lysostaphin,” *Journal of bacteriology*, vol. 190, no. 24, pp. 7904–7909, 2008.
- [94] V. Vadillo-Rodriguez, T. J. Beveridge, and J. R. Dutcher, “Surface viscoelasticity of individual gram-negative bacterial cells measured using atomic force microscopy,” *Journal of bacteriology*, vol. 190, no. 12, pp. 4225–4232, 2008.
- [95] M. Shibata, H. Yamashita, T. Uchihashi, H. Kandori, and T. Ando, “High-speed atomic force microscopy shows dynamic molecular processes in photoactivated bacteriorhodopsin,” *Nature nanotechnology*, vol. 5, no. 3, pp. 208–212, 2010.
- [96] G. E. Fantner, R. J. Barbero, D. S. Gray, and A. M. Belcher, “Kinetics of antimicrobial peptide activity measured on individual bacterial cells using high-speed atomic force microscopy,” *Nature Nanotechnology Letters*, pp. 1–6, 2010.
- [97] M. Micic, D. Hu, Y. D. Suh, G. Newton, M. Romine, and H. P. Lu, “Correlated atomic force microscopy and fluorescence lifetime imaging of live bacterial cells,” *Colloids and surfaces. B, Biointerfaces*, vol. 34, no. 4, pp. 205–212, 2004.
- [98] M. T. Montero, M. Pijoan, S. Merino-Montero, T. Vinuesa, and J. Hernández-Borrell, “Interfacial membrane effects of fluoroquinolones as revealed by a combination of fluorescence binding experiments and atomic

- force microscopy observations,” *Langmuir*, vol. 22, no. 18, pp. 7574–7578, 2006.
- [99] M. Radmacher, J. P. Cleveland, M. Fritz, H. G. Hansma, and P. K. Hansma, “Mapping Interaction Forces with the Atomic Force Microscope,” *Biophysical journal*, vol. 66, no. 6, pp. 2159–2165, 1994.
- [100] H.-J. Butt and M. Jaschke, “Calculation of thermal noise in atomic force microscopy,” *Nanotechnology*, vol. 6, pp. 1–7, 1995.
- [101] J. L. Hutter and J. Bechhoefer, “Calibration of atomic-force microscope tips,” *Review of Scientific Instruments*, vol. 64, no. 7, p. 1868, 1993.
- [102] J. L. Hutter, “Comment on Tilt of Atomic Force Microscopy Cantilevers,” *Langmuir*, vol. 21, pp. 2630–2632, 2005.
- [103] R. W. Stark, T. Drobek, and W. M. Heckl, “Thermomechanical noise of a free v-shaped cantilever for atomic-force microscopy,” *Ultramicroscopy*, vol. 86, no. 1-2, pp. 207–215, 2001.
- [104] M. a. Beckmann, S. Venkataraman, M. J. Doktycz, J. P. Nataro, C. J. Sullivan, J. L. Morrell-Falvey, and D. P. Allison, “Measuring cell surface elasticity on enteroaggregative *Escherichia coli* wild type and dispersin mutant by AFM,” *Ultramicroscopy*, vol. 106, no. 8-9, pp. 695–702, 2006.
- [105] H. C. van der Mei, H. J. Busscher, R. Bos, J. de Vries, C. J. Boonaert, and Y. F. Dufrène, “Direct Probing by Atomic Force Microscopy of the Cell Surface Softness of a Fibrillated and Nonfibrillated Oral Streptococcal Strain,” *Biophysical journal*, vol. 78, no. 5, pp. 2668–2674, 2000.
- [106] C. B. Volle, M. A. Ferguson, K. E. Aidala, E. M. Spain, and M. E. Núñez, “Spring constants and adhesive properties of native bacterial biofilm cells measured by atomic force microscopy,” *Colloids and surfaces. B, Biointerfaces*, vol. 67, no. 1, pp. 32–40, 2008.
- [107] N. Andreeva, D. Bassi, F. Cappa, P. S. Cocconcelli, F. Parmigiani, and G. Ferrini, “Nanomechanical analysis of *Clostridium tyrobutyricum* spores,” *Micron*, vol. 41, no. 8, pp. 945–952, 2010.
- [108] J. H. Hoh and C. A. Schoenenberger, “Surface morphology and mechanical properties of MDCK monolayers by atomic force microscopy,” *Journal of cell science*, vol. 107, no. 5, pp. 1105–1114, 1994.

- [109] M. J. Rosenbluth, W. A. Lam, and D. A. Fletcher, "Force microscopy of nonadherent cells: a comparison of leukemia cell deformability," *Biophysical journal*, vol. 90, no. 8, pp. 2994–3003, 2006.
- [110] V. Vadillo-Rodriguez, S. R. Schooling, and J. R. Dutcher, "In situ characterization of differences in the viscoelastic response of individual gram-negative and gram-positive bacterial cells," *Journal of bacteriology*, vol. 191, no. 17, pp. 5518–5525, 2009.
- [111] F. Gaboriaud, B. S. Parcha, M. L. Gee, J. A. Holden, and R. A. Strugnell, "Spatially resolved force spectroscopy of bacterial surfaces using force-volume imaging," *Colloids and surfaces. B, Biointerfaces*, vol. 62, no. 2, pp. 206–213, 2008.
- [112] P. Schaer-Zammaretti and J. Ubbink, "Imaging of lactic acid bacteria with AFM - elasticity and adhesion maps and their relationship to biological and structural data," *Ultramicroscopy*, vol. 97, no. 1-4, pp. 199–208, 2003.
- [113] G. Longo, L. M. Rio, A. Trampuz, G. Dietler, A. Bizzini, and S. Kasas, "Antibiotic-induced Modifications of the Stiffness of Bacterial Membranes," *Journal of Microbiological Methods*, vol. 93, pp. 80–84, Feb. 2013.
- [114] D. Alsteens, E. Dague, P. G. Rouxhet, A. R. Baulard, and Y. F. Dufrêne, "Direct measurement of hydrophobic forces on cell surfaces using AFM," *Langmuir*, vol. 23, no. 24, pp. 11977–11979, 2007.
- [115] L. S. Dorobantu, S. Bhattacharjee, J. M. Foght, and M. R. Gray, "Atomic force microscopy measurement of heterogeneity in bacterial surface hydrophobicity," *Langmuir*, vol. 24, no. 9, pp. 4944–4951, 2008.
- [116] F. Ahimou, F. A. Denis, A. Touhami, and Y. F. Dufrene, "Probing Microbial Cell Surface Charges by Atomic Force Microscopy," *Langmuir*, vol. 18, no. 25, pp. 9937–9941, 2002.
- [117] G. Francius, S. Lebeer, D. Alsteens, L. Wildling, H. J. Gruber, P. Hols, S. D. Keersmaecker, J. Vanderleyden, and Y. F. Dufrêne, "Detection, Localization, and Conformational Analysis of Single Polysaccharide Molecules on Live Bacteria," *ACS NANO*, vol. 2, no. 9, pp. 1921–1929, 2008.
- [118] J. Tang, D. Krajcikova, R. Zhu, A. Ebner, S. Cutting, H. J. Gruber, I. Barak, and P. Hinterdorfer, "Atomic force microscopy imaging and single molecule recognition force spectroscopy of coat proteins on the surface of *Bacillus subtilis* spore," *Journal of Molecular Recognition*, vol. 20, pp. 483–489, 2007.

- [119] V. Dupres, F. D. Menozzi, C. Locht, B. H. Clare, N. L. Abbott, C. Bompard, D. Raze, and Y. F. Dufre, “Nanoscale mapping and functional analysis of individual adhesins on living bacteria,” *Nature Methods*, vol. 2, no. 7, pp. 515–521, 2005.
- [120] M. Benoit, D. Gabriel, G. Gerisch, and H. E. Gaub, “Discrete interactions in cell adhesion measured by single-molecule force spectroscopy,” *Nature cell biology*, vol. 2, no. 6, pp. 313–317, 2000.
- [121] C. J. P. Boonaert, V. Toniazzo, C. Mustin, Y. F. Dufrene, and P. G. Rouxhet, “Deformation of *Lactococcus lactis* surface in atomic force microscopy study,” *Colloids and Surfaces B: Biointerfaces*, vol. 23, pp. 201–211, 2002.
- [122] S. B. Velegol, S. Pardi, X. Li, D. Velegol, and B. E. Logan, “AFM Imaging Artifacts due to Bacterial Cell Height and AFM Tip Geometry,” *Langmuir*, no. 11, pp. 851–857, 2003.
- [123] D. Alsteens, C. Verbelen, E. Dague, D. Raze, A. R. Baulard, and Y. F. Dufrêne, “Organization of the mycobacterial cell wall: a nanoscale view,” *Pflügers Archiv : European Journal of Physiology*, vol. 456, no. 1, pp. 117–125, 2008.
- [124] C. Bustamante and D. Keller, “Scanning Force Microscopy in Biology,” *Physics Today*, pp. 32–38, 1995.
- [125] H.-J. Butt, B. Cappella, and M. Kappl, “Force measurements with the atomic force microscope: Technique, interpretation and applications,” *Surface Science Reports*, vol. 59, no. 1-6, pp. 1–152, 2005.
- [126] L. Cui, X. Ma, K. Sato, K. Okuma, F. C. Tenover, E. M. Mamizuka, C. G. Gemmell, M.-N. Kim, M.-c. Ploy, N. E. Solh, and V. Ferraz, “Cell Wall Thickening Is a Common Feature of Vancomycin Resistance in *Staphylococcus aureus*,” *Journal of Clinical Microbiology*, vol. 41, no. 1, pp. 5–14, 2003.
- [127] A. Vinckier and G. Semenza, “Measuring elasticity of biological materials by atomic force microscopy,” *FEBS letters*, vol. 430, no. 1-2, pp. 12–16, 1998.
- [128] G. Longo, L. M. Rio, A. Trampuz, G. Dietler, A. Bizzini, and S. Kasas, “Antibiotic-induced modifications of the stiffness of bacterial membranes,” *Journal of microbiological methods*, vol. 93, no. 2, pp. 80–84, 2013.
- [129] K. Amako, A. Umeda, and K. Murata, “Arrangement of Peptidoglycan in the Cell Wall of *Staphylococcus* spp.,” *Journal of bacteriology*, vol. 150, no. 2, pp. 844–850, 1982.

- [130] S. Yamada, M. Sugai, H. Komatsuzawa, S. Nakashima, T. Oshida, A. Matsumoto, and H. Suginaka, "An autolysin ring associated with cell separation of *Staphylococcus aureus*," *Journal of bacteriology*, vol. 178, no. 6, pp. 1565–1571, 1996.
- [131] J. N. Reddy, *Theory and Analysis of Elastic Plates*. Taylor and Francis, 1999.
- [132] Y. F. Dufrêne and P. Hinterdorfer, "Recent progress in AFM molecular recognition studies," *Pflügers Archiv: European journal of physiology*, vol. 456, no. 1, pp. 237–245, 2008.